# A PROFICIENT METHODOLOGY FOR LUNG CARCINOMA DETECTION AT PREMATURE STAGE USING DEEP LEARNING TECHNIQUES

Thesis Submitted for the Award of the Degree of

# DOCTOR OF PHILOSOPHY

In

**Computer Science and Engineering** 

By

Isha Bhatia

Registration No. 41900586

**Supervised By** 

Dr. Aarti - 25209

School of Computer Science and Engineering,
Lovely Professional University



LOVELY PROFESSIONAL UNIVERSITY, PUNJAB 2025

# **DECLARATION**

I, hereby declared that the presented work in the thesis entitled "A Proficient Methodology for Lung Carcinoma Detection at Premature Stage using Deep Learning Techniques." in fulfilment of degree of Doctor of Philosophy (Ph.D.) is outcome of research work carried out by me under the supervision Dr. Aarti, working as Professor, in the of Lovely Professional University, Punjab, India. In keeping with the general practice of reporting scientific observations, due acknowledgements have been made whenever work described here has been based on findings of another investigator. This work has not been submitted in part or full to any other University or Institute for the award of any degree.



(Signature of Supervisor)

Name of the scholar: Isha Bhatia

(Signature of scholar)

Lovely Professional University, Punjab, India

**Registration Number:** 41900586

**Department/school:** Computer Science and Engineering,

# **CERTIFICATE**

This is to certify that the work reported in the Ph.D. thesis entitled "A Proficient Methodology for Lung Carcinoma Detection at Premature Stage using Deep Learning Techniques." submitted in fulfilment of the requirement for the reward of degree of Doctor of Philosophy (Ph.D.) in the Computer Science and Engineering, is a research work carried out Isha Bhatia, 41900586 is bonafide record of her original work carried out under my supervision and that no part of thesis has been submitted for any other degree, diploma or equivalent course.



(Signature of Supervisor) Name of supervisor: Dr. Aarti

**Designation**: Associate Professor

**Department/School:** Department of Computer Science & Engineering,

Lovely Professional University, Punjab, India

Place: Lovely Professional University, Punjab

**Date:** 23/07/2025

**ACKNOWLEDGEMENT** 

First and foremost, I would like to extend my sincerest gratitude to the almighty

God, without whom this work would not have been possible. I would like to

express my sincere gratitude and deep appreciation to my supervisor, Dr. Aarti,

for their invaluable guidance. Their enduring, continual guidance and support

motivated me in every phase of my research as well as in life. I am grateful to

them for teaching me lots of things that not only led my thesis to fruition but also

inculcated good researcher traits in me.

I would like to thank my parents, Mr. Lakhmi Chand Bhatia and Mrs. Har Bhatia,

for their emotional support, love, and blessings, who have worked hard day and

night to make me what I am today.

I would also like to thank my Research Committee Members for providing

insightful and constructive comments. I would like to thank my friends and well-

wishers who helped me directly or indirectly throughout my Ph.D. research at

Lovely Professional University, Punjab.

Place: Lovely Professional University, Punjab

**Date:** 23/07/2025

Name: Isha Bhatia

Registration No: 41900586

iii

# **ABSTRACT**

Lung carcinoma has a high mortality rate; however, early prediction can significantly improve patient outcomes. Although various methods have been developed for premature-stage lung carcinoma prediction, many still suffer from issues such as low accuracy, high noise, poor contrast, and the lack of integrated risk screening. To address these challenges, this study proposed a lung carcinoma prediction and risk screening model using Transfer Learning with a P-ReLU-ResNet (P-ResNet) framework. The proposed model operates on 2D CT scan slices. Initially, lung computed tomography (CT) scan images were preprocessed to reduce noise and enhance edges using the Intra-class Variance-Anisotropic Diffusion Filter (I-ADF) and Unsharp Mask Filter (UMF). The enhanced images were then segmented using a Bates-distributed Coati Optimization Algorithm integrated with Region Growing Segmentation (B-RGS). Features were extracted from the segmented images and selected using the Binomial-distributed Chisquare Test (BD-CST). The selected features are then classified using the TLbased P-ReLUResNet model to determine whether the input is normal or abnormal. For abnormal cases, a risk screening module further categorizes the risk as low or high. Experimental results validated the effectiveness of the presented method. The research achieved superior performance in premature stage lung cancer prediction, achieving recall, accuracy, and precision scores of 97.36%, 98.21%, and 98.71%, respectively, outperforming existing approaches across all key metrics. This study focused solely on lung carcinoma detection, rather than other pulmonary conditions observable in lung imaging. Future work aims to incorporate advanced tools for more accurate prediction of cancer type and severity.

Keywords: Lung carcinoma, Anisotropic Diffusion Filter, Chi-square test, TL-based P-ReLUResNet algorithms

# **ORGANIZATION OF THESIS**

The thesis is structured into eight chapters: Introduction, Literature Survey, Research Methodology, Deep Learning for Lung Cancer Detection, Transfer Learning for Lung Cancer Detection, Hybrid Approach, Comparative Analysis, Conclusion, and Future Scope.

#### Chapter 1

A brief introduction to cancer and lung cancer is given in this chapter. This chapter includes an explanation of the work's motivation, an outline of the thesis, details on the thesis's structure, and contributions.

## Chapter 2

The background information on the detection techniques and medical facts about lung cancer have been thoroughly explained in Chapter 2. From a medical perspective, data on lung cancer prevalence worldwide and associated details have been provided. This chapter explains the need for automated detection algorithms. Technical details about the suggested framework's technical background and methods for detecting lung cancer in the literature have been provided. This chapter presents a thorough literature review on lung nodule detection.

#### Chapter 3

This chapter presents the research methodology that includes the following: Role of deep learning models in cancer detection at the premature stage. Study of different deep learning models for lung cancer detection. Data collection for lung CT images from the LIDC-IDRI dataset and pre-processing of these images. Implementation of P-ResNet algorithm for the detection of lung nodules. Study & implementation of transfer learning for lung cancer detection. Calculate performance in terms of accuracy, precision, and recall. Design and implementation of a hybrid model P-ResNet with ReLU function. Parameters fine-tuning of all implemented models for better accuracy. Calculate the performance of P-ResNet. Comparison between pre-trained & current model.

#### Chapter 4

Performed an analysis of pre-existing algorithms using various benchmark datasets. In this, the traditional models that were demonstrating the outcomes were discussed. Using benchmark datasets, the traditional CNN, MPA, and NBC models are reviewed, and their outcomes are presented.

#### Chapter 5

To forecast the discovery of lung cancer in a patient, the improved segmentation method was tested using both benchmark datasets and the proposed dataset. This chapter presents the different optimizers for testing the suggested system.

#### Chapter 6

A detailed description of the novel model is given from the beginning. The topics addressed included preprocessing, segmentation, feature extraction, feature selection, and classification methods. The results of several datasets utilized in the recommended research are displayed in this chapter. Lastly, the accuracy of the suggested system is verified using real-time video. Using different accuracy metrics, the system's performance is compared to that of modern systems.

#### Chapter 7

Presents a detailed comparison of different models and methodologies for lung cancer detection. The performance and diagnostic relevance of each approach are discussed.

#### **Chapter 8**

This chapter gives a summary of the research work and highlights the main findings of the proposed TL-based P-ReLUResNet model for early lung cancer detection. It also explains how the model helps improve accuracy by using different types of data. Finally, the chapter discusses future work, such as using the model to predict cancer types and severity with the help of better techniques and larger datasets.

<b>TABLE</b>	OF	CONTENTS
DE	CLARATION	•••••••••••••••••••••••••••••••••••••••
CE	CRTIFICATE	i
AC	CKNOWLEDGEMENT	ii
ABS	STRACT	iv
OR	RGANIZATION OF THESIS	
CH	APTER 1 INTRODUCTION	
1.1.	Introduction to Lung Cancer and Its Globa	l Impact
1.2.	The Fundamentals of Lung Cancer	,
1.3.	Overview of Lung Imaging and Diagnostic	e Techniques
1.4.	General Steps of Lung Cancer	
1.5.	Significance and Urgency of Early Lung C	ancer Detection
1.6.	Motivation and Research Objective	
1.7.	Research Contributions	
CHA	IAPTER 2 LITERATURE SURVEY	
2.1.	Overview of Existing Research on Lung C	ancer
2.2.	Review of Deep Learning Approaches for	Lung Nodule Detection10
2.3.	Techniques for Enhancing and Analyzing I	Lung Cancer Images14
2.4.	Datasets Available for Implementation	1
2.5.	Summary	1
CHA	IAPTER 3 HYPOTHESIS AND OBJECTIVE	S1
3.1.	Identified Research Gaps	1′
3.2.	Research Objectives	1′

3.3.	Proposed Framework	
3.4.	Summary	19
CHA	PTER 4 PROPOSED SEGMENTATION AND CLASSIFICATION	20
4.1.	Deep Learning-Based Framework for Lung Nodule Detection	20
4.1.1.	Pre-processing stage	20
4.1.2	Segmentation of Lung Nodules	22
4.2	Classification Techniques	23
4.2.1.	Convolutional layer network	23
4.2.2	Memory of the Marine Predator Algorithm (MPA)	26
4.3	Classification Using Traditional ML Algorithms	29
4.3.1	Naïve Bayes Classifier Workflow and Architecture	29
4.4	Datasets Used in ML-Based Lung Cancer Detection	31
4.5	Performance Comparison of Deep Learning and Traditional Models	32
4.6	Chapter Summary	33
CHA	PTER 5 ENHANCING ALGORITHMS THROUGH	
OPTI	MIZATION METHODS	34
5.1.	Problem definition	34
5.2.	Problem-Solving Approach	35
5.3.	Proposed Methodology1: Lightweight Deep Neural Network for Early	
Lung Cano	cer Detection	35
5.3.1.	Ricker Wavelet Iterative Center Weighted Median Filter (RWICWM)	37
5.3.2.	Sørensen-Dice Index K-means clustering	37
5.3.3.	Semi-supervised and contrastive learning-based DNN	39
5.3.4.	Risk Score Screening	41

	5.3.5.	Dataset Overview for Lightweight DNN Model	42
5.4. Proposed Methodology 2: Lung Carcinoma Detection Using Tran		Proposed Methodology 2: Lung Carcinoma Detection Using Transfer	
Lea	arning	44	
	5.4.1.	Iterative Adaptive Decision Fusion (I-ADF)	47
	5.4.2.	Knuckle Point Using (B-RGS)	48
	5.4.3.	Unmask Sharp Filter	48
	5.4.4.	Binomial Distributed Chi-Square	49
	5.4.5.	Dataset Overview for Transfer Learning Model	50
5.5	<b>5.</b>	Chapter Summary	51
	СНАР	TER 6 LUNG TUMOR SCREENING USING SMART	
	DECIS	SION-MAKING TECHNIQUES	52
6.1	•	Advanced DNN Risk Screening for Early Lung Carcinoma	52
	6.1.1.	Image Preprocessing for Lung CT Enhancement and Denoising	52
	6.1.2.	Noise Suppression	52
	6.1.3.	Lung Nodule Segmentation for Region of Interest Identification	54
	6.1.4.	Optimized Segmentation Using K-means and Dice Index	54
	6.1.5.	Experimental Results and Comparative Performance Analysis	56
6.2		TL-Based P-ResNet Framework for Early Lung Cancer Detection	60
	6.2.1.	Enhanced Filtering Techniques for Lung CT Image Preprocessing	62
	6.2.2.	Precise Lung Image Segmentation Using BRGS Optimized with BD-COA	66
	6.2.3.	Extraction of Discriminative Features from Segmented Lung Regions	69
	6.2.4.	Selection of Optimal Features Using Statistical and Spatial Criteria	71
	6.2.5.	Classification of Lung Abnormalities Using the Proposed P-ResNet Model	72
	6.2.6.	Risk Screening of Lung Carcinoma Using: TL-based P-ReLUResNet	74
	6.2.7.	Results and Discussion on Proposed Models' Effectiveness	74

6.3.	Chapter Summary		79
	CHAPTER 7	COMPARATIVE ANALYSIS	81
7.1.	Chapte	er Summary	83
	CHAPTER 8	CONCLUSION AND FUTURE SCOPE	84
8.1.	Conclu	usion	84
8.2.	Future	e Scope	85
	REFERENCE	S	86
	ANNEXURE	I	94
	ANNEXURE	2	105

# LIST OF TABLES

Table 2.1 Summary of Widely Used Public Datasets for Lung Cancer Detection	15
Table 4.1 The result of the MPA algorithm and its comparisons with others	28
Table 4.2 Description and Techniques for the MPA Algorithm	30
Table 6.1 Evaluation of the suggested models and the current models	
performance	57
Table 6.2 Analysis of the existing and prospective models: Performance of PSNR,	
SSIM, and ET	59
Table 6.3 Comparative Assessment of Proposed vs. Current Lung Cancer	
Models	75
Table 6.4 Analysis of the projected model's and current models' MSE, PSNR,	
and SSIM performance	78
Table 6.5 Comparison of the accuracy of the suggested model and the literature	
survey model	79
Table 7.1 Comparative Analysis of Proposed Methodologies	82

# LIST OF FIGURES

Figure 1.1 Types of Cancer in the Human Body	2
Figure 1.2 Growth of cancer cells in the human body	2
Figure 1.3 Diagnostic Imaging Tools for Lung Abnormalities	4
Figure 1.4 Basic steps of Lung Cancer Detection	5
Figure 2.1 Basic Steps of Lung Cancer Detection	9
Figure 3.1 Proposed Framework for Premature stage Lung Cancer Detection	18
Figure 4.1 Workflow of the Proposed Lung Nodule Detection Framework	
Using CNN and MPA	20
Figure 4.2 Step-by-Step Preprocessing Workflow for CT Lung Images	21
Figure 4.3 Image Left and Right without and with pre-processing	22
Figure 4.4 Illustration of Lung Image Segmentation	22
Figure 4.5 Image Left and Right without and with segmentation	23
Figure 4.6 Convolutional Feature Mapper	24
Figure 4.7 Input and Output Activation Maps	25
Figure 4.8 Max pooling in CNN	25
Figure 4.9 Flow chart of the present MPA-CNN method	27
Figure 4.10 Flow chart of Naïve Architecture	30
Figure 4.11 Malignant nodules of various sizes on CT slices	31
Figure 5.1 Block schematic of the suggested model	36
Figure 5.2 Dataset Utilization for Cancer Detection	40
Figure 5.3 The left, center, and right images illustrate distinct kinds of cancer	41
Figure 5.4 Sample input images in the proposed framework.	43
Figure 5.5 Left and Right with Cancer and Highlighted Cancerous Image	44
Figure 5.6 Pre-Diagnosis of Lung Cancer Detection	46
Figure 5.7 Sample images of the planned model	50
Figure 6.1 Block Diagram of Lightweight DNN for Lung Cancer Detection	52
Figure 6.2 Architecture of the TL-Based P-ReLUResNet (P-ResNet) Risk	
Screening System	61
Figure 6.3 Architecture of the Proposed P-ResNet Model	72

# LIST OF GRAPHS

Graph 4.1 Accuracy and Sensitivity Comparison	28
Graph 4.2 Comparison of several suggested nodule detection models	33
Graph 6.1 Comparison of Preprocessing Techniques Based on Accuracy5	58
Graph 6.2 SSIM and Runtime Analysis of Proposed vs. Baseline Models	59
Graph 6.3 Evaluation of processing methods	75
Graph 6.4 Performance Comparison of P-ResNet with Existing Models	76
Graph 6.5Training Time Comparison Between Proposed and Existing Models	76
Graph 6.6 Dice Score Comparison Between Proposed and Existing Models	77
Graph 6.7 Comparison of Performance Metrics for Existing and Proposed	
Models	78
Graph 6.8 Accuracy Comparison Between Proposed Model and Literature	
Models	79
Graph 7.1 Comparative accuracy of the proposed TL-based P-ResNet model	
with DNN and other models	83

#### LIST OF ABBREVIATIONS

I-ADF Intra-class Variance-Anisotropic Diffusion Filter

BD CST Binomial distributed Chi-Square Test
B-RGS Bates Region Growing Segmentation

UMF Unsharp Mask Filter

SVM Support Vector Machine

AI Artificial Intelligence

DL Deep Learning

ANN Artificial Neural Network

SIFT Scale Invariant Feature Transform

LBP Local Binary Pattern

CIA Cancer Imaging Archive

MPA Marine Predator Algorithm

HRCT High-Resolution Computed Tomography

MRI Magnetic Resonance Imaging

HoG Histogram of Oriented Gradients

GLCM Gray-level co-occurrence matrix

CNN Convolutional Neural Network

BF-SSA Best Fitness-based Squirrel Search Algorithm

ADC Adenocarcinoma

SCC Squamous Cell Carcinoma

SCLC Small Cell Lung Cancer

NSCLC Non-Small Cell Lung Cancer

MLPs Multi-Layer Perceptron's

RWICWM Region-Wise Intensity Correction and Weighted Mean

HE Histogram Equalization

RoI's Regions of Interest

WDSI-LSO Weighted Dice Similarity Index with Local Search Optimization

OL Outer Lesion

EL Enhanced Lesion or Early Lesion

SSCL Semi-Supervised Classification Learning Deep Neural Network

CNN Convolution Neural Network

#### CHAPTER 1 INTRODUCTION

#### 1.1. Introduction to Lung Cancer and Its Global Impact

Lung cancer is one of the most prevalent and deadly diseases globally. Compared to other cancers, it exhibits a higher rate of metastasis and is a leading cause of cancer-related deaths. In this study, we conducted a comprehensive review of the existing literature on the epidemiology, diagnosis, and treatment of lung cancer. The disease has become a significant global health concern, primarily caused by smoking, environmental pollution, and lifestyle factors. Among these, smoking remains the most prominent risk factor. Additional contributors include indoor air pollution and dietary habits. Furthermore, genetic mutations and inherited gene changes are also associated with lung cancer development. A major challenge is the delayed diagnosis, which often leads to a poor prognosis and a high mortality rate.

In recent years, advancements in anticancer drugs have improved the efficacy-to-toxicity ratio [22][48]. However, to further reduce lung cancer mortality, strong public health measures are required, especially those aimed at discouraging smoking. Moreover, many patients suffer due to incorrect medication dosage, often resulting from inaccurate diagnosis or poor interpretation of medical data. To address these issues, this work aims to enhance the accuracy of existing lung cancer detection algorithms [15][26]. It is well known that various diseases affect the human body, and some can be extremely harmful. If not detected early, such diseases can lead to severe consequences. Among them, cancer is one of the most life-threatening conditions.

The term "cancer" is derived from the Latin word crab, likely referring to the crab-like appearance of malignant tumors as they invade surrounding tissues. Cancer is also known by other terms such as malignancy, neoplasm, or malignant tumor. The various types of cancer are illustrated in Figure 1.1, such as brain cancer, kidney cancer, bladder cancer, and liver cancer. It can affect multiple organs, including the breast, prostate, colon, and lungs. On the left side of the image, four significant cancers are listed vertically. Brain Cancer is shown at the top, referencing abnormal cell growth in the brain, which can disrupt neurological functions. Lung Cancer follows, with an image depicting tumors within the lungs, a condition that is often linked to smoking or environmental exposure. Colorectal Cancer is next, representing malignancies in the colon or rectum, commonly influenced by diet, genetics, and lifestyle. At the bottom, Leukemia Cancer is displayed, indicating cancer of the blood or bone marrow, where abnormal white blood cell production occurs. On the right side, the image presents another four types of cancers: Kidney Cancer is placed at the top, referring to tumors forming in the renal tissues, which can affect the body's waste filtration system. Liver Cancer is shown below, often associated with chronic liver diseases and hepatitis infections.

Bladder Cancer follows, highlighting malignancy in the bladder lining, typically identified through symptoms like blood in the urine. At the bottom, Pancreatic Cancer affects digestive enzyme production and insulin regulation.

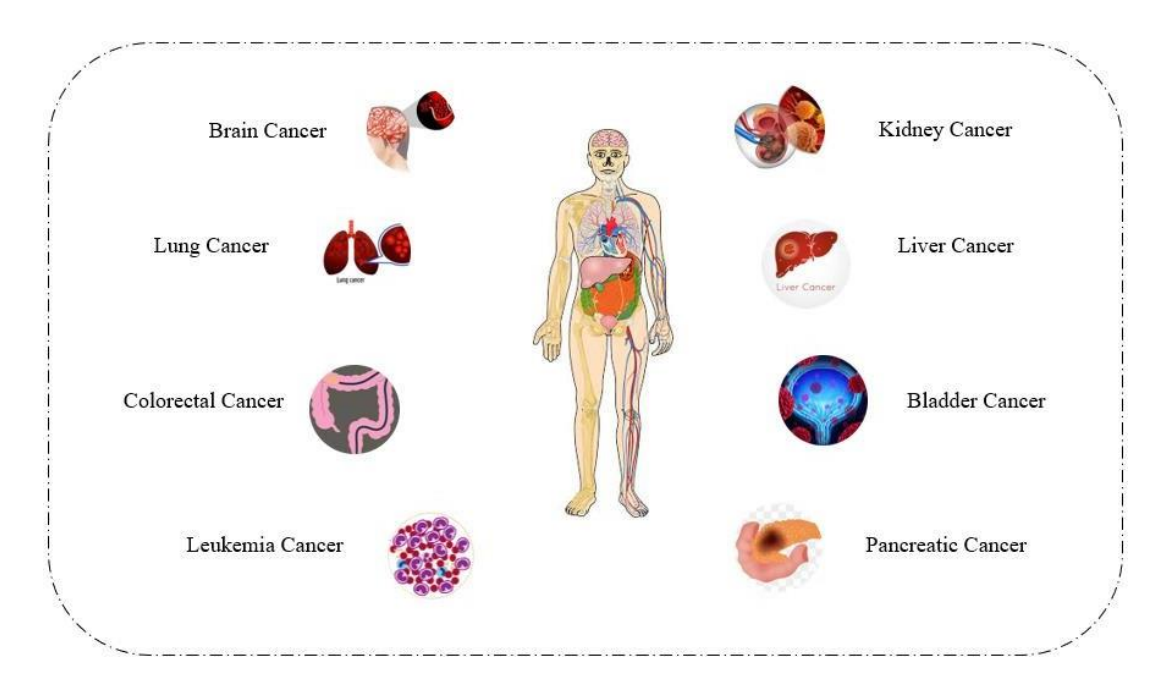


Figure 1.1 Types of Cancer in the Human Body

Among these, lung cancer is the most fatal, accounting for the highest number of cancer-related deaths worldwide. This thesis specifically focuses on the early detection of lung cancer using advanced deep learning techniques, due to its high mortality rate and diagnostic challenges.

## 1.2. The Fundamentals of Lung Cancer

A tumor forms when abnormal cells in the lungs grow uncontrollably and cluster together, as shown in Figure 1.2.

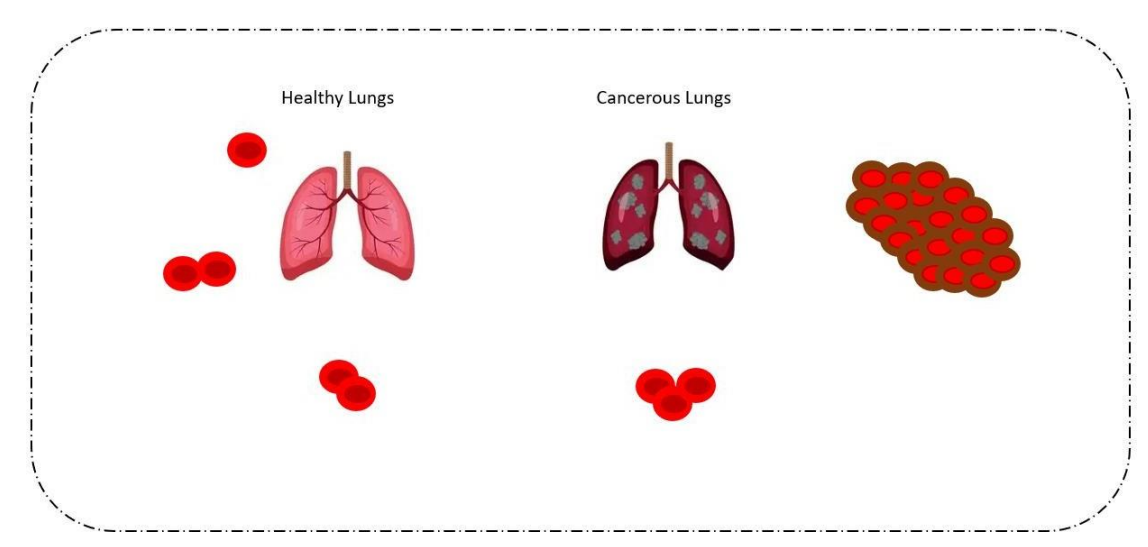


Figure 1.2 Growth of cancer cells in the human body

Source: <a href="https://www.lungcancers.eu/lung-tumor/lung-tumors/">https://www.lungcancers.eu/lung-tumor/lung-tumors/</a>

Figure 1.2 illustrates how cancer cells, unlike normal cells, multiply rapidly and damage healthy lung tissue. The body's organs can't function properly when cancer cells grow. Simply, lung cancer is the uncontrolled growth of abnormal cells in one or both lungs. These faulty cells cannot perform like healthy lung cells or perform the functions of regular lung cells. The abnormal cells have the potential to develop into tumors as they reproduce, which could harm the lungs. The lungs supply oxygen to the body. Lung cancer is a severe disease and is the most common cancerrelated cause of death. Today, a major health concern in all countries is tumours. Lung cancer is the most common disease and acts as a silent killer among both men and women. After receiving a diagnosis, more than half of patients with lung cancer pass away within a year. The two primary sorts of lung tumors are small cell lung cancer (SCLC) and non-small cell lung cancer (NSCLC). Carcinoid lung cancer is a third and less frequent kind of lung cancer. Often, small cell lung cancer is linked with cigarette smoking. Two distinct forms of small cell lung cancer exist: 1) Oat cell type, 2) Combined small cell carcinoma. In general, chemotherapy is used to treat small-cell lung cancer. Non-small cell Lung Cancer (NSCLC) is more prevalent as compared to other cancers, and about 80% of cases of lung cancer are caused by it. Compared to small cell lung cancer, this kind of cancer often develops and spreads to other areas of the body more slowly. Three distinct forms of non-small cell lung cancer exist: 1) Adenocarcinoma, 2) Squamous cell carcinoma, and 3) Large cell carcinoma.

## 1.3. Overview of Lung Imaging and Diagnostic Techniques

Lung imaging techniques are essential for diagnosing and monitoring lung diseases, including malignancies. These methods provide detailed views of the lungs and surrounding structures, enabling medical professionals to identify abnormalities, monitor disease progression, and develop effective treatment plans [22]. Common imaging techniques used for lung evaluation include below as shown in Figure 1.3:

- **a. Chest X-rays (CXR):** CXRs are often used as an initial screening tool for lung conditions. They provide a two-dimensional image of the chest, showing the lungs, heart, and ribs. CXRs can help detect masses, infections, lung malignancies, and other abnormalities [34].
- **b.** Magnetic Resonance Imaging (MRI): Although MRI is less commonly used for lung imaging due to motion artifacts from breathing [52], it is a valuable tool for accurately diagnosing certain lung cancers [32][94][83]. MRI is highly sensitive to soft tissue contrast and can offer additional information about vascular structures and tissue characteristics [22].
- **c. Positron Emission Tomography (PET) Scan:** PET scans visualize the body's metabolic activity using a radioactive tracer [57][72]. PET-CT scans, which combine PET and CT images, are commonly employed to detect and stage lung cancers. The tracer accumulates in

regions with high metabolic activity, such as malignant cells [91][53].

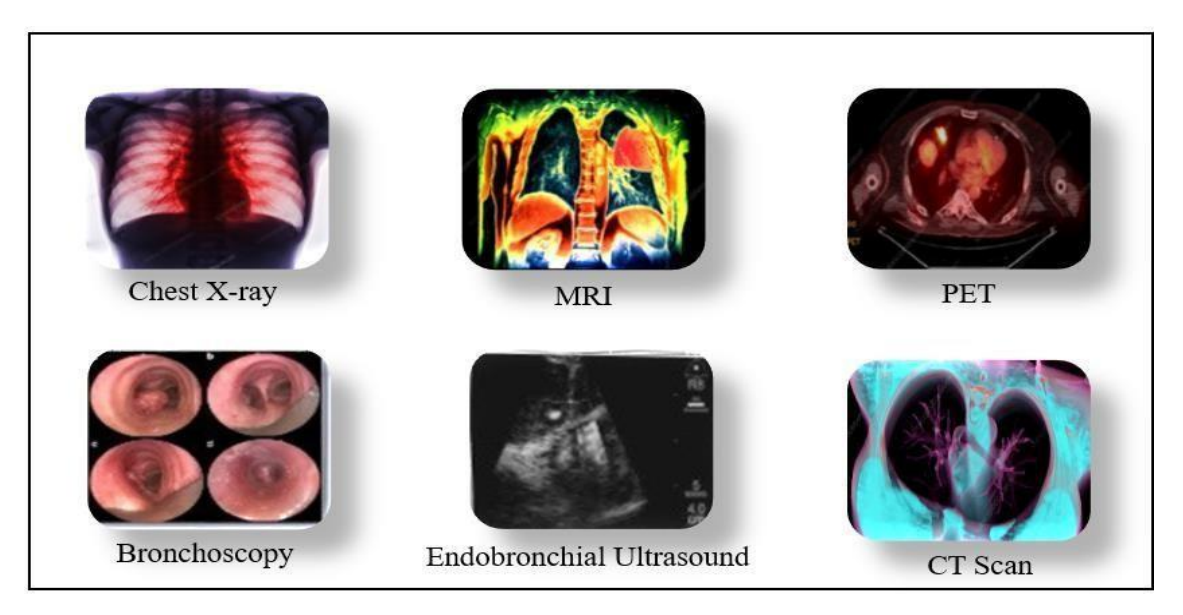


Figure 1.3 Diagnostic Imaging Tools for Lung Abnormalities

- **d. Bronchoscopy:** A thin, flexible tube is inserted through the mouth or nose into the airways during a bronchoscopy [3]. This procedure allows for clear imaging of the airways and assists in the staging and diagnosis of lung tumors. Biopsies can also be taken for pathological examination during the procedure [2].
- **e. Endobronchial Ultrasound** (**EBUS**): EBUS combines bronchoscopy and ultrasound to visualize and collect samples from lymph nodes and surrounding tissues [66]. It is frequently used to stage lung cancer and assess lymph node involvement [45].
- **f. VATS** (Video-Assisted Thoracoscopic Surgery): Also known as thoracoscopy, VATS involves making a few small incisions in the chest to insert a camera and surgical instruments. It is used to obtain tissue samples for biopsy and to diagnose or treat lung conditions [24].
- **g.** Computed Tomography (CT) Scans: CT scans provide detailed and high-resolution images of the lungs and surrounding tissues [4]. These scans play a crucial role in detecting and diagnosing lung malignancies. They help determine the presence, size, and exact location of tumors and assess whether cancer has spread to nearby lymph nodes or other tissues [14].

#### 1.4. General Steps of Lung Cancer

Traditional or general steps of lung cancer detection are shown in Figure 1.4.

#### **Step 1: Image Acquisition**

Basically, a database is a repository that can store data or images in an organized manner. Various databases are used in image processing. One such database is the Lung Image Database Consortium image collection (LIDC-IDRI), which contains 1,018 cases of annotated lesions on thoracic computed tomography (CT) scans used for diagnostic purposes and lung cancer

screening [4][77]. This dataset was developed through collaboration between academic institutions and eight medical imaging companies.

#### **Step 2: Grey Level Conversion**

As we know, the input image is captured in RGB format; therefore, color conversion and filtering are applied.

(i) Colour Conversion: The primary aim of using color conversion is to reduce the number of colors. By separating the R, G, and B components from each pixel's 24-bit color value, an 8-bit grayscale value at position (i, j) is obtained.

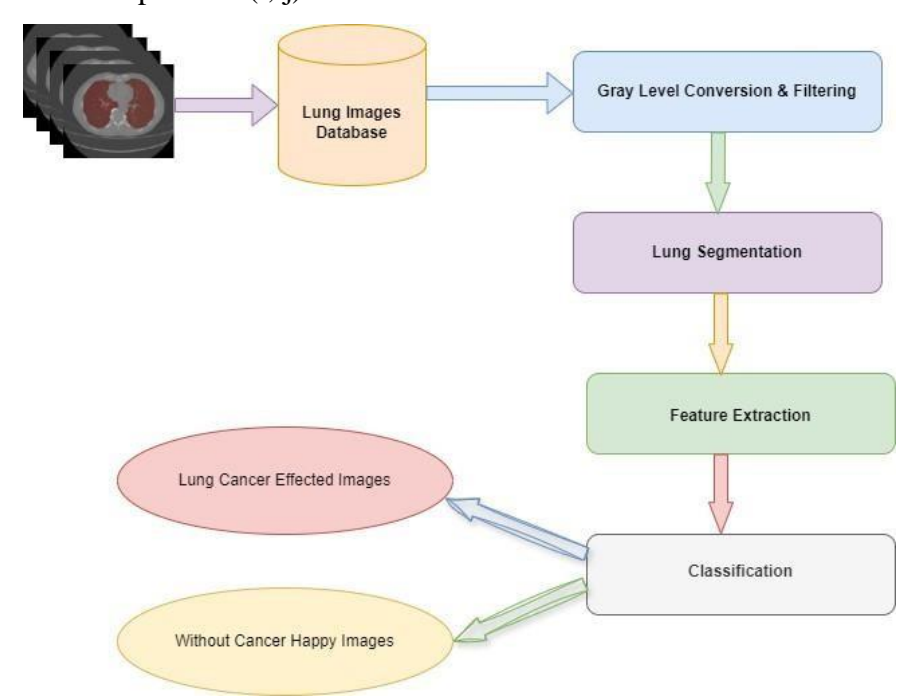


Figure 1.4 Basic steps of Lung Cancer Detection.

(ii) Colour Filtering: The main goal of filtering is to remove noise and distortion from the image. The noise may originate from the external environment or the camera during image capture [33]. Simply put, filtering eliminates all distortion and noise, resulting in a clearer image.

#### **Step 3: Lung Segmentation**

Lung segmentation is a vital step in analyzing lung CT images, as it helps isolate the lung area from other chest structures. This process ensures that subsequent tasks, such as feature extraction and disease classification, focus only on the relevant region.

To understand lung segmentation, it's important to first understand image segmentation. Image segmentation is a common technique in computer vision, where an image is divided into meaningful parts or regions. These regions often correspond to objects or boundaries within the image, such as edges or shapes [14]. Generally, there are two types of image segmentation:

**Local segmentation** targets specific portions of the image.

**Global segmentation**, which considers the entire image for identifying significant patterns or regions.

Segmentation helps in accurately identifying the lungs from CT scans by separating them from nearby organs and tissues. This improves the efficiency and precision of automated detection systems used in medical imaging [34].

#### **Step 4: Feature Extraction**

One type of complexity reduction in image processing is feature extraction. Finding the most relevant details in the original data and representing them in a smaller dimensionality space is the primary objective of feature extraction [44].

# **Step 5: Classification**

Image classification is one of the most crucial components of digital image analysis. The task of collecting information classes from a multiband raster is known as image classification, and it is quite pleasant to have a "pretty picture" or image that illustrates different features across the spectrum of colors. The core area of medical image analysis is picture categorization, where deep neural networks are crucial [15][86]. The process of image classification begins with the input images and ends with an output classification that indicates the presence or absence of the disease. Supervised and Unsupervised classification are the two primary classification techniques [8].

# 1.5. Significance and Urgency of Early Lung Cancer Detection

Pollution is increasing day by day, and due to the competitive world, work schedules have become hectic across all sectors. As a result, people are unable to focus on their health, leading to a rise in health problems, particularly lung cancer. Consequently, many scientists and researchers are actively working in this area. Another reason for this growing interest is the increasing market demand for lung cancer detection modules. The use of automated lung cancer detection provides immediate assistance to patients. With the rapidly increasing number of nuclear families, lung cancer detection has become a critical area of research.

#### 1.6. Motivation and Research Objective

Lung cancer is one of the major causes of cancer-related deaths worldwide, primarily due to its late identification and the lack of accurate premature stage screening techniques. Existing lung cancer detection systems usually rely only on limited information, such as smoking history, which reduces their effectiveness and accuracy. Furthermore, many of these models are inaccurate and fail to consider individual risk factors. This study is motivated by the need to overcome these challenges by creating a more advanced and accurate method for predicting early lung cancer risk. The main goal is to develop a deep learning-based framework that combines

medical scans with various aspects of patient data, such as environmental exposure, genetic traits, and lifestyle factors, to provide a more accurate and personalized evaluation. P-ResNet, the proposed method, enhances premature-stage lung cancer diagnosis using a hybrid approach. Unlike traditional models, this framework is designed to incorporate individual risk factors and support more accurate identification. In recent years, deep learning models such as Convolutional Neural Networks (CNNs), ResNet, and VGG16 have been widely used for lung cancer detection. However, each of these models has limitations. CNNs tend to be less accurate for complex tasks like premature-stage lung cancer detection and are difficult to train when they have many layers. ResNet may suffer from the "dying ReLU" problem (inactive neurons), while VGG16 has a large number of parameters, making it slow and computationally expensive. To address these challenges and improve early detection, this research introduces a novel model called TL-based P-ReLUResNet, which integrates multiple types of features to provide a more accurate assessment of lung cancer risk. To evaluate the effectiveness of the proposed framework, publicly available CT scan datasets were used, and standard performance metrics, including accuracy, precision, and recall, were applied. This study uses 2D axial CT image slices extracted from full 3D CT scans. These 2D slices are widely used due to their efficiency in training deep learning models. More details about the datasets and methods used can be found in the subsequent chapters of this thesis.

#### 1.7. Research Contributions

This thesis presents several significant advancements in the field of premature-stage lung cancer diagnosis using deep learning techniques. A Lightweight Advanced Deep Neural Network (DNN) model was developed using RWICWM filtering, K-means clustering, and WDSI-LSO. This integration enabled accurate lung nodule diagnosis and risk assessment while keeping computational costs low. A Transfer Learning-based P-ResNet system was also developed to effectively screen for lung cancer risk. The study introduced novel preprocessing approaches, such as Inverse Log Transformation and Convex Hull-based augmentation, which resulted in improved image quality and segmentation accuracy. A comparison between the proposed and existing models was conducted using evaluation metrics such as SSIM, PSNR, recall, and precision. The findings validated the enhanced reliability and robustness of the proposed techniques. To improve model performance, optimization techniques such as Iterative Adaptive Decision Fusion (I-ADF) and Binomial Chi-Square-based feature selection were employed, resulting in higher prediction accuracy and lower error rates.

#### CHAPTER 2 LITERATURE SURVEY

#### 2.1. Overview of Existing Research on Lung Cancer

The scientific term for cancer is *carcinoma*, which refers to the uncontrolled multiplication of abnormal cells. In such cases, cancerous cells proliferate rapidly and accumulate, ultimately damaging the affected organ, whether it is the lungs or another part of the body, thus resulting in what is known as carcinoma. When this instability in cell growth occurs in the lungs, this condition is specifically referred to as lung cancer [5].

Unlike normal cells, cancerous cells grow without regulation or control. These abnormal cells destroy the surrounding healthy lung tissue and disrupt normal lung function. As they continue to grow, they interfere with the function of vital internal organs. In summary, lung cancer is characterized by the abnormal and irregular growth of cells in one or both lungs [7]. These abnormal cells fail to develop into functional lung tissue and cannot perform the functions of healthy lung cells [90]. When left unchecked, their proliferation can lead to the formation of a tumor and further impair lung function.

Lung cancer is considered a life-threatening disease because the respiratory system relies entirely on the lungs. The oxygen inhaled through the nose travels directly to the lungs, where it is filtered and then circulated throughout the body via the bloodstream. Given the lungs' crucial role in sustaining life, any disease that affects them poses a serious threat to survival. As such, lung cancer is recognized as a global health concern and is often referred to as a "silent killer" [10]. Studies indicate that over half of all lung cancer patients die within the first year of diagnosis.

There are two primary types of lung cancer: small cell lung cancer (SCLC) and non-small cell lung cancer (NSCLC) [82][44]. SCLC is further classified into two subtypes: small cell carcinoma and mixed or large cell carcinoma [1]. Research has identified tobacco use as the leading cause of small-cell lung cancer. In contrast, NSCLC is more frequently observed in patients with this chronic illness [78]. Together, SCLC and NSCLC account for approximately 80% of lung cancer cases worldwide. Essential Techniques for Lung Cancer Diagnosis.

**General Steps:** Diagnosing the disease is the first and most crucial step before beginning any form of treatment. In simple terms, the entire approach to lung cancer revolves around early detection, as proper treatment cannot be administered without it. This section aims to guide you through the step-by-step process of diagnosing lung cancer.

Figure 2.1 illustrates the general procedures for identifying lung cancer. It presents all five steps in a logical sequence [92]. The first step involves the use of a dataset or database. A brief explanation of each stage is provided below.

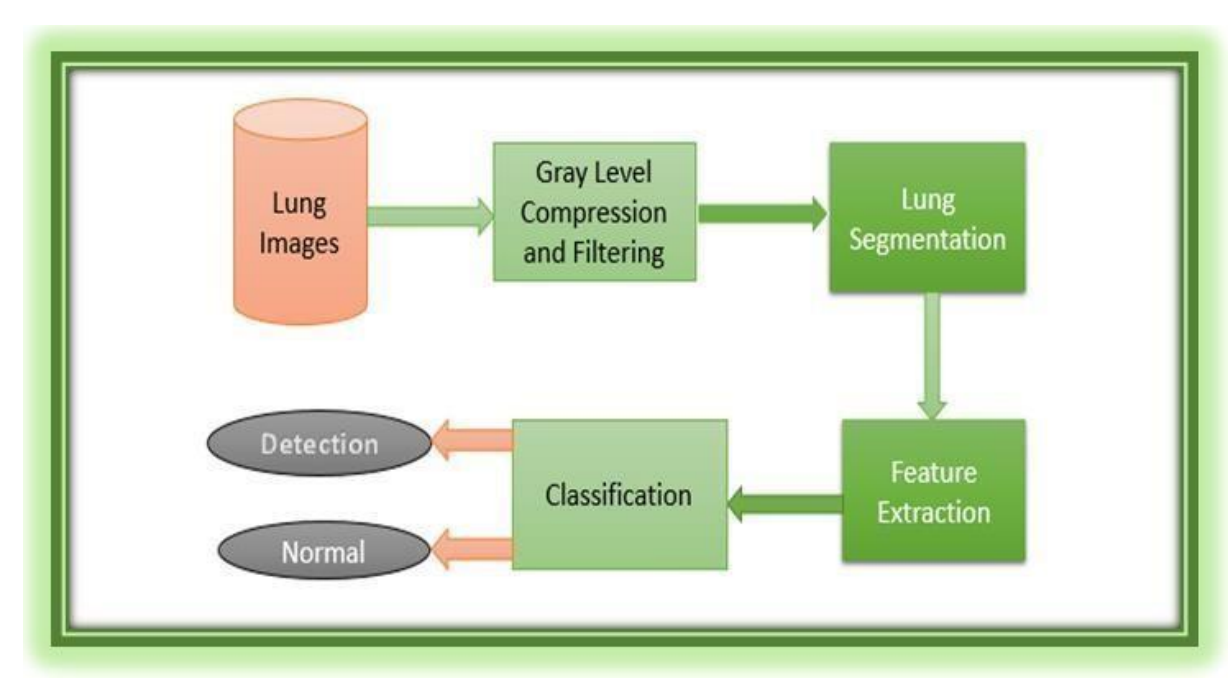


Figure 2.1 Basic Steps of Lung Cancer Detection

In basic terms, a database is a structured pool used to store and organize data or visual content. Various types of databases are used in image processing applications [62][58]. One such example is the Lung Image Database Consortium (LIDC), which includes an array of pulmonary computed tomography (CT) scans used for diagnosing affected lung regions. This dataset was created through collaboration among eight medical institutions and academic centers, involving 1,018 cases to build a comprehensive set of diagnostic images [79]. Since the digital images in this database are captured using the RGB (Red, Green, Blue) color model, color conversion and filtering techniques are applied during preprocessing.

Color Conversion: The main objective of color conversion is to reduce the number of colors in an image while preserving essential visual details. Each 24-bit pixel (I, J) in the image consists of three 8-bit channels: R (Red), G (Green), and B (Blue). These are converted into an 8-bit grayscale value to simplify further processing.

Color Filtering: The purpose of filtering is to eliminate noise and distortion that may arise during image acquisition, either due to camera limitations or external environmental factors [39]. This step helps maintain image clarity by removing any interference or visual anomalies. Before discussing lung segmentation, it is important to understand the concept of image segmentation. Image segmentation is a digital technique that divides an image into multiple meaningful segments to simplify analysis. This includes the identification of points, lines, curves, and boundaries within the image, a process sometimes referred to as image vivisection or segmentation. Image segmentation is generally categorized into two types: local segmentation and global segmentation [44].

- Local segmentation focuses on a specific region of the image.
- Global segmentation considers the entire image for analysis.

One of the most critical steps in radiological lung image analysis is lung segmentation [51]. It involves a computer-based method for isolating lung boundaries from surrounding tissues, such as the trachea, in CT images. This is crucial for further image analysis and diagnosis. Next, feature extraction plays a vital role in image processing. It refers to techniques used to eliminate redundant or irrelevant data from the dataset [79]. The main objective is to extract the most significant and useful information from the original image for analysis.

Finally, the most essential component of digital image processing is image classification, particularly in the context of neural networks used in medical applications. In simple terms, image classification involves extracting relevant and targeted data from image matrices to recognize patterns or disease-specific features [30].

# 2.2. Review of Deep Learning Approaches for Lung Nodule Detection

Joshua, one of the researchers, proposed a 3D CNN-based unsupervised learning model for the diagnosis of lung cancer. A gradient activation function was employed in this binary classification strategy to enhance the visualization of lung tumors. Using the LUNA dataset [81], the proposed AlexNet detection model was evaluated against a well-known 2D CNN learning classifier [37]. However, the model performed poorly due to insufficient testing data, as only 10% of the training dataset was utilized [41].

To assist in the premature-stage detection of squamous cell carcinoma (SCC) and adenocarcinoma (ADC), Chaunzwa et al. developed a supervised CNN-based prediction model. This CNN was validated using real-time non-small cell lung cancer (NSCLC) patient data collected at Massachusetts General Hospital during the premature-stage of the disease [16]. The dataset consisted of 311 collected patient records. The CNN model, built upon the VGG network, achieved an area under the curve (AUC) of 71%, which was considered inadequate. One limitation of the VGG-based CNN was its lack of preprocessing, such as noise removal and CT image segmentation, which could have improved its prediction accuracy [12][50].

Chaturvedi et al. reviewed the latest techniques for lung cancer detection and classification. Their study covered modern methods for lung nodule diagnosis, localization, and classification using standard datasets such as LIDC-IDRI, LUNA16, and the Super Bowl Dataset 2019. They also discussed supervised learning methods, including SVM, KNN, and CNN [68]. According to the authors in [9], these datasets represent the most commonly used CT data thresholds for disease diagnosis. Kalaivani et al. introduced a DenseNet-based binary classification model using a deep

convolutional neural network to distinguish between aggressive and benign lung cancer cases [17].

Following a review of these studies, presented in tabular form in ANNEXURE 2, this research aims to develop an automated method for early disease detection and patient health status assessment. The following section provides a brief overview of various optimization strategies employed in deep learning to identify cancerous nodules at a premature-stage.

A work that utilized wavelet feature descriptors in conjunction with an artificial neural network for classification was presented. The computed mathematical properties, such as autocorrelation, entropy, contrast, and energy, are generated when the wavelet transform is applied and then used as input parameters for the neural network classifier [43]. However, this method uses ANN for classification, and it has a slow learning progression; hence, computation time is high.

The Cancer Imaging Archive (TCIA) database provides an analysis of the Lung Image Database Consortium image collection (LIDC-IDRI) [66] using the SVM-LASSO model. Using the two CT radiomic properties of the anteroposterior dimension of the bounding box and the directional change of local homogeneity, it was possible to predict the malignancy. Nonetheless, there were no radiomic characteristics that distinguished spiculated or lobulated borders in particular [24]. A study was presented in which Wavelet feature descriptors were used in conjunction with an artificial neural network (ANN) for classification. The wavelet transform was applied to extract mathematical properties such as autocorrelation, entropy, contrast, and energy. These computed features were then used as input parameters for the neural network classifier [28]. However, the method's reliance on ANN led to a slow learning process, resulting in high computational time. The Cancer Imaging Archive (TCIA) database includes an analysis of the Lung Image Database Consortium image collection (LIDC-IDRI) [66] using an SVM-LASSO model. By employing two CT radiomic features, the anteroposterior dimension of the bounding box and the directional change of local homogeneity, it was possible to predict malignancy. However, no specific radiomic features were identified that could reliably distinguish spiculated or lobulated tumor borders.

The Regression Neural Network (RNN) segmentation technique was proposed in [74][51], offering high accuracy in identifying nearby lesions of similar intensity. Due to the presence of adjacent vascular and pleural lesions, this method provided improved boundary identification during segmentation. RNN, as a learning algorithm, addresses challenges in automatic lesion detection. However, the model primarily focused on the segmentation accuracy of lung parenchyma and the precise identification of boundaries for juxtapleural and juxtavascular lesions [78]. A two-pronged approach to lung segmentation was presented in [61]. The first

component employed thresholding and morphological techniques, while the second addressed nodule-type classification using a naïve approach. This study explored the segmentation problem in the context of limited ground-truth data related to nodule types [43]. However, the classification approach was flawed, as it incorrectly categorized nodules attached to the pleural surface or vascular structures as fat nodules [36].

Another study demonstrated feature extraction from computed tomography (CT) images using artificial intelligence algorithms to analyze benign and malignant pulmonary nodules. CT images of pulmonary nodules were collected and processed using an Expectation Maximization (EM)-based lung nodule feature extraction model [54]. Nonetheless, detecting these nodules in the premature-stage remains challenging, as the associated symptoms often lack classical specificity, and most patients do not present with clear clinical signs during the initial phase.

Lung carcinoma is one of the most prevalent and widespread types of cancer [5], with a mortality rate higher than that of other common cancers, such as prostate, breast, and colon cancer [4]. Lung carcinoma is classified into two main types: small-cell lung carcinoma (SCLC) and non-small-cell lung carcinoma (NSCLC). Both are primarily caused by smoking; however, a harsh reality is that even individuals who have never smoked can develop this deadly disease.

This may be attributed to several factors, including prolonged exposure to air pollution, smoke, contaminated water, and, in some cases, hazardous gases, all of which have been reported as potential causes of lung cancer. Accurate identification of the premature-stage NSCLC is essential [74][24]; however, there is currently no exact method available [2]. Early diagnosis significantly reduces the lung cancer mortality rate [16], saving countless lives.

A variety of modern techniques are now available for the diagnosis and treatment of lung cancer [29]. With the advancement of medical imaging technology, tools such as lung biopsy, Positron Emission Tomography (PET) [58], High-Resolution Computed Tomography (HRCT), Computed Tomography (CT) scans, and X-rays have greatly improved the detection of malignant nodules in one or both lungs [53][68].

The rise in early detection rates can also be attributed to CT imaging, which radiologists and oncologists now routinely use [27]. CT scans help assess various parameters, including the size, location, and type of lung lesions [19][93]. However, there is still a pressing need for progress in the medical field, particularly in the early identification and screening of lung malignancy [43]. Enhancing early screening practices can help minimize risk factors [36] and improve survival outcomes for patients.

Accurate segmentation of tumors and surrounding organs is also critical. Inaccurate segmentation may lead to either under- or over-irradiation of healthy tissue and tumors [65]. Image

segmentation reduces image complexity by dividing the image into smaller, manageable regions [33]. Previously, segmentation was done manually, often resulting in unreliable and inconsistent outcomes [88]. In contrast, automatic segmentation techniques such as region-growing or multiseed approaches have improved the reproducibility of results and enhanced the quality of radiomic features [94].

Additionally, a risk prediction model has been developed in China to identify individuals at the highest risk for lung cancer during CT screening. This model demonstrated good bias control and accuracy and was built using easily obtainable clinical classifiers suitable for large-scale screening scenarios. However, it relied entirely on self-reported data, making it susceptible to measurement errors [32].

Several machine learning techniques have been proposed to develop efficient models for identifying individuals at high risk of developing lung carcinoma, enabling early intervention to prevent long-term consequences. The results indicated that the model demonstrated improved performance in detecting lung cancer. However, due to privacy concerns, accessing critical medical data remains a significant challenge [56].

In another study, a deep learning (DL) classification system for lung cancer was developed using CT scans. A dataset of 311 patients with premature-stage lung carcinoma was used to train and validate convolutional neural networks (CNNs) [50][90][34], focusing on the two most common histological subtypes: squamous cell carcinoma (SCC) and adenocarcinoma (ADC). The results showed that the model was effective in classifying lung cancer and could serve as a supportive tool for radiologists. However, its performance was limited due to the small sample size.

Lung cancer prediction was also explored using a machine learning approach combined with enhanced image processing, as presented in [54]. An improved deep neural network (DNN) was used to segment affected regions of noise-reduced lung CT images, extracting various features from the segmented areas [27]. This model showed better classification performance, though its overall accuracy remained suboptimal [55].

Another approach recommended the use of enhanced dense clustering with deep learning in a directly trained neural network for lung cancer detection from CT images [21]. The technique segmented the affected regions by calculating pixel similarity values. Based on these similarities, regions were grouped, and features relevant to spectral analysis were extracted. Classification techniques were then applied to learn and categorize these features [57]. The results demonstrated accurate lung cancer predictions; however, this method did not incorporate risk assessment.

In [9], deep CNN models were proposed for classifying lung cancer from CT scans [30][49], each utilizing a distinct network architecture. Combining predictions from multiple CNNs using

ensemble learning [38] led to improved classification performance. However, the ensemble method also resulted in high computational costs.

A classification and prediction system for lung cancer was also developed using machine learning and image processing techniques [81][80]. This method involved preprocessing CT images with a geometric mean filter, which enhanced image quality and improved the performance of artificial neural networks in predicting lung cancer. Despite these improvements, the model showed an increased likelihood of prediction errors [71].

The authors of [84] revisited the problem of lung cancer segmentation in CT images [54]. Their method integrated data from adjacent CT slices and combined the discrete wavelet transform (DWT) with deep supervision in the model architecture to enhance textural analysis. However, due to the unpredictable nature of cancer, the model was only partially successful in its predictions. Using extracted features from the Gray-Level Co-Occurrence Matrix (GLCM) [37], along with reliable machine learning (ML) and image enhancement techniques [47], a lung cancer prediction system was developed. The procedure involved extracting GLCM features from enhanced images [62] and applying optimized ML classification algorithms [44]. The results indicated that the model could be highly effective in improving lung cancer prognosis, aiding further diagnosis, and potentially reducing the mortality rate through expert radiologist support. However, the model's performance was limited by the small size of the dataset used [61].

#### 2.3. Techniques for Enhancing and Analyzing Lung Cancer Images

Image preprocessing primarily aims to enhance and improve image quality by reducing noise and removing unwanted distortions. In simple terms, it serves as a data-mining strategy that not only addresses missing data but also transforms raw image data into meaningful and usable information [64]. Today, a variety of preprocessing techniques and tools, such as OpenCV, CUDA, and Keras, are commonly used to enhance image quality.

Image segmentation, in simple terms, involves dividing an image into meaningful regions or segments. This is particularly useful when analyzing complex images, as segmentation helps isolate and understand distinct objects within the image. The goal of segmentation is to accurately detect the edges and boundaries of these objects [24]. Several segmentation techniques exist, including clustering-based, edge-based, region-based, and watershed-based methods [19]. In essence, segmentation enhances the visual representation of the image for more effective analysis [28].

With segmentation, adjacent pixels are analyzed for similarity, and those with similar characteristics are grouped into the same region [26]. Once segmentation is completed, the next critical step is feature extraction, which highlights the most significant attributes of the detected

object. Feature extraction plays a vital role in many applications, such as pattern recognition used in Android mobile security and spam detection software [20].

In the context of medical imaging, feature extraction helps isolate the shape and region of interest (ROI) within an image, allowing for detailed analysis and accurate diagnosis. It relies on a combination of methodologies and algorithms to assess various characteristics of the segmented image, such as eccentricity, perimeter, area, and average pixel intensity [22]. These features are then used to determine whether the image content is normal or abnormal, supporting effective clinical decision-making.

## 2.4. Datasets Available for Implementation

Selecting an appropriate dataset is crucial when developing lung cancer detection systems, as it ensures effective training, analysis, and validation of the models. Below Table 2.1 shows a list of commonly used publicly available datasets that are widely utilized for designing and validating algorithms in lung cancer detection.

Table 2.1 Summary of Widely Used Public Datasets for Lung Cancer Detection

<b>Dataset Name</b>	Modality	Description	Application
LIDC-IDRI (Lung	CT scans	Contains annotated chest CT	Widely used for training and
Image Database		images with lung nodules	benchmarking lung nodule
Consortium Image		marked by multiple radiologists.	detection algorithms.
Database Resource			
Initiative)			
TCIA (The Cancer	CT, PET,	Provides multiple datasets	Useful for multi-modal lung
Imaging Archive)	MRI	related to lung cancer imaging	cancer diagnosis and deep
		from different modalities.	learning training.
JSRT (Japanese	Chest X-	Offers X-ray images labeled with	Used for evaluating X-ray-
Society of	rays	the presence or absence of lung	based detection methods.
Radiological		nodules.	
Technology)			
Deep Lesion Dataset	CT scans	Includes a large collection of CT	Suitable for evaluating
-		images with various lesion	nodule/lesion detection and
		annotations.	classification algorithms.

LIDC-IDRI and Deep Lesion datasets offer CT scans with annotated nodules or lesions, ideal for training and testing detection models. TCIA provides multi-modal data, including CT, PET, and MRI, supporting advanced diagnostic approaches. Meanwhile, the JSRT dataset includes labeled chest X-rays, useful for assessing 2D image-based detection techniques. Together, these datasets play a crucial role in developing and benchmarking deep learning models for lung cancer diagnosis.

#### 2.5. Summary

Reducing mortality rates and improving patient outcomes largely depends on the early detection of lung cancer. One promising area of artificial intelligence (AI) that enhances the accuracy and

efficiency of premature-stage lung cancer diagnosis is deep learning. Researchers have developed sophisticated algorithms, particularly convolutional neural networks (CNNs) and other deep learning architectures, that can analyze medical imaging data, such as CT scans and chest X-rays, to identify suspicious lung nodules indicative of cancer.

Trained on large collections of labelled medical images, these deep learning models have demonstrated remarkable sensitivity and specificity in detecting lung nodules. By automatically extracting features from imaging data, the algorithms are capable of identifying subtle patterns that may be overlooked by human radiologists but are associated with premature-stage lung cancer.

Moreover, deep learning systems can support radiologists by aiding in complex cases and offering a second opinion. This assistance can help reduce diagnostic errors and improve overall workflow efficiency in the medical field.

# CHAPTER 3 HYPOTHESIS AND OBJECTIVES

#### 3.1. Identified Research Gaps

- i. Detecting lung carcinoma largely depends on identifying abnormalities in the bronchioles and ribs. However, predicting such abnormalities at a premature stage is challenging due to their rapid and irregular changes.
- ii. Captured CT images often contain inconsistencies and low-resolution pixels, leading to various types of noise, such as Gaussian and Poisson noise, which significantly reduce the accuracy of the classification process [77].
- iii. Manual analysis of earlier medical imaging data is difficult, and segmentation results heavily depend on convergence time and accuracy. Therefore, there is a need to develop new and more precise techniques for lung image segmentation [56].
- iv. Existing preprocessing methods for lung CT images often result in poor illumination correction and insufficient edge enhancement, primarily due to sequential and outdated processing techniques. Although risk screening helps identify premature-stage lung cancer more frequently, it may delay necessary diagnosis if performed too early. Hence, risk screening should ideally be conducted after the classification stage for more reliable results.
- v. While common segmentation techniques can extract regions of interest (ROIs) from lung images, the resulting features often exhibit high similarity to neighboring classes and suffer from low confidence during the detection phase.

#### 3.2. Research Objectives

The primary objective of this work is to recognize lung carcinoma at a premature-stage. The other key objectives are as follows:

- To detect lung carcinoma using a P-ReLU activated transfer learning-based ResNet model, referred to as TL-based P-ReLUResNet (P-ResNet).
- ii. To remove noise from CT images using the Intra-class Variance–Anisotropic Diffusion Filter (I-ADF).
- iii. To perform lung segmentation through a Region Growing Segmentation (RGS) method integrated with the Bates Distributed Coati Optimization Algorithm (B-RGS), incorporating knuckle point partitioning.
- iv. To enhance edge clarity using the Unsharp Mask Filter (UMF).
- v. To improve model accuracy by selecting optimal features using the Binomial Distributed Chi-Square Test (BD-CST).

#### 3.3. Proposed Framework

Lung cancer is the most prevalent type of cancer worldwide. Due to its high mortality rate, researchers have been motivated to conduct extensive studies focused on its early detection and diagnosis [6]. When lung cancer is identified at a premature stage, the survival rate can increase significantly, by approximately 70–80%.

To facilitate early prediction, a novel deep learning-based framework has been proposed. This system comprises the following key stages: preprocessing, lung partition segmentation, feature extraction, feature selection, classification, and carcinoma-based risk screening, as you can see in Figure 3.1.

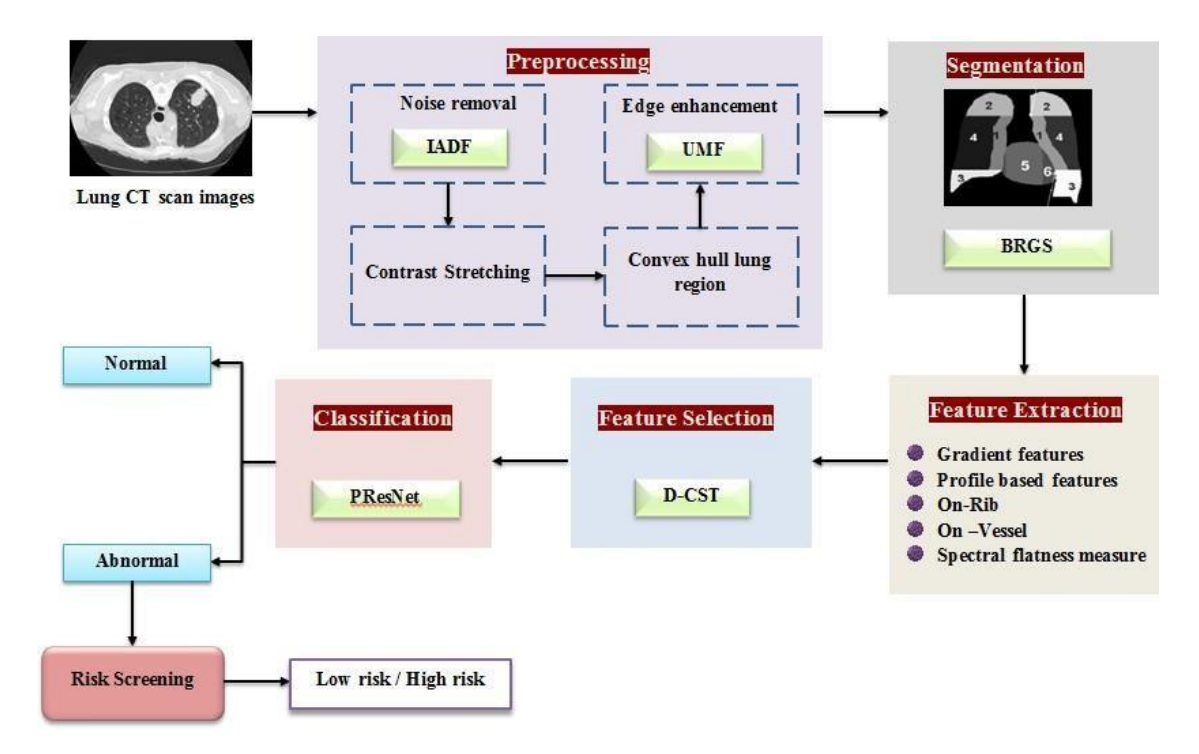


Figure 3.1 Proposed Framework for Premature Stage Lung Cancer Detection

For risk screening purposes, the sensitivity of abnormal CT images was individually assessed to calculate the packet index of each image. This packet index helped identify individuals at high risk, particularly those diagnosed with Large Cell Carcinoma and Squamous Cell Carcinoma, while others were classified as low risk. Based on this screening, patients were categorized accordingly, and the results are presented in the subsequent section.

#### 3.4. Summary

Lung cancer, a common malignant tumor, primarily originates from abnormalities in the bronchial mucosa. As a result, individuals diagnosed with lung cancer often experience symptoms such as chest pain, coughing, dysphonia, and general discomfort in the throat and lungs. These symptoms may be further complicated by conditions such as malignant pleural effusion and pulmonary inflammation. Therefore, early prediction of lung cancer is critical for assessing individual risk and improving patient outcomes.

Globally, lung cancer remains the leading cause of cancer-related mortality. Approximately 85% of lung cancer cases are attributed to cigarette smoking. Common symptoms include persistent cough, chest discomfort, weight loss, and, less commonly, haemoptysis (coughing up blood). However, many patients present with metastatic disease, often without any clear clinical symptoms.

Diagnosis typically involves imaging techniques such as chest X-rays or computed tomography (CT) scans, followed by confirmation through biopsy. Treatment options depend on the stage of the disease and may include surgery, chemotherapy, radiation therapy, or a combination of these approaches. Historically, the prognosis for lung cancer has been poor, with a five-year survival rate of only about 15%.

To address this challenge and improve both prognosis and early classification of carcinoma subtypes, this study proposes a novel deep learning-based model for the accurate and early detection of lung cancer.

# CHAPTER 4 PROPOSED SEGMENTATION AND CLASSIFICATION

# 4.1. Deep Learning-Based Framework for Lung Nodule Detection

Convolutional Neural Networks (CNNs) have recently demonstrated remarkable automation capabilities in the medical field. They are widely used in deep learning applications for cancer diagnosis. Compared to other classification techniques, CNNs process input images directly, requiring minimal preprocessing [49], and they can efficiently learn parameters with sufficient training. These networks are designed to process visual data in a way that resembles the functioning of neurons in the human brain. A graphical representation of the research process is shown in Figure 4.1.

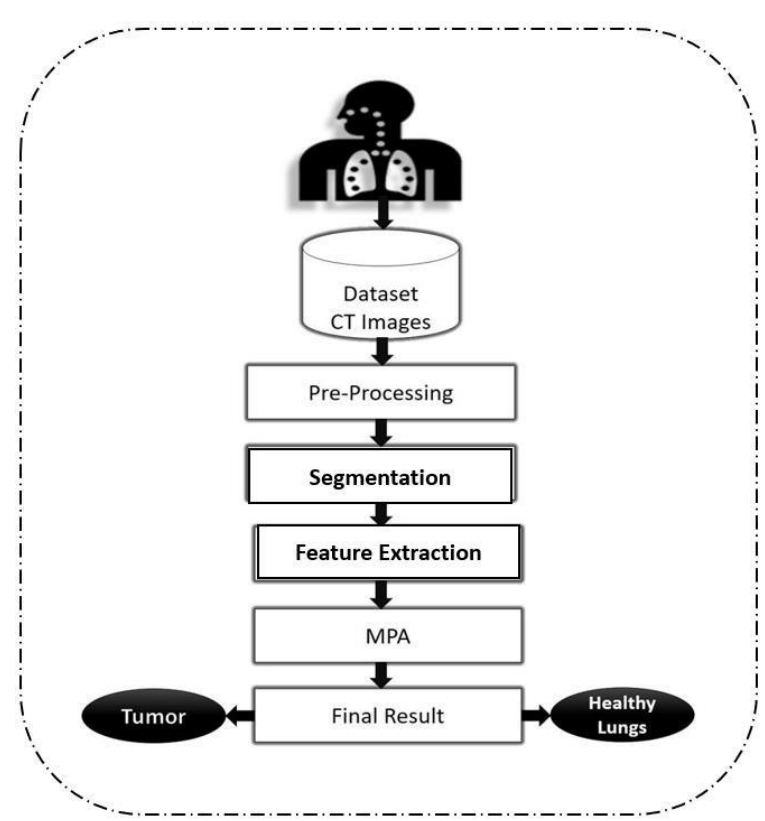


Figure 4.1 Workflow of the Proposed Lung Nodule Detection Framework Using CNN and MPA **4.1.1. Pre-processing stage** 

The pre-processing stage plays a crucial role in enhancing the quality of lung CT scan images before feeding them into the classification model. The primary objective is to eliminate unwanted distortions and enhance key features for accurate detection. The key preprocessing steps applied in this study are shown in Figure 4.2:

1. Noise Removal: A median filter is applied to eliminate salt-and-pepper noise from CT images.

This filter smooths the image by replacing each pixel value with the median of neighboring pixel intensities, effectively preserving edges while reducing noise.

- Expected Output: A cleaner image with reduced background interference.
- 2. Contrast Enhancement: Techniques such as histogram equalization are employed to improve the contrast of CT images, making the nodules more distinguishable from surrounding tissues.
- 3. Expected Output: Enhanced visibility of nodular regions and clearer lung boundaries.
- 4. Unsharp Masking: This step sharpens the image by enhancing the edge details, allowing better boundary detection of suspected lesions.
- 5. Expected Output: Sharper and more defined anatomical structures.
- 6. Watershed Segmentation: Used to separate overlapping structures or nodules in the image by treating the grayscale image as a topographic surface.
- 7. Expected Output: Segmented image with distinct lung nodule boundaries.

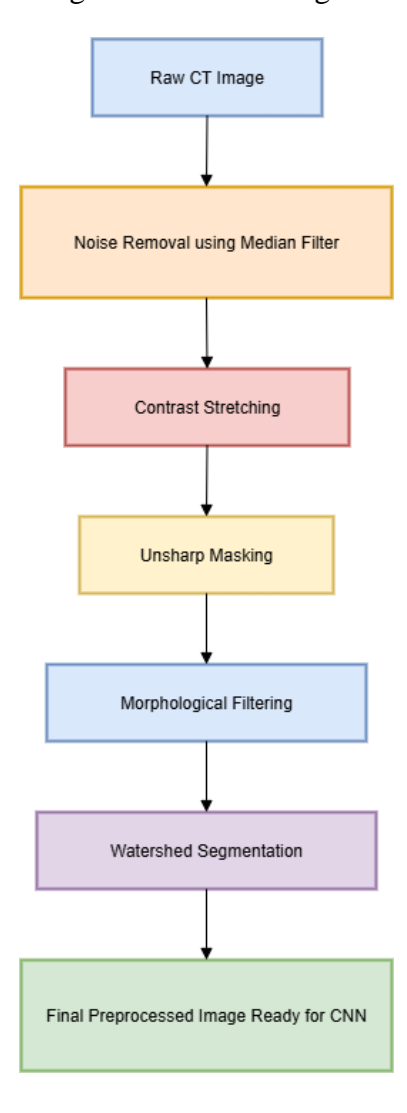


Figure 4.2 Step-by-Step Preprocessing Workflow for CT Lung Images

These processed images are then input into a CNN model specifically designed and trained for accurate classification. The effectiveness of these preprocessing steps directly contributes to reducing noise, enhancing features, and improving the overall detection performance of the system, as shown in Figure 4.3.

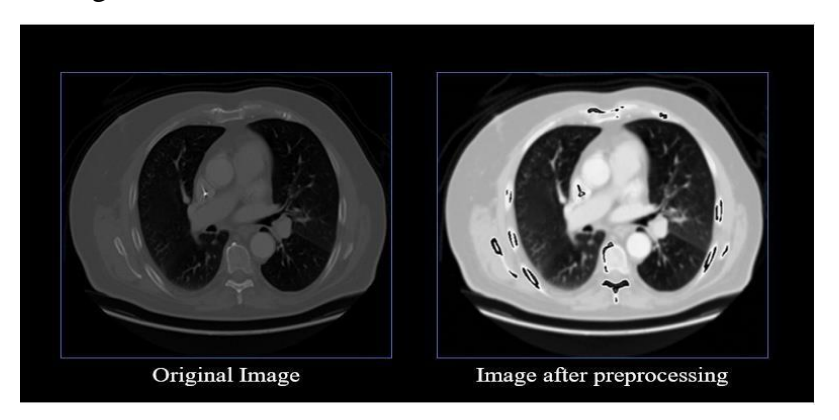


Figure 4.3 Image Left and Right without and with pre-processing

The intrinsic ability of the median filter to moderate intensity levels makes it possible to remove these artifacts without sacrificing image quality. It also effectively preserves image borders while reducing brightness fluctuations. Moreover, it efficiently removes "salt-and-pepper" noise, which is caused by abrupt and severe disruptions [19].

#### 4.1.2 Segmentation of Lung Nodules

The primary aim of lung nodule dissection is to isolate individual lesions from the respiratory system, which is a crucial step in assessing nodule size and distinguishing non-cancerous lesions.

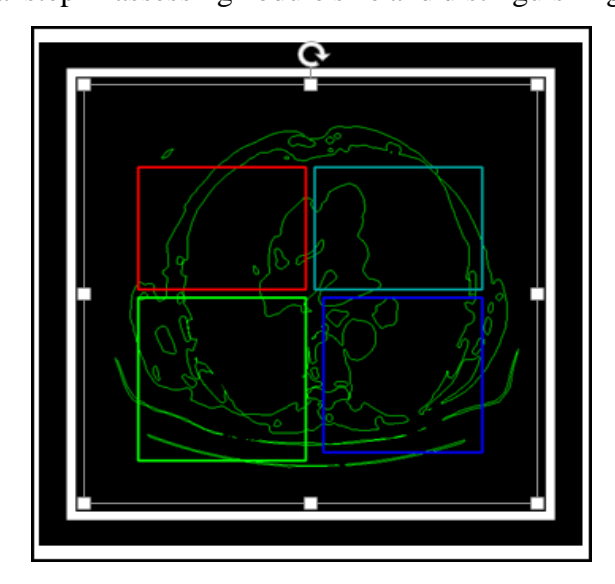


Figure 4.4 Illustration of Lung Image Segmentation

Figure 4.4 shows a segmented lung CT scan where the lung region is outlined in green. The scan is divided into four color-coded sections (red, green, blue, and cyan) representing different zones

of the lung for analysis. This type of segmentation helps focus on specific lung areas to detect abnormalities like nodules. The visual breakdown supports easier observation and diagnosis.

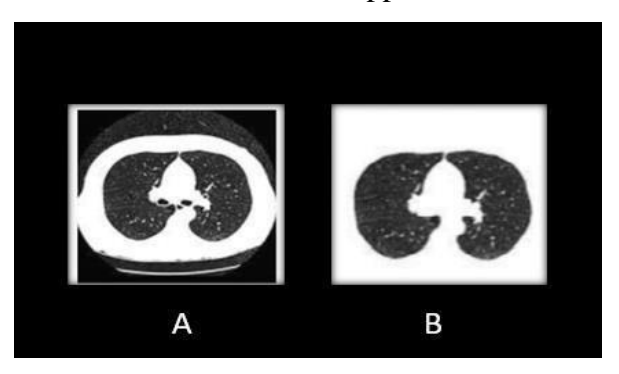


Figure 4.5 Image Left and Right without and with segmentation

Figure 4.5 shows two lung CT scan slices labelled A and B. Image A represents the original CT scan, clearly displaying the lung structure and surrounding chest area in high contrast. Image B shows a processed version where only the lung region is highlighted, and non-cancerous areas are removed. This type of transformation is commonly used to enhance the analysis and detection of lung tissue for improved disease diagnosis. It helps radiologists or AI systems examine the lungs more accurately.

#### 4.2 Classification Techniques

# 4.2.1. Convolutional layer network

This method utilizes convolutional layers, max-pooling layers, and neural network layers, similar to other deep learning architectures. Essentially, the input data is treated like any typical input, it passes through multiple convolutional and pooling layers. Network training involves minimizing the output error between the expected and actual results by optimizing parameters such as weights and biases [43]. In this study, supervised learning is employed, where input-output examples guide the training process. The error is reduced by adjusting the network's output to match the desired target [49]. As illustrated in Figure 4.6, the deep neural network developed for this work comprises three main types of layers: convolutional, max-pooling, and a combination of both. The convolutional layer contains kernels (filters), represented as three-dimensional weight matrices, that perform convolution operations on the neuron inputs [40]. Three convolutional layers are used in this architecture, and the filter size significantly influences performance [63]. A Softmax layer is added after the convolutional blocks to manage class probabilities and reduce dimensionality. By applying  $2 \times 2$  filters in pooling layers, the number of output features is significantly reduced, which decreases the number of parameters and increases computational efficiency. Images are used as input in this study to reduce complexity, storage demand, and computational overhead [81]. However, as the input image size increases, the network's

sensitivity tends to decline. Similar to the convolutional layer, each neuron in the pooling layer is connected to the outputs of a few neurons in the previous layer. The pooling layer is used to accelerate computation and reduce data volume [75][68]. Even after convolution and pooling, a considerable amount of small-sized feature data remains [61]. During the training phase, these features are passed to a Softmax classifier, which assigns class labels to the input images [79]. The final output layer, called "Flatten," transforms the multi-dimensional tensor into a 1D vector to facilitate weight optimization. Finally, various TensorFlow activation functions are tested using the RMSprop optimizer, which aims to minimize cross-entropy loss.

Visualization Method: This mapping technique highlights the area's most influential in a model's decision by providing visual explanations. It serves as a powerful tool for making the model more interpretable to domain experts. Through visual depictions of the model's decision-making process, this technique enhances trust and facilitates validation during debugging and optimization [34]. By analyzing these visual outputs, researchers can identify weak points in the model and implement architectural improvements. In this study, Grad-CAM is applied for visual recognition in single-module classification. The goal is to explore and enhance 3D CNN as shown in Figure 4.6 to more accurately and reliably detect lung nodules in CT scan data compared to existing models [76][55]. Ultimately, this approach aims to support early lung cancer detection, improving patient prognosis and survival outcomes.

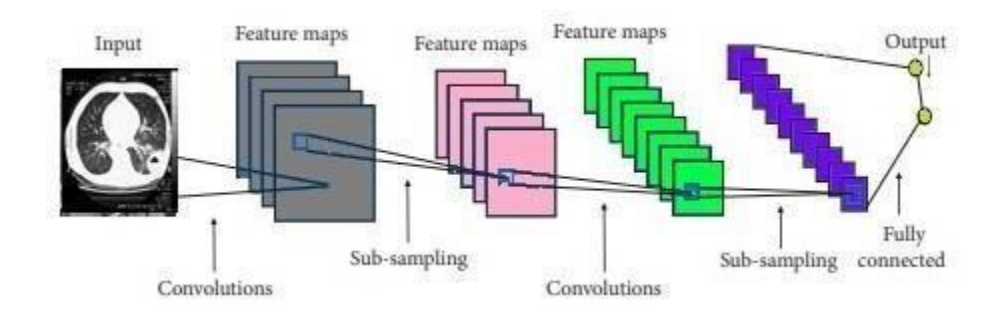


Figure 4.6 Convolutional Feature Mapper

Source: <a href="https://medium.com/data-science/convolutional-neural-network-feature-map-and-filter-visualization-f75012a5a49c">https://medium.com/data-science/convolutional-neural-network-feature-map-and-filter-visualization-f75012a5a49c</a>

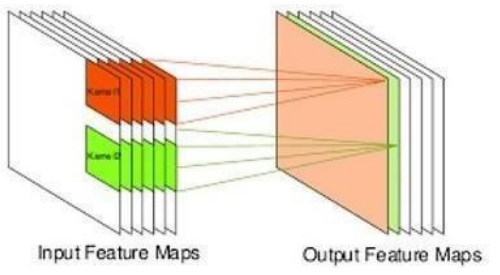


Figure 4.7 Input and Output Activation Maps

Source: <a href="https://www.researchgate.net/figure/An-example-of-low-resolution-input-activation-maps-and-the-corresponding-high-resolution\_fig3\_338420687">https://www.researchgate.net/figure/An-example-of-low-resolution-input-activation-maps-and-the-corresponding-high-resolution\_fig3\_338420687</a>

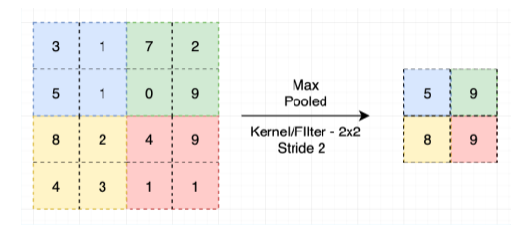


Figure 4.8 Max pooling in CNN

Source: https://www.mdpi.com/1999-4893/15/11/391

Grad-CAM can be regarded as a generalized form of Class Activation Mapping (CAM), offering researchers a way to interpret the inner workings of 3D CNN-based models visually. This approach is especially helpful for developers and medical professionals, as it visually highlights the regions in a CT scan that influence the model's decision.

Grad-CAM works by performing a weighted combination of the forward activation maps, followed by the application of a ReLU function to introduce non-linearity. Since the ReLU activation is applied in every layer of the output feature map, the resulting CNN becomes more nonlinear, improving its ability to model complex patterns. In the suggested algorithm, the rectified linear unit has been employed as the activation function. It functions as follows:

$$LN^{a}_{grad-cam} = \underset{k}{\text{ReLU}} \left( \sum_{k} \alpha^{c} A^{k} \right)$$
(Equation 4.1)

Where,

 $LN_{grad-cam}^a$  = Grad-CAM output localization map for class activation.

ReLU= Rectified Linear Unit, an activation function that outputs max (0, x).

 $\alpha_k^c$  = Importance weight of the feature map  $A^k$  For class C.

 $A^k$  = Activation map of the K<sup>th</sup> feature in the last convolutional layer.

This method helps us visualize how the model makes decisions by highlighting the specific areas in lung images that it relies on. It's especially useful in medical imaging because it shows where the model is focusing, which helps experts understand and validate its predictions during lung nodule detection.

#### 4.2.2 Memory of the Marine Predator Algorithm (MPA)

Marine predators, such as marine wolves, possess remarkable memory skills that help them repeatedly locate successful hunting grounds. This behavior is mimicked in the Marine Predator Algorithm (MPA), where memory retention is used to simulate predator behavior. After incorporating the effects of Fish Aggregating Devices (FADs) and prey movements, the algorithm evaluates its solution matrix for potential improvements by updating the elite solutions [58][69].

In each iteration, if the current solution demonstrates better fitness than the previous one, it replaces the earlier solution. This process mirrors the way predators revisit prey-rich areas, thereby progressively enhancing the solution quality. In this study, the MPA aims to optimize the **learning rate parameter**. Fitness is evaluated using the **Root Mean Square Error (RMSE)** between the actual label vector and the predicted output vector.

The steps of the proposed method are as follows:

- 1. Initialize algorithm parameters.
- 2. Evaluate the initial population.
- 3. Compare and update solutions based on fitness values.
- 4. Iteratively enhance solutions by simulating predator foraging behavior.
- 5. Optimize the learning rate to improve classification accuracy.

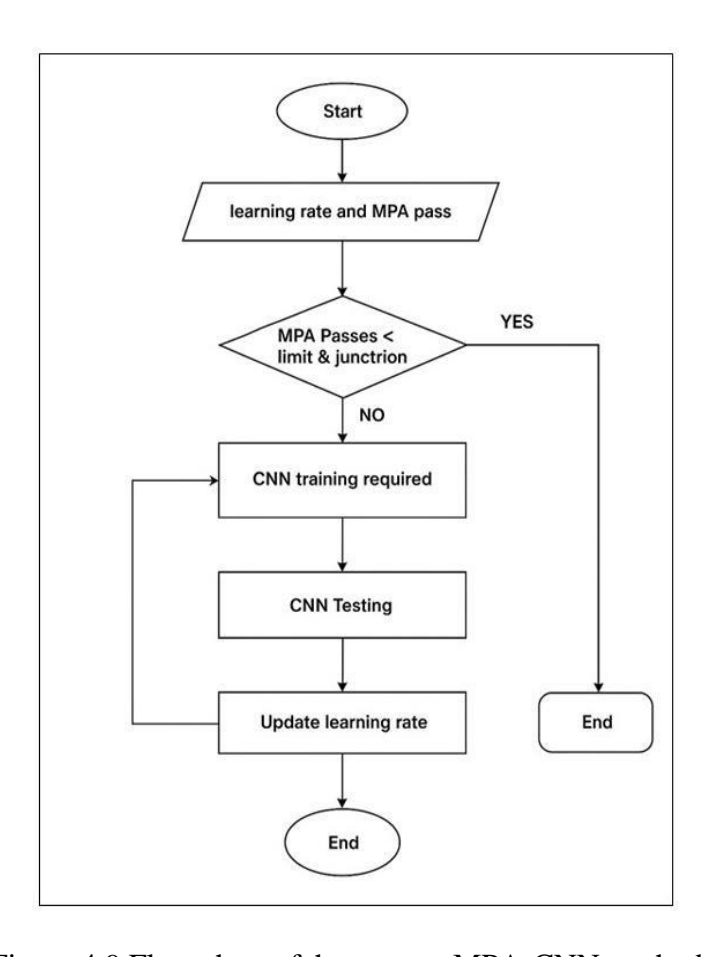


Figure 4.9 Flow chart of the present MPA-CNN method

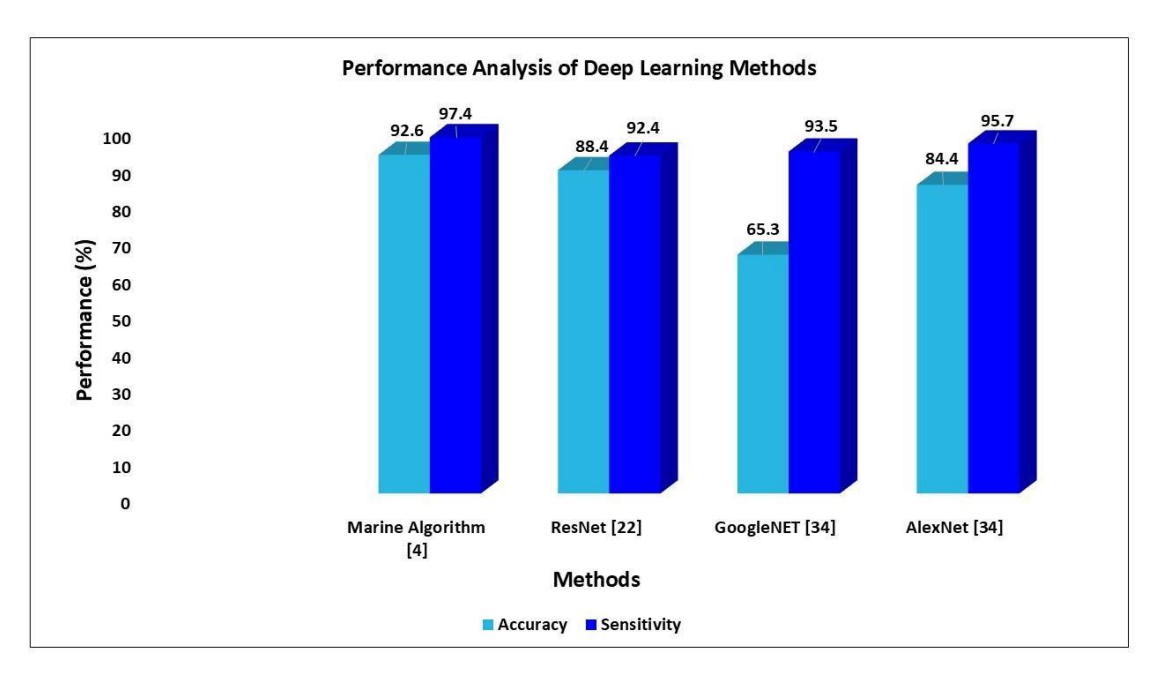
The Flowchart in Figure 4.9 illustrates the iterative CNN training process guided by MPA passes and learning rate adjustments. It continues training and testing until a predefined condition is met, ensuring optimal performance tuning. Train the optimized CNN model on the training data and evaluate its performance on the test data. When performance on a k-fold validation dataset no longer increases after training the model for an arbitrary number of epochs, halt training (k = 5). This method allows one to adjust the ideal value for the classification process. The MPA algorithm is programmed to execute up to 100 times. If the error value stays constant after 10 iterations, the MPA is said to have converged. After the experiment is set up, use the CNN training technique [52]. The learning rate is changed if the search agent's findings reveal a smaller mistake than the preceding number. For the predetermined number of iterations, the MPA runs. Test the model once the CNN training is finished. How accurately the model predicts the actual values in the test dataset is shown by the CNN accuracy test. The relevance of deep learning technologies in identifying significant elements from complex datasets in the current medical era is well demonstrated by their application. In the proposed method of this study, there is no overlap between the training and test data. Eighty percent of the images from the dataset are randomly selected for training, while the remaining twenty percent are used for testing. The training dataset

is fed into a Deep Neural Network (DNN) with a batch size of 32, trained over 200 iterations. This approach delivers superior results compared to other methods. Table 4.1 presents the simulation results of the proposed method along with comparisons to existing techniques.

Table 4.1 The result of the MPA algorithm and its comparisons with others.

Accuracy	Sensitivity
92.6	97.4
88.4	92.4
65.3	93.5
84.4	95.7
•	92.6 38.4 65.3

The proposed technique demonstrates higher accuracy than the other evaluated methods, as shown in Table 4.1.



Graph 4.1 Accuracy and Sensitivity Comparison

The accuracy and sensitivity of various techniques for detecting lung cancer are compared in Graph 4.1. With a sensitivity of 97.4% and an accuracy of 92.6%, the Marine Predator Algorithm outperforms competing methods such as ResNet, GoogleNET, and AlexNet. These enhanced

metrics suggest that the Marine Predator Algorithm can reliably diagnose lung cancer from CT-based imaging data. One of its key advantages is the use of metaheuristic optimization, specifically, the Marine Predators Algorithm, to optimize network architecture and improve classification accuracy. This approach yields more precise and dependable results by extracting high-level features from deep networks, thereby enhancing both classification and diagnostic performance. Additionally, the higher sensitivity of the Marine Predator Algorithm guarantees fewer false negatives, making it a potentially useful tool for lung cancer early detection and intervention.

# 4.3 Classification Using Traditional ML Algorithms

Traditional classification approaches play a vital role in many machine learning tasks, particularly when addressing segmentation challenges. These methods provide a baseline for evaluating more advanced techniques and are often effective when applied to simpler or well-structured datasets. This section focuses on the Naïve Bayes classifier, a widely used classical classification method.

### 4.3.1 Naïve Bayes Classifier Workflow and Architecture

The preprocessing layer normalizes and rescales the pixel values of CT scan images to a standardized range, enhancing the quality of inputs for training. The Convolutional Neural Network (CNN) serves as the core component of the framework, consisting of multiple convolutional layers that extract significant features from the CT images [45]. These layers are designed to detect patterns that are potentially associated with cancerous regions [13]. To minimize overfitting and improve generalization, dropout layers are incorporated within the dense layers [30]. For classification, the model employs the Softmax activation function, which calculates the probability distribution across the output classes (cancerous or non-cancerous) based on the dense layer outputs. During training, the loss function measures the discrepancy between the predicted outputs and actual labels [43]. The model's weights are optimized using well-established optimization algorithms, with the Adam optimizer being preferred for its adaptive learning rate and computational efficiency [20][29]. The flowchart in Figure 4.10 outlines the complete lung cancer detection pipeline, starting from data preprocessing to performance evaluation. Each stage of segmentation, feature extraction, selection, and classification works in sequence to ensure accurate diagnostic results.

# Step-by-step procedure to detect the lung carcinoma using a naïve base classifier

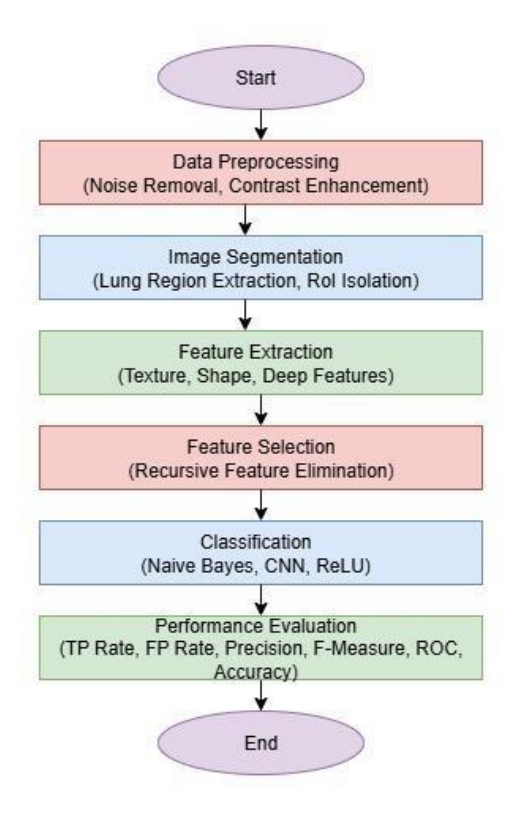


Figure 4.10 Flow chart of Naïve Architecture

Figure 4.10 presents a systematic approach for lung cancer detection using machine learning techniques. It begins with preprocessing the CT images to enhance quality, followed by segmenting lung regions and isolating regions of interest (ROI). Features such as texture and shape are extracted and refined using recursive selection. Finally, classification algorithms like Naive Bayes and CNN are applied, and the model's performance is evaluated using metrics like accuracy, precision, and ROC.

Table 4.2 Description and Techniques for the MPA Algorithm

Step	Stages	Techniques	Reference
1	Data collection and labelling	Public datasets	[18], [25], [77]
2	Data pre-processing normalization	Image resizing	[44], [80]
3	Data split	Training, validation, and testing sets	[25], [77]
4	Classification	Naive Bayes classifier	[37], [85]
5	Feature Extraction Networks	Convolutional Neural Network (CNN)	[20], [39], [86]
6	Non-linearity introduction function	Rectified Linear Unit (ReLU) activation	[73], [84]
7	Mapping to output classes	Fully connected layer	[36], [80]

Table 4.2 shows the main steps used in the Marine Predator Algorithm (MPA) for lung cancer detection. First, CT scan images are collected and labeled. Then, the images are resized and divided into training and testing sets. A Naïve Bayes model is used for classification, and important features are taken from the images using a CNN. ReLU is used to add non-linearity, and finally, the results are given using a fully connected layer.

Apart from the proposed segmentation and classification models, various AI-driven approaches have emerged for early lung cancer detection. Convolutional Neural Networks (CNNs), for instance, have shown significant promise in analyzing CT images to detect malignant nodules with high accuracy [41]. These AI algorithms can process large medical image datasets and identify patterns indicative of cancer. While imaging-based techniques remain central to this study, other emerging methods such as liquid biopsy, breath analysis, and optical coherence tomography are also being explored for non-invasive detection [13][39]. Though promising, these methods are still under research and fall beyond the image-based scope of this chapter.

## 4.4 Datasets Used in ML-Based Lung Cancer Detection

A large number of medical images is required to train a deep learning model for early lung cancer detection [55][15]. The dataset should include both cancerous and non-cancerous cases, along with detailed information on the stage and subtype of the tumor [17][9][40]. The National Lung Screening Trial (NLST) is one of the most commonly used datasets for this purpose [14][24]. It contains over 53,000 CT scans from more than 33,000 patients, with both positive and negative lung cancer cases [49][12][7]. To train deep learning models to distinguish between benign and malignant nodules, this dataset comprises annotations and classifications of the nodules [6] [40].

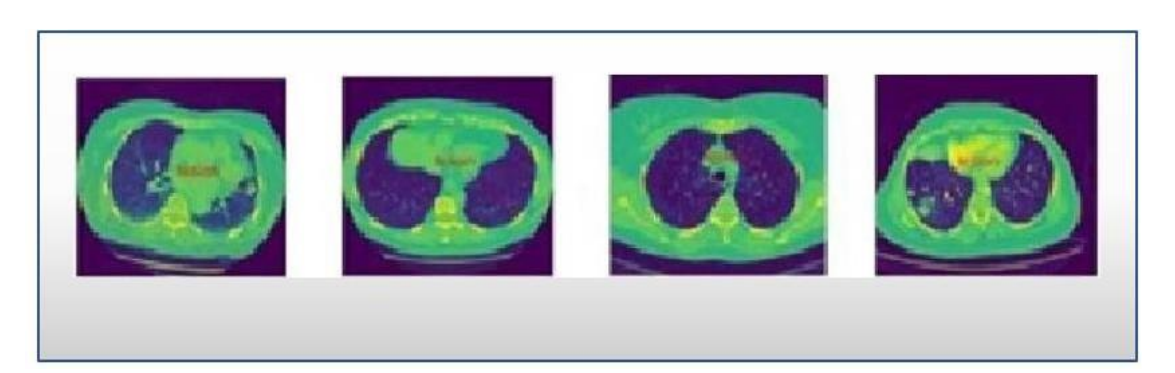


Figure 4.11 Malignant nodules of various sizes on CT slices.

Figure 4.11 shows sample CT scan slices from a benchmark lung cancer detection dataset. These images highlight both healthy and abnormal lung regions, which are essential for training deep learning models. The scans demonstrate varied patterns, helping machine learning systems learn to differentiate between benign and malignant nodules. As shown in Figure 4.14 above, CT scan images labeled A and D display irregular bright regions indicating potential lung nodules or

abnormal tissue, suggesting unhealthy cases. In contrast, images B and C show clearer lung fields without such irregularities, representing healthy examples.

Table 4.3 Nodule annotations for cancer detection

Dataset Name	Imaging Modality	Annotation Type	Nodule Type	Number of Patients	of Number of Nodules	Reference
LIDC- IDRI	СТ	Radiologist	Lung	1,018	2,174	[12]
NLST	CT	Radiologist	Lung	53,452	7,191	[26]
ANODE09	CT	Radiologist	Lung	1,004	1,004	[15]
Kaggle Dat Science Bow		Radiologist	Lung	1,944	1,861	[25]
LUNGx	CT	Radiologist	Lung	2,426	3,495	[20]
LUNA16	CT	Computer- aided	Lung	888	1,186	[77]

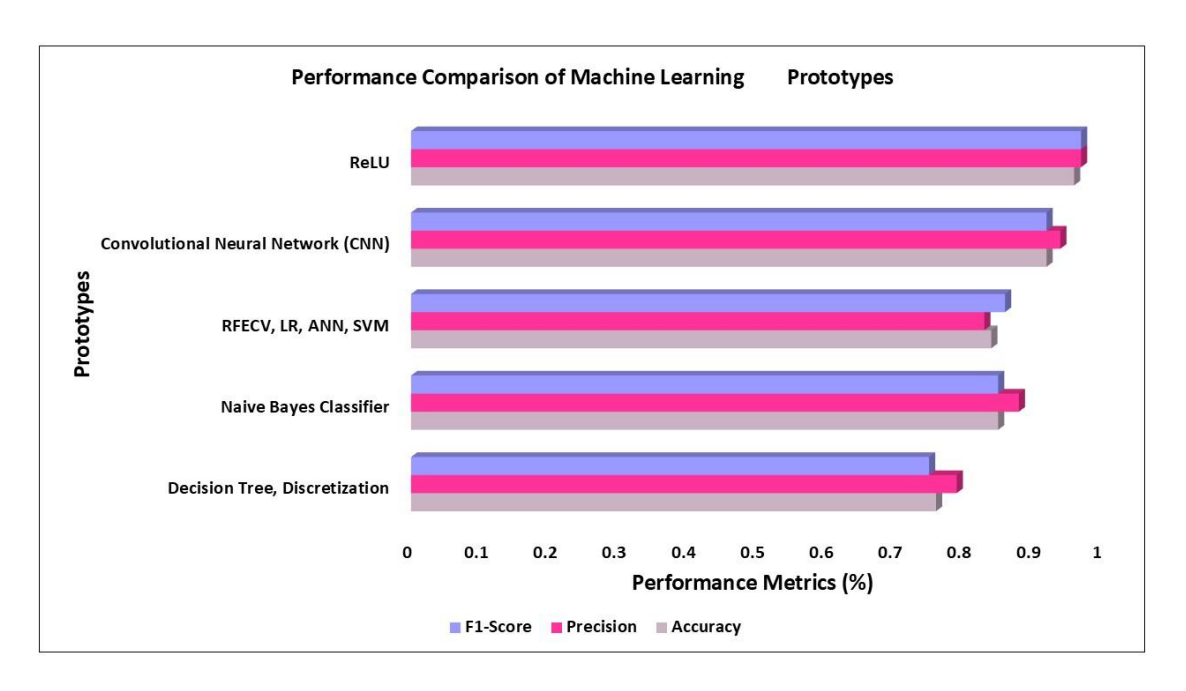
Table 4.3 presents commonly used benchmark datasets for lung cancer detection using machine learning. It lists each dataset's imaging method (mostly CT scans), annotation type (usually radiologist-verified), and details such as the number of patients and nodules included. For instance, the NLST dataset stands out with over 53,000 patients and 7,191 lung nodules, offering rich and diverse data. Other datasets like LIDC-IDRI, LUNA16, and Kaggle also provide valuable CT images, helping researchers train and evaluate deep learning models for accurate lung nodule detection and classification. An accurate deep learning model for lung cancer early detection must be trained on a sizable and varied collection of medical images.

#### 4.5 Performance Comparison of Deep Learning and Traditional Models

Table 4.4 Comparative results of the different proposed Lung nodule detection models.

Prototype	Accuracy	Precision	F1-Score	Citation
Decision Tree, Discretization	0.76	0.79	0.75	[20] Kavitha & Naveen, 2023
Naive Bayes Classifier	0.85	0.88	0.85	[34] Rawat et al., 2023
RFECV, LR, ANN, SVM	0.84	0.83	0.86	[17] Hasan et al., 2023
Convolutional Neural Network	0.92	0.94	0.92	[39] Praveena et al., 2022
ReLU	0.96	0.97	0.97	[44] Shakeel et al., 2022

Table 4.4 shows that deep learning models like CNN and ReLU outperform traditional methods in terms of accuracy, precision, and F1-score. ReLU achieves the highest performance, indicating its strong capability in lung cancer detection.



Graph 4.2 Comparison of several suggested nodule detection models

Graph 4.2 illustrates the performance of different machine learning and deep learning models used for lung cancer detection. It compares accuracy, precision, recall, and F1-score for five techniques. Among them, ReLU-based models and CNNs achieved the highest scores across all metrics, indicating strong predictive power. In contrast, traditional methods like decision trees performed lower, showing that deep learning models are more reliable for this task.

#### 4.6 Chapter Summary

The review concluded that lung cancer in CT images can be accurately detected using deep learning algorithms. The algorithm achieved high accuracy (AUC = 0.96 for nodule detection) in diagnosing the premature-stage lung cancer. These findings suggest that deep learning algorithms are highly effective in detecting premature-stage lung cancer from CT images, potentially enabling earlier diagnosis and better patient outcomes. However, further research is required to evaluate these algorithms in clinical settings and across larger datasets. This study primarily focused on lung cancer detection rather than other pulmonary issues visible in lung imaging. In the future, the proposed methods may also help identify a broader range of pulmonary conditions.

# CHAPTER 5 ENHANCING ALGORITHMS THROUGH OPTIMIZATION METHODS

#### 5.1. Problem definition

Due to changes in lifestyle, environment, and dietary habits, cancer, particularly lung cancer, has emerged as a serious threat to global public health. Research attributes lung cancer to multiple factors, including cigarette smoking, indoor air pollution, genetic tendency, chronic illnesses, and poor diet. Among these, smoking is the most dominant cause, responsible for approximately 85% of lung cancer cases. Lung cancer often starts with abnormal growth in the bronchial mucosa, leading to symptoms such as persistent coughing, chest pain, and breathing difficulty. Unfortunately, these symptoms frequently appear only in advanced stages, by which point metastasis has often occurred. As a result, timely and accurate premature-stage detection is critical to improving survival rates and treatment outcomes. Currently, diagnosis relies on image analysis techniques such as chest X-rays, CT scans, and is confirmed by biopsy. However, traditional methods were not able to provide early and accurate results. Thus, this study proposes a novel deep learning framework for precise, premature-stage lung cancer detection.

The proposed model introduces the following innovations:

# (a) Segmentation using B-RGS (Bates-distributed Coati Optimization + Region Growing Segmentation):

Why: Lung segmentation is critical to isolate the lung area from the surrounding structure. The proposed B-RGS approach enables more accurate partitioning of lung regions by incorporating knuckle point detection, leading to precise region growth for better tumor localization.

- **(b)** Edge enhancement using Unsharp Mask Filter (UMF): Why: CT images often suffer from low contrast and weak boundaries. UMF improves edge clarity, helping the model focus on critical boundaries between healthy and abnormal tissues, thus improving segmentation and classification accuracy.
- (c) Feature selection using Binomial Distributed Chi-Square Test (BD-CST): Why: Deep learning models benefit from selecting only the most relevant features. BD-CST reduces noise and redundant information, enhancing model performance and reducing training complexity.

## **5.2.** Problem-Solving Approach

To overcome the identified challenges, this research proposes a comprehensive, deep learning-based model for premature-stage lung cancer prediction, specifically using TL-based P-ReLUResNet (P-ResNet). The model incorporates the following key contributions:

- a. TL-based P-ReLUResNet for lung cancer detection: P-ResNet integrates transfer learning and PReLU activation, offering improved gradient flow and better feature representation, especially beneficial for complex CT data.
- **b. I-ADF for noise removal:** Iterative Adaptive Decision Fusion effectively removes imaging noise while preserving key image features, improving the clarity of CT scans used for diagnosis.
- **c.** Lung segmentation using B-RGS: Combines metaheuristic optimization and region growing to isolate lung structures with higher accuracy.
- **d. Edge enhancement using UMF:** Enhances contrast at tissue boundaries, aiding the model in distinguishing tumor regions from healthy tissue.
- e. Feature selection using BD-CST: Prioritizes the most discriminative features, leading to higher accuracy and reduced false Positive rates.

# 5.3. Proposed Methodology1: Lightweight Deep Neural Network for Early Lung Cancer Detection

This proposed framework is shown in Figure 5.1 and works under the following phases:

- 1. Pre-processing (Noise elimination and Contrast enhancement)
- 2. Segmentation phase
- 3. Classification phase.
- 4. Risk score prediction phase

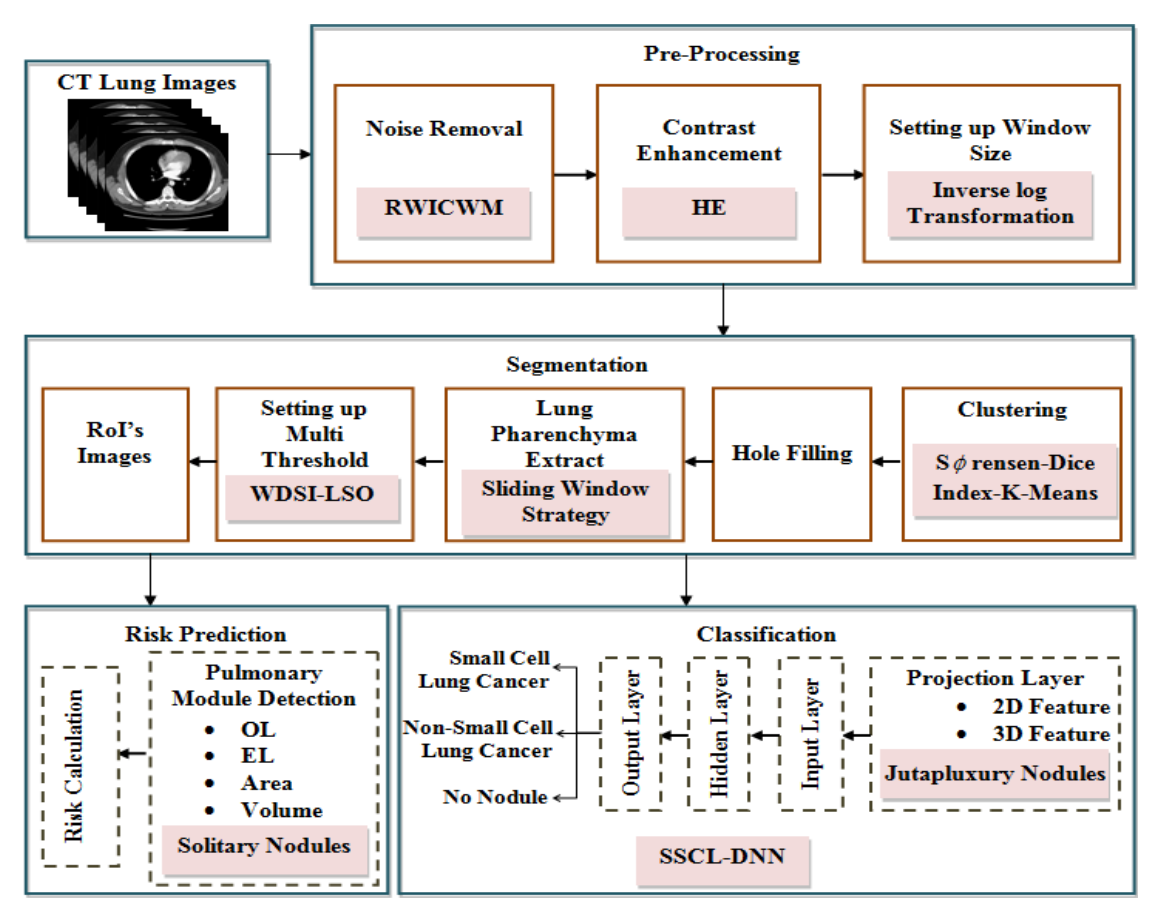


Figure 5.1 Block schematic of the suggested lightweight model

The explanation, details, and contributions of our developed approach are given below. In this research, we propose a lightweight model to overcome noisy regions, such as graininess, tissues [11], and vessels, a Ricker Wavelet Iterative Center Weighted Median Filter (RWICWM).

- To reduce false positives of the disease prediction accuracy, Sørensen-Dice Index-based K-means clustering has been suggested.
- ii. To detect varying-sized nodules of the lungs, Light Spectrum Optimizer-based pulmonary nodule detection (WDSI-LSO) has been used.
- iii. To differentiate lung parenchyma from the segmented lung, a sliding window strategy has been suggested.
- iv. To screen patients for future analysis, a risk screening has been made based on solitary nodule detection using PLCOm.
- v. To appropriately classify lung cancer with high accuracy, a semi-supervised and contrastive learning-based Deep Neural Network (SSCL-DNN) has been proposed.
- vi. The proposed algorithm evolved using a hybrid method and was compared to other algorithms, such as MLP, CNN, and RNN. Google DeepMind was the first to use reinforcement learning technology.

#### **5.3.1. Ricker Wavelet Iterative Center Weighted Median Filter (RWICWM)**

First, input lung CT images are collected from the LIDC dataset in DICOM format and are given to the Ricker Wavelet Iterative Center Weighted Median Filter (RWICWM). The suggested filter improves variance field estimation by making use of the image Ricker wavelet coefficients' innerand inter-scale dependence. By smoothing the noisy wavelet coefficient variances iteratively, this filter maintains the edge information found in the large-magnitude wavelet coefficients [40]. Here results will be evaluated for parameters, such as PSNR, MSE, and SSIM, with conventional denoising filters, such as the Gaussian filter, Guided filter, and Wiener filter. A histogram equalization technique is adopted for contrast enhancement [4][25]. After determining the proper window size level, the slope and intercept are rescaled using the inverse log transformation.

#### 5.3.2. Sørensen-Dice Index K-means clustering

The pre-processed images will be computed for various intensities, and then given to Sørensen-Dice Index K-means clustering. After that, the cluster centers will be initialized, and this step is repeated until convergence is reached. Since Euclidean and other distances are not scale-invariant, meaning that the distances computed could be skewed depending on the features' units, the Sørensen-Dice Index distance is thus employed as the data index distance calculation [6][56]. Sørensen's initial formula was intended for use with discrete data. It is defined as specified, 2 sets, X and Y, as

$$DSE = \frac{2 \cdot}{|\lambda|}$$
 (Equation 5.1)

This equation measures how similar two sets X and Y are. It calculates the overlap (intersection) between the two sets and divides it by the total size of both sets combined. A value close to 1 indicates strong similarity (more common elements), and A value near 0 means very little overlap. Used in clustering to compare the similarity between segmented regions in CT images. The 2 sets of cardinalities, or the number of essentials in every set, are represented by the variables |X| and |Y|. Divide the whole number of elements in each set by the total sum of items that both sets share twice to get the Sørensen index. By using the definitions of (FN), which stands for false negative, true positive (TP), and false positive (FP), one can write boolean data as follows. The cardinalities, or the number of members in each set, of the two sets are represented by the variables |X| and |Y|[45]. Divide the overall sum of elements in each set by the total sum of items that both sets share twice to get the Sørensen index. By using the definitions of true positive (TP), false positive (FP), and false negative (FN), one can characterize boolean data as [34][16].

$$DSE = \frac{2 \cdot TP}{2 \cdot TP + FP + FN}$$
 (Equation 5.2)

Where TP = True Positives, FP = False Positives, FN = False Negatives. It is commonly used in image segmentation to evaluate how well predicted regions match actual tumor areas. Conversely, true positives are only counted once in the numerator and denominator of the Jaccard index. The similarity quotient, or DSC, has a range of 0 to 1[26][9]. It can be seen as a set-level similarity metric. The established operations can be described in terms of vector operations over binary vectors a and b, just like the Jaccard index does:

$$S_v = rac{2 \cdot |a \cdot b|}{|a| + |b|}$$
 (Equation 5.3)

Here, *a* and *b* are binary vectors (pixel values: tumor vs non-tumor). The formula compares two vectors by checking how many matching values they have. Useful when comparing pixel-wise predictions with ground truth segmentations. This provides a broader similarity metric across vectors and yields the same result for binary vectors. The coefficient is well-defined as two-fold the collective information (intersection) over the total cardinalities for sets X and Y of keywords utilized in information retrieval. Therefore, from each cluster center, the centroid intensity will be determined using the Sørensen-Dice Index as a distance measure. For every data point, this process is repeated [24][36]. Conventional clustering techniques, such as the K-means clustering algorithm, centroid-based clustering, and density-based clustering methods, will be evaluated for comparison. The results of this clustering method for parameters, such as true positive and false positive rates, are compared with those of previous methods.

$$C = K$$
-means $(IRWI \cdot CW \cdot M)$ 

(Equation 5.4)

This shows the result *C* of applying K-means clustering to the preprocessed image *I R W I C W M*. K-means is used to group similar pixels, like tumor, background, etc. The clustered regions are denoted by the C. Srensen-Dice Index with K-means Clustering: Using the Srensen-Dice Index as the similarity metric, we employ K-means clustering to separate the preprocessed image into K clusters. After choosing K cluster centers, each pixel is subsequently given to the nearest cluster based on the Dice similarity.

$$I_{\text{segmented}} = f(I_{\text{preprocessed}}, K, \text{Dice Similarity})$$

(Equation 5.5)

This equation indicates that segmentation is performed on the preprocessed image using K-clusters and Dice similarity as the distance metric. The segmented image is represented by the keyword segmented. K-means stands for the K-means clustering procedure. K represents the number of clusters, which normally stand in the foreground and background. The similarity metric used in K-means clustering is Dice similarity [14]. The segmented pulmonary nodules are included in the final product, where each pixel is assigned to a cluster depending on how similar it is to the cluster centers using the Sørensen-Dice Index. The result obtained at this stage is then given for pulmonary nodule detection. For pulmonary nodule detection, lung parenchyma is extracted [38] using a sliding window strategy, and from this, lung nodule detection will be done using Weighted Dice Similarity Index with Local Search Optimization based pulmonary nodule detection (WDSI-LSO) [5][47].

Here, Light Spectrum Optimizer is taken, and due to its being restricted by the transmission coverage, the scale factor distribution is modified using the Weibull distribution. Here, the images' grey level values will be initialized, and the goal function is to find the best threshold by histogram analysis and evaluating each gray level to see which one maximizes the likelihood that the threshold value will occur for each class of probability [57]. Many ROIs with different intensities are obtained from this ideal threshold due to optimal multilayer thresholds. Eventually, these ROIs are concealed using a segmented lung mask to create the collective form of an ROI picture. From this ROI, the features, such as the range of area, volume range, tolerance in Overlap (OL) feature, and elongation (EL) feature, are calculated [15][7]. This result will be evaluated for nodule count, Dice Similarity Coefficient (DSC), sensitivity, Positive predictive value (PPV), and specificity for U-DNet, NoduleNet, and Faster R-CNN.

$$I_{WDSI\text{-}LSO} = WDSI_{LSO}(IRWI \cdot CW \cdot M, C)$$
 (Equation 5.6)

Where  $I_{WDSI-LSO}$  represents the enhanced image after applying WDSI-LSO. The segmentation process can be visualized as a binary image, where pixels corresponding to pulmonary nodules. This shows the image.  $I_{WDSI-LSO}$  It is generated by applying the Light Spectrum Optimizer (WDSI-LSO) on the preprocessed image and cluster result.

# 5.3.3. Semi-supervised and contrastive learning-based DNN

As proposed methodology discussed in the above section, Preprocessing steps typically include Contrast Stretched, Convex Hull, and Edge Enhanced for resizing the images, normalizing the pixel values, and possibly augmenting the data to increase the variety and robustness of the training set, as shown in Figure 5.2 below. In the context of lung cancer, labels would indicate the presence or absence of nodules and, if available, the malignancy of detected nodules. Common

architectures used for medical image classification include Convolutional Neural Networks (CNNs) like ResNet, VGG, and proposed. Divide the dataset into training, validation, and test sets. A common split is 70-20-10. Train your DNN using the training set. Use the validation set to tune hyperparameters and avoid overfitting. After classification, the Optimizers like Adam or RMSprop and the risk analyzer are frequently used.

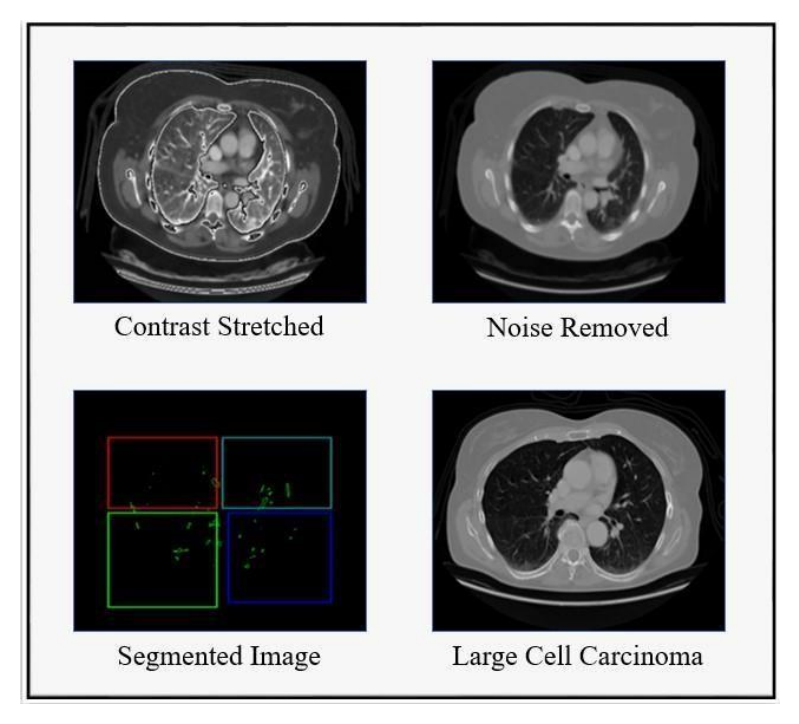


Figure 5.2 Dataset Utilization for Cancer Detection

The LUNA16 CT imaging dataset, which was split into three sets (Test, Training, and Validation), served as the data sample for this study. Each image in the dataset is assigned a single label: normal, large cell carcinoma, or squamous cell carcinoma. CT scans were performed throughout the patients' clinical care schedules. Before training the deep learning models on the dataset, two board-certified physicians reviewed and labeled the images. To ensure accuracy, a third expert further assessed the image labels. In both the training and test sets, there was a significant class imbalance. Additionally, some samples from the training set were also present in the test set, creating overlap. To address this, the training and test sets were combined, shuffled, and randomly reordered to form a new training set. Figure 5.3 displays images corresponding to cases of squamous cell carcinoma, large cell carcinoma, and normal conditions.



Figure 5.3 The left, center, and right images illustrate distinct kinds of cancer.

For classification, the segmented nodules were taken as input to the semi-supervised and contrastive learning-based DNN (SSCL-DNN). Output SSCL-DNN = SSCL-DNN (IWDSI-LSO, C, PLCOm). Where Output SSCL-DNN represents the output of the neural network, which could include nodule detection scores and risk assessments. By incorporating several projector layers, a contrastive loss term, semi-supervised label propagation, and contrastive learning [1] for classification, DNN is divided into two sub-networks. 1. The classifier will receive segmented results as a training set. 2. The network has pre-trained models (semi-supervised learning) and it propagates the incoming images into classes, such as small-cell lung, non-small cell lung malignancy [31], and no nodule. 3. Then, contrastive learning [40] is introduced in the network by adding a projection layer and considering contrast loss. 4. Due to contrasting learning, the input images will be augmented both strongly and weakly, then combined in the projection layer for the extraction of 2D features and 3D features. These features will be mapped as feature vectors in the same layer 5. These results will be given to DNN classification layers, and the upshot will be non-small cell lung [7], small-cell lung malignancy, as well as no nodule [37].

#### **5.3.4. Risk Score Screening**

Here, risk screening [6] will be done based on solid nodules found in the segmentation result. This will be done based on environmental factors, such as smoking, family history, and other chronic diseases. Along with this, if positive solid nodules were found, the risk assessment would be performed using the PLCOm risk model. PLCOm risk assessment also considers the environmental features stated earlier to result in high-level and low-level risk. This was done to predict the survival rate of the entire database and make precautionary care in the future.

$$Risk_{PLCOm} = PLCOm(I_{patient\_data})$$
(Equation 5.7)

Where *Ipatientdata* contains patient-specific information.

This equation represents the risk score calculated using the PLCOm model based on a patient's environmental data (like smoking history, family history, etc.).

#### 5.3.5. Dataset Overview for Lightweight DNN Model

The Lung Image Database Consortium image collection serves as the dataset for this proposed work (LUNA-16) [28]. Thoracic computed tomography (CT) scans with marked-up, labeled lesions are used for both lung cancer screening and diagnosis [6]. This 1018-case data collection was produced in collaboration with seven university organizations and eight medical imaging companies [38]. Images from a clinical thoracic CT scan and an XML file containing the annotation process findings, completed in two steps by four seasoned thoracic radiologists, are included for each topic. At the first blinded-read stage, each radiologist independently reviewed each CT image [2] and classified lesions into three categories: "non-nodule > or =3 mm", "nodule < 3 mm", and "nodule > or = 3 Mm". Here, the sample image of the suggested methodology is shown in Figure 5.4. In Figure 5.4A, the original CT sample images are displayed. As can be seen in Figure 5.4B, the contrast stretch applied to the input images is preprocessed to remove noise using RWICWM. Next, in the picture of Figure 5.4C, we see the edge enhancement image. After, in Figure 5.4D, we see segmentation. Finally, in Figure 5.4E, the classified output is largecell cancer, squamous cell cancer [51], and normal (without carcinoma). RWICWM. Next, in the picture of Figure 5.4C, we see the edge enhancement image. After, in Figure 5.4D, we see segmentation. Finally, in Figure 5.4E, the classified output is large-cell cancer, squamous cell cancer [51], and normal (without carcinoma).

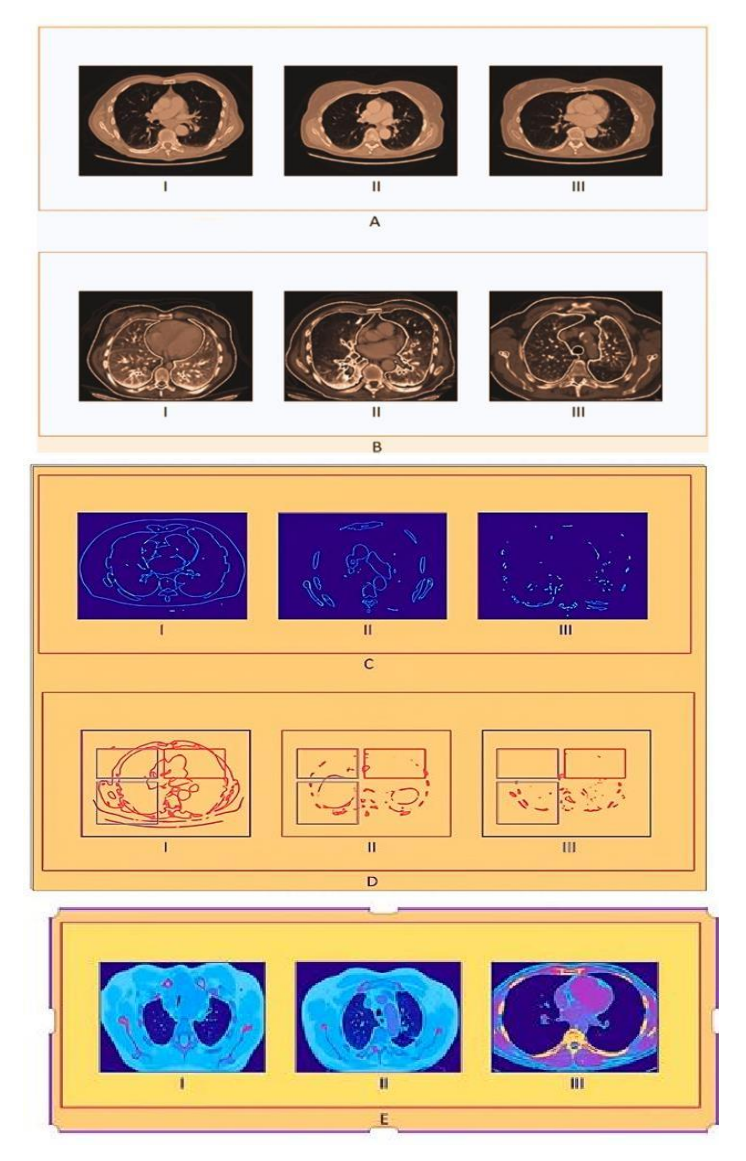


Figure 5.4 Sample input images in the proposed framework.

(A, B) The Top and Bottom Images show the original CT sample Images and the contrast–stretched Images. (C, D) The Top and Bottom Images show the edge enhancement Image and segmentation. (E) The images show the classified output: large cell cancer, squamous cell cancer [24], and normal (without carcinoma).

In Figure 5.4, the images help doctors make well-informed decisions and improve patient care strategies by providing a thorough awareness of the extent and distribution of malignant tumors through a visual contrast between normal cancerous images on the left side and enhanced cancerous diseased tissue images on the right side.

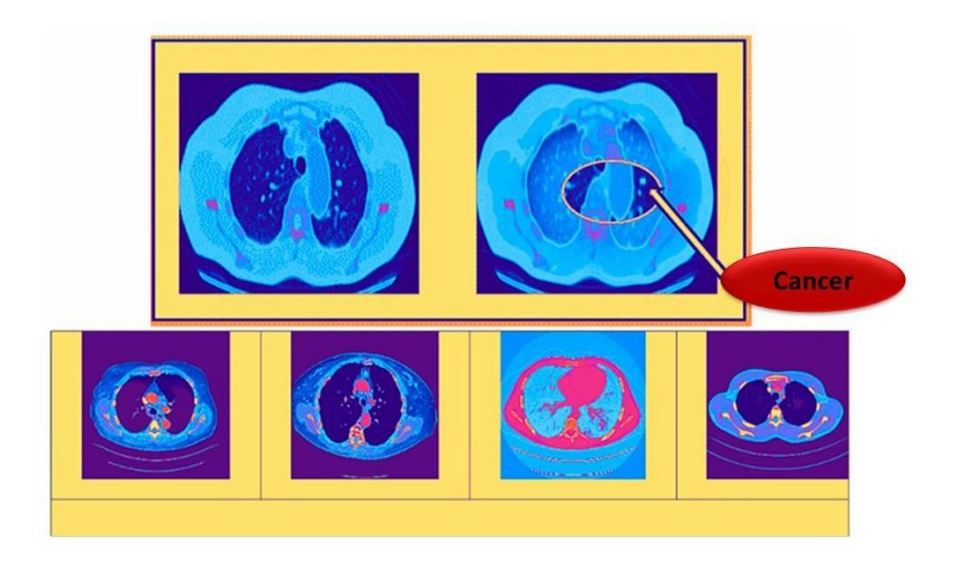


Figure 5.5 Left and Right with Cancer and Highlighted Cancerous Image.

The area highlighted in Figure 5.5 (using the arrow) is the cause for concern and requires additional investigation because it shows cancerous cells. Herein, we have used red color to indicate the tumor. This might be a side and enhanced cancerous diseased tissue images on the right side, and might be a tumor, nodule, or another abnormality that has to be examined more closely to rule out malignancy or benignity

# 5.4. Proposed Methodology 2: Lung Carcinoma Detection Using Transfer Learning

Proposed Methodology: Advanced Lung Carcinoma Prediction and Risk Screening Model Using Transfer Learning: Globally, lung cancer is the most prevalent type of cancer. Due to the high death rate associated with lung cancer, researchers were compelled to conduct an extensive investigation into the early identification and diagnosis of cancer. When lung cancer is detected early (in the first stage), the survival rate increases by 70 to 80%. To predict them in a premature stage, a novel framework with deep learning has been proposed. The novel framework consists of the following stages: Pre-processing, Lung partition Segmentation, Feature extraction, Feature selection, Classification, and Risk Screening based on carcinoma. Segmentation and nodule detection were performed on each 2D CT slice independently. A Lung CT scan image is taken as input, and this image itself has some noise, such as Gaussian and Poisson noises, which should be removed. Also, the image should be enhanced for its high level of classification. Hence, the image first undergoes noise removal using Intra-class variance-Anisotropic Diffusion Filter (I-ADF). Conventional Anisotropic Diffusion Filter (ADF) is chosen for its characteristic of without blurring edges. Still, it has the disadvantage of constant diffusion magnitude that might affect the Signal to Noise Ratio (SNR) of the filter. Hence, it is modified to follow inter-class variance. This novel filter will be evaluated for variance and SNR and will be compared with conventional methods, such as Wavelet transform filter (WTF), Gilbert Filter (GF), and Median Filter (MF) [66][29]. From this, the noise-removed image will then be given for contrast stretching. This is to increase the range of intensity values as it contains a span of desired values. This contraststretched image will then be given for the convex hull operation to separate the lung region from the whole image, and then proceed with this result in the image again [12]. Further, this lung region will then be given for edge enhancement using an Unsharp Mask Filter (UMF). UMF is selected for its increased edge sharpness in the image, and this pre-processed image will then be given for segmentation. For segmentation purposes, Bates distributed the coati optimization algorithm, and integrated Region Growing Segmentation (B-RGS) has been proposed. Here, Region Growing Segmentation (RGS) is selected for its high segmentation accuracy if the edges are clear; still, it has certain limitations when used in lung CT images to segment the carcinoma region due to the overlapping shadow of vessels, tissue mass, and ribs. Hence, to overcome this issue, the seed of the region growing section is assumed to be the knuckle point of the lung image. This knuckle point is selected using the Bates distributed Coati Optimization algorithm (BD-COA). This will be done by collecting the contour values of both lungs (left and right) and then conforming them. This gives a conformity index by selecting the highest conformity value. Here, the Coati Optimization algorithm (COA) is selected for its high meta-heuristic property, and still, it has a limitation of high computation complexity; hence, it is modified in the r iguana updating rate using the Bates distribution. This B-RGS will then be evaluated for segmentation accuracy, error, etc., and will be compared with RGS, Watershed algorithm, and Density-based segmentation algorithm. Features, such as gradient features, profile-based features, on-rib, onvessel, and spectral flatness measures, have been extracted. These features were typically related to carcinoma categories. Feature selection will be done using a Binomial distributed Chi-square test (BD-CST). The Chi-square test is chosen for feature reduction due to its low processing time. Still, it has a limitation of choosing the significance level randomly that might affect the processing result; hence, it is modified to follow the Binomial Distribution (BD). This method will then be evaluated for its feature selection algorithms, such as Genetic algorithm (GA), Linear Discriminant analysis (LDA), and Principal Component Analysis (PCA). The selected features will then be given for the classification of carcinoma. For classification, TL-based P-ReLUResNet P-ResNet (P-ResNet) has been proposed. P-ResNet is selected for its high efficiency in medical image classification. However, it suffers from a low learning rate and a high computation time for the kernel activation function. Hence, to address this issue, this transfer learning modified ResNet model will provide improved learning rate, and thus it will be further modified with P-ReLU activation function for its efficiency. This model will be evaluated for

Accuracy, precision, recall, etc., and will be compared with existing deep learning models, such as Deep Neural Network (DNN), Convolutional Neural Network (CNN), and Artificial Neural Network (ANN). The classifier results as normal and abnormal, such as Adenocarcinoma, Squamous cell carcinoma, and Large Cell Carcinoma, are classified. As this transfer learning modified P- P-P-ResNet model will provide an improved learning rate, and thus it will be further modified with P-ReLU activation function for its efficiency. For risk screening purposes, the sensitivity of the abnormal images was considered and calculated individually to find the packet index of the CT image. This packet index in turn shows that persons with Squamous cell carcinoma and Large Cell Carcinoma were at high risk, and others are at low risk. Thus, the patients were screened, and the results will be presented.

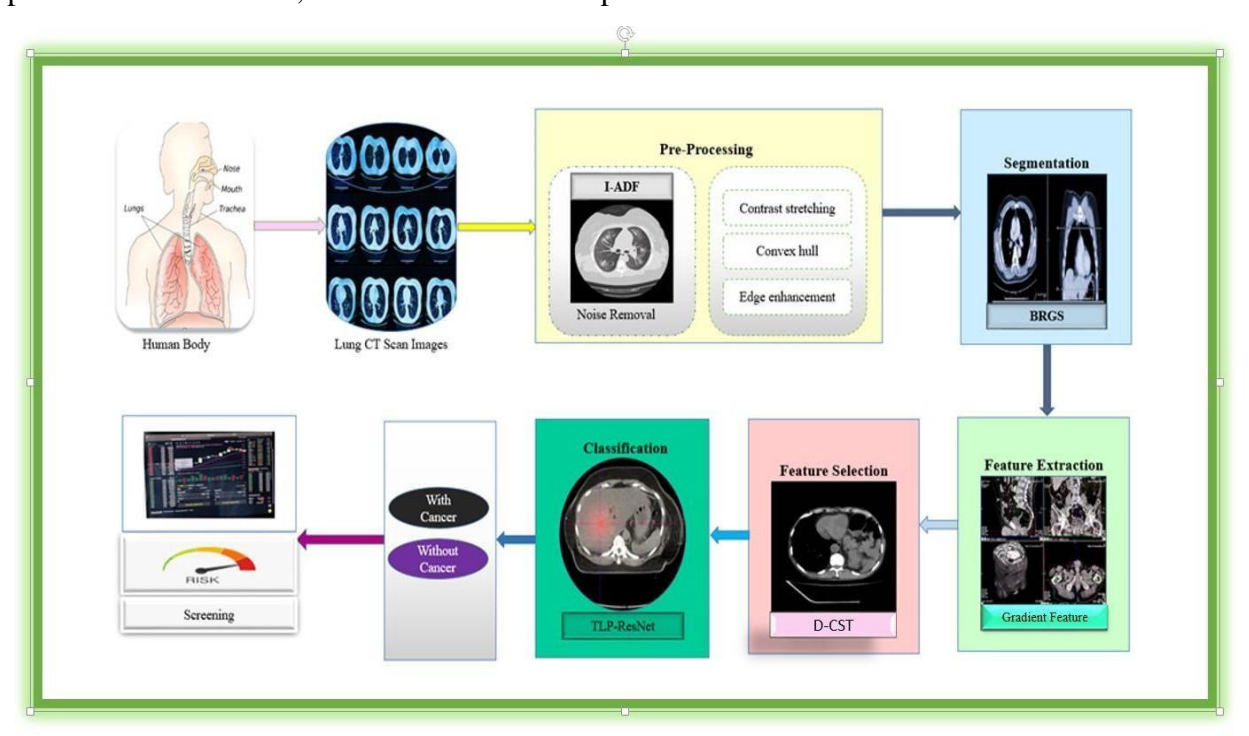


Figure 5.6 Pre-Diagnosis of Lung Cancer Detection

The TL-based P-ReLUResNet (P-ResNet) for lung cancer diagnosis combines a number of cutting-edge ideas from medical image processing and machine learning. An essential part of this process is Transfer Learning (TL), which allows the model to use the knowledge it has learned during training on big datasets in related fields like object identification or even general medical imaging. Through the application of this acquired knowledge, the model is able to adjust and become more specialized for the goal of detecting lung cancer, possibly using less data and achieving faster convergence. Based on the Residual Neural Network (P-ResNet) framework, which is well known for its capacity to efficiently train very deep neural networks through the use of skip connections, P-ResNet's architecture was developed. Because of these connections, the model can learn residual mappings, which facilitates the training of deep networks without

causing the vanishing gradient issue. The network is further enhanced by the integration of Parametric Rectified Linear Unit (P-ReLU) activation functions. P-ReLU modifies the normal ReLU activation function to include more learnable parameters, which allows the network to simulate more intricate relationships in the data. The ability of P-ResNet to increase lung cancer detection's sensitivity and specificity is one of its main benefits. The ability of the model to precisely recognize true positive cases of lung cancer is referred to as sensitivity, while the ability to correctly identify true negative cases is measured by specificity. P-ResNet seeks to balance these two metrics by adding P-ReLU activations and fine-tuning the pre-trained model weights using TL to reduce false positives and false negatives. Furthermore, P-ResNet may improve the effectiveness of procedures for diagnosing and screening for lung cancer. Radiologists can detect possible cancers more quickly and precisely by using P-ResNet, which automates the detection of problematic regions in lung imaging studies, such as CT or X-rays. This could shorten the time it takes to diagnose a patient, allowing for earlier interventions and better patient outcomes.

#### **5.4.1.** Iterative Adaptive Decision Fusion (I-ADF)

Through iterative decision fusion, the Iterative Adaptive Decision Fusion (I-ADF) technology offers a novel approach to lung cancer detection with the goal of improving diagnosis accuracy and dependability. In contrast to conventional techniques that depend exclusively on a single classifier or algorithm, I-ADF utilizes several classifiers and repeatedly combines their conclusions to attain enhanced performance. I-ADF functions primarily through a sequence of iterative processes. First, some classifiers, each intended to evaluate distinct features of lung imaging data, are used to produce distinct conclusions about the existence or non-existence of malignant anomalies. These classifiers could make use of a variety of methods, including rule-based systems, conventional machine learning algorithms, and deep learning models. An adaptive decision fusion technique is utilized to combine the judgments made by each classifier after the first classification phase.

The individual choices are combined dynamically throughout this fusion process, which adjusts to the properties of the input data and the effectiveness of each classifier. Through iterative improvement of the fusion method based on input from prior rounds, I-ADF can efficiently combine the advantages of several classifiers while minimizing the drawbacks of each one separately. Because I-ADF is iterative, decision fusion may be continuously improved, allowing the system to learn from its performance and adjust to changing patterns in the data. The fusion process gets more and more precise with each iteration, improving lung cancer detection's resilience and accuracy. The utilization of I-ADF exhibits considerable potential in enhancing the dependability of lung cancer detection and diagnosis. I-ADF may lessen the drawbacks of single

algorithms and offer more precise evaluations of worrisome lesions in lung imaging scans by skillfully integrating the insights from several classifiers. In the end, this method may help identify lung cancer early, which would improve patient outcomes and allow for quicker therapies.

#### **5.4.2.** Knuckle Point Using (B-RGS)

By identifying conspicuous places within lung imaging data, Knuckle Point diagnosis (KPD) using Binary-Robust Geometric Sampling (B-RGS) presents a viable tool for improving lung cancer diagnosis. Using B-RGS, this method seeks to identify important characteristics along the outlines of lung anomalies, such as tumors or nodules, similar to knuckle points in fingerprints. The capacity to precisely identify critical locations along aberrant outlines has substantial diagnostic significance when it comes to lung cancer identification. These points can help distinguish between benign and malignant lesions by acting as reference markers when examining the size, shape, and textural traits of possible cancers. The KPD approach effectively recovers significant points from lung imaging data, even in the presence of noise or fluctuations in picture quality, by utilizing B-RGS. Significant spots may be identified based on their geometric qualities thanks to the combination of strong geometric sampling and binary image processing techniques found in B-RGS. Through the provision of useful landmarks for analysis to automated diagnostic systems and radiologists, the combination of KPD with B-RGS advances the identification of lung cancer. More precise and dependable diagnosis is made possible by the knowledge of the geographical distribution and structural features of lung anomalies provided by these identified knuckle spots. Once everything is looked at, the exact localization of important characteristics within lung imaging data through the use of KPD employing B-RGS provides a potential method to improve lung cancer diagnosis. This technique has the potential to improve early detection rates and treatment methods for individuals with lung cancer by utilizing the advantages of contour analysis and geometric sampling.

# **5.4.3.** Unmask Sharp Filter

The UMF Unmask Sharp Filter is a cutting-edge method for lung cancer diagnosis that improves the sharpness and clarity of medical imaging data, especially in lung imaging modalities like computed tomography (CT) scans and X-rays. This method concentrates on enhancing the visibility of minute anomalies and structures in lung pictures, which are essential for precise diagnosis and timely identification of lung cancer. Fundamentally, the UMF Unmask Sharp Filter preserves significant anatomical information while improving picture sharpness through the use of sophisticated image processing methods [16][25]. This filter "unmasks" hidden elements in the image so that automated diagnostic systems and medical experts may more easily identify them by selectively enhancing high-frequency components and reducing noise. The UMF

Unmask Sharp Filter's increased sharpness has several benefits for lung cancer diagnosis. It enhances the visibility of aberrant structures, lesions, and tiny nodules that might be signs of lung cancer in its premature stage. Furthermore, by improving contrast and detail, the filter helps medical professionals distinguish between benign discoveries and those that are cancerous, resulting in more precise and trustworthy diagnoses. Additionally, the UMF Unmask Sharp Filter is compatible with a range of imaging modalities and software systems and is made to fit easily into current medical imaging processes. Its adaptability and simplicity of usage allow it to be applied in research and clinical practice contexts, which promotes broad acceptance and use. Through enhanced picture sharpness and clarity, the UMF Unmask Sharp Filter is a useful tool for improving lung cancer diagnosis. In the fight against lung cancer, this approach has the potential to enhance patient outcomes by improving diagnostic visibility, improving early detection rates, and facilitating more accurate diagnosis by uncovering subtle abnormalities.

## **5.4.4.** Binomial Distributed Chi-Square

Summing the squares of independent standard normal random variables yields the Binomial Distributed Chi-Square, frequently referred to as the Chi-Square Distribution, whose degrees of freedom are equivalent to the total number of categories minus one. In statistical analysis, this distribution is commonly seen, especially in goodness-of-fit and hypothesis testing [31]. Chi-Square Distribution is used in hypothesis testing to assess the difference between observed and predicted frequencies in categorical data. A substantial divergence between the observed and expected distributions can be found by statisticians by comparing the perceived frequencies with those predicted by a null hypothesis. When assessing the relationship between two categorical variables, the chi-square test for independence is one prominent use of the Binomial Distributed Chi-Square. Researchers can determine if there is a statistically significant association between the variables by calculating the chi-square statistic from the observed frequencies in a contingency table. Additionally, evaluating the goodness of fit, the degree to which an observed frequency distribution matches a theoretical or predicted distribution. Requires careful consideration of the Chi-Square Distribution. This application is frequently used to evaluate the suitability of statistical models and hypotheses in a variety of domains, including economics, psychology, and biology.

A fundamental probability distribution in statistical research, the Binomial Distributed Chi-Square provides useful tools for goodness-of-fit evaluation, independence assessment, and hypothesis testing.

# 5.4.5. Dataset Overview for Transfer Learning Model

The data includes one folder for normal cells and three distinct sorts of chest sarcoma: Squamous cell cancer, Adenocarcinoma, and large cell cancer. The test, train, and validation folders can be found inside the data folder, which is the main folder holding all of the step files. A training set is indicated by the term "train," a testing set by "test," and a validation set by "valid". The training set utilized 80% of the data during analysis, followed by the testing set (20%).

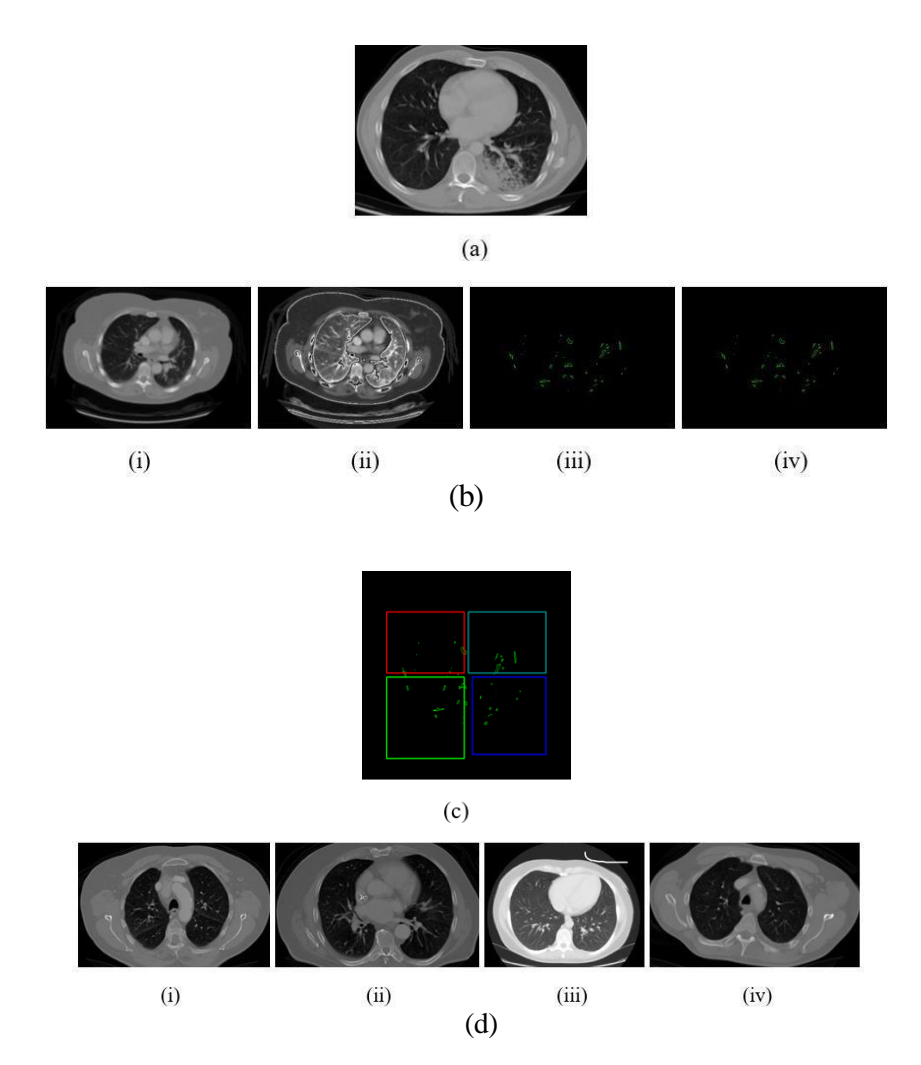


Figure 5.7 Sample images of the planned model.

(a) input picture, (b) pre-processed images, (c) segmented images, and (d) classified output images

Here, Figure 5.7 demonstrates the sample image of the proposed methodology. The input image is shown in (a). After that, the input image is pre-processed by using I-ADF and UMF, has been shown in (b). Then, b(i) represents the noise-removed image, b(ii) represents the contrast-stretched image, b(iii) represents the convex hull image, and b(iv) represents the edge enhancement image. Then, the segmented image is shown in (c), and finally, the classified output

is d (i) Adeno carcinoma, d (ii) large cell cancer, d(iii) squamous cell cancer, and d(iv) normal (without carcinoma). The outputs d (i), d (ii), and d (iii) represent the abnormal class.

# 5.5. Chapter Summary

In this, the chi-squared distribution is a fundamental tool in hypothesis testing because it makes it easier to compare actual and anticipated frequencies in categorical data. Statisticians can estimate the degree of disparity between the observed and predicted distributions to help them decide whether a hypothesis is true or not. The chi-square test for independence is a popular use of the Binomial Distributed Chi-Square that enables researchers to conclude if there is a statistically significant association between two categorical variables. Understanding the relationship between variables is obtained by computing the chi-square statistic from observed frequencies in contingency tables. When determining the goodness-of-fit of observed frequency distributions, the Chi-Square Distribution is an invaluable tool for comparing them to theoretical or predicted distributions. This evaluation is essential for confirming the reliability of statistical models and hypotheses in a variety of fields. As a fundamental idea in statistical analysis, the Binomial Distributed Chi-Square gives academics and professionals the means to test hypotheses, look at correlations between variables, and validate statistical models.

# CHAPTER 6 LUNG TUMOR SCREENING USING SMART DECISION-MAKING TECHNIQUES

#### 6.1. Advanced DNN Risk Screening for Early Lung Carcinoma

In this work, a Lightweight Advanced Deep Neural Network (DNN) Model is proposed for premature-stage lung carcinoma prediction by utilizing the SSCL-DNN and WDSI-LSO approaches as discussed in chapter 5. The proposed methodology comprises several key phases: pre-processing, feature extraction, segmentation, classification, feature selection, and risk assessment. Figure 6.1 presents the block diagram of the proposed model.

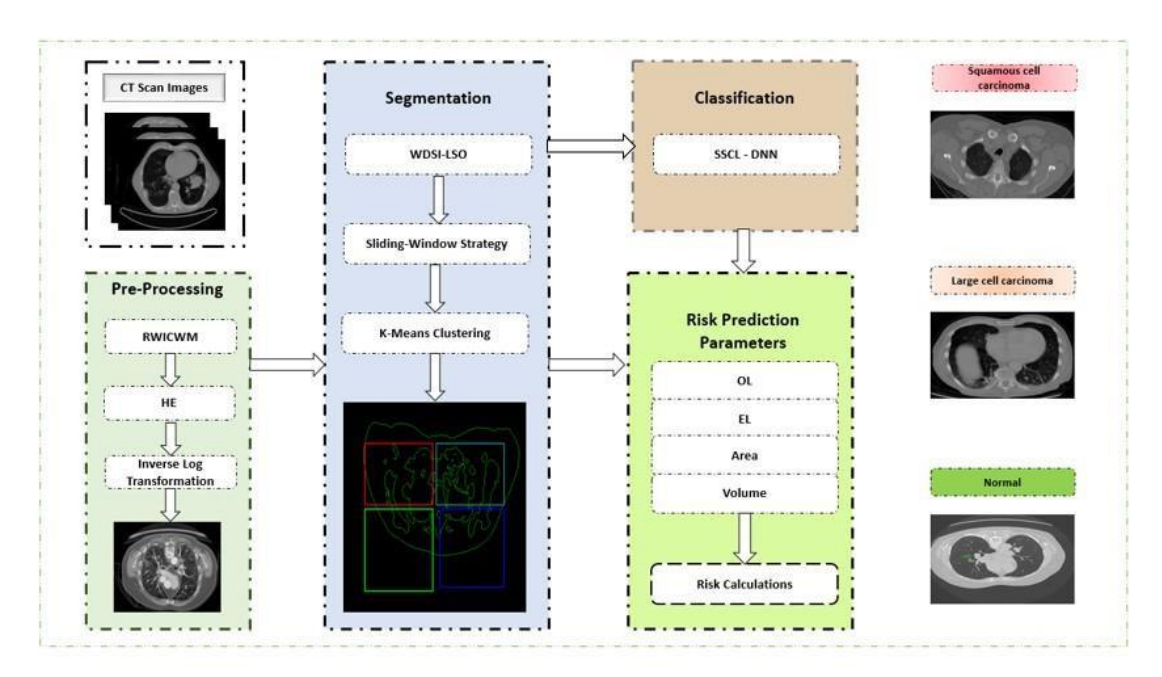


Figure 6.1 Block Diagram of Lightweight DNN for Lung Cancer Detection

# 6.1.1. Image Preprocessing for Lung CT Enhancement and Denoising

Three essential preprocessing steps are included in the proposed DNN model: RWICWM, K-means clustering, and WDSI-LSO. RWICWM enhances image quality by smoothing and highlighting important features. K-means clustering is used to segment the image and identify potentially malignant areas. WDSI-LSO ensures robust feature extraction by enhancing these regions and assigning scores based on their similarity to known malignant patterns. These steps collectively improve the precision and effectiveness of the DNN in identifying lung cancer.

#### **6.1.2.** Noise Suppression

By integrating wavelet transform and median filtering, the Ricker Wavelet Iterative Center Weighted Median Filter (RWICWM) improves medical images as discussed in section 5.2.1.

$$\psi(t) = \left(1 - rac{p^2}{\sigma^2}
ight) \cdot e^{rac{p^2}{2\sigma^2}}$$
 (Equation 6.1)

Here, p represents time or spatial location, and  $\sigma$  controls the width of the wavelet. The wavelet is symmetric and has a zero mean, making it effective for highlighting variations in intensity (like edges) and detecting features such as nodules in lung images. RWICWM improves significant characteristics and efficiently lowers noise in medical images to help in abnormality diagnosis.

#### **Image Contrast Enhancement Using Histogram Equalization (HE)**

A method for increasing image contrast by more uniformly spreading pixel intensity values is called histogram equalization, or HE. It determines how frequently each intensity level shows up in the image.

CDF: Compute the Cumulative Distribution Function

$$ext{CDF}(i) = \sum_{j=0}^{i} ext{histogram}(j)$$
 (Equation 6.2)

Histogram (j) is the frequency of occurrence of intensity level j in the image. CDF (i) gives the total number of pixels with intensity values from 0 to i. The CDF helps redistribute pixel intensity values to enhance image contrast, especially in low-light or low-contrast medical images like lung CT scans.

**Transform Intensity Levels:** 

$$I_{
m new}(x,y) = {
m round}\left(rac{{
m CDF}(I,(x,y)) - {
m CDF}_{
m min}}{1 - {
m CDF}_{
m min}} imes (L-1)
ight)$$
 (Equation 6.3)

This equation is used for histogram equalization, a contrast enhancement technique commonly applied in medical imaging to improve the visibility of anatomical structures.

I new (x, y): The new pixel value at location (x, y) after histogram equalization.

CDF (I(x, y)): The cumulative distribution function value for the pixel's original intensity. CDF  $CDF_{min}$ : The minimum non-zero value of the CDF (used to avoid division by zero).

L: The total number of possible intensity levels in the image (typically 256 for 8-bit images). round (.): Rounds the result to the nearest integer to maintain valid intensity values.

It increases the overall contrast and increases the visibility of image details. It is used in digital imaging, photography, medical imaging (e.g., improving X-rays), and other fields. Although histogram equalization works well, it can cause noise in photos by over-enhancement.

#### **Detail Enhancement Using Inverse Logarithmic Transformation**

An inverse logarithmic function is used to pixel intensities in the Inverse Log Transformation process, which improves image contrast. This technique is very helpful for bringing out the

details in dark areas of an image, which makes it better suited for visual evaluation. To emphasize the darker areas, the inverse log transformation is applied to every pixel intensity value:

$$I_{
m new}(x,y) = e^{lpha \cdot I(x,y)} - 1$$
 (Equation 6.4)

This equation is used in non-linear contrast enhancement methods, specifically exponential transformation.

I new (x, y): The transformed pixel value at coordinates (x, y).

I(x, y): The original intensity value of the pixel.

 $\alpha$ : A positive constant that controls the degree of enhancement.

e: The base of the natural logarithm.

The scaling constant that regulates the level of amplification is called  $\alpha$ . Usually, the image's dynamic range is taken into consideration while selecting  $\alpha$ .

# 6.1.3. Lung Nodule Segmentation for Region of Interest Identification

The technique of splitting a visual into relevant parts in order to separate items or areas of interest is known as image segmentation. K-means clustering is a useful technique for this. It divides the image into k k groups according to the intensity levels of the individual pixels.

# 6.1.4. Optimized Segmentation Using K-means and Dice Index

In image segmentation and clustering, to assess the overlap between expected and actual segments is the Sørensen-Dice Index (SDI), which is a measure of similarity between two sets. It can be utilized in conjunction with K-means clustering to improve the precision and analysis of clustering outcomes.

SDI: Sørensen-Dice Index.

$$SDI = \frac{2 \cdot |A \cap A|}{|A| + |A|}$$
 (Equation 6.5)

The Sørensen–Dice Index (SDI) is a similarity measure used to quantify the overlap between two sets, commonly applied in image segmentation to evaluate how well an algorithm's output matches the ground truth.

Where.

|A| and |B| are the sizes (number of elements) of sets A and B.

 $A \cap B$  is the number of elements in their intersection.

# Morphological Hole Filling for Complete Nodule Segmentation

In binary pictures, where the backdrop is represented by black pixels (value 0) and the foreground items are represented by white pixels (value 1), hole filling is a technique used to fill in the gaps or missing areas. This procedure entails the identification of holes, the selection of a marker within the hole, and the propagation of the marker's value across the hole until it reaches the boundary, utilizing morphological procedures such as dilation. By adding nearby pixels, the dilation procedure expands the region iteratively. The final product is integrated with the original image once the hole has been filled. Hole filling ensures that every space between items is filled in, resulting in a full representation. This improves image quality for more accurate feature extraction and analysis, especially for applications like optical character recognition, medical imaging, and object detection.

# **Localized Feature Detection Using Sliding Window Technique**

The sliding window strategy is a fundamental technique in image processing and computer vision used for object detection and feature extraction. This method involves moving a window of a fixed size across an image to analyze sub-regions sequentially.

# **Optimized Nodule Scoring Using WDSL-LSO Technique**

Stand for Weibull Distributed Scale Factor Integrated-Light Spectrum Optimizer for Pulmonary Nodule Detection. By using the Weibull distribution together with light spectrum optimization, this method improves the precision of pulmonary nodule detection, a sign of lung cancer. A flexible probability distribution that is frequently utilized in survival analysis and reliability engineering is the Weibull distribution. The two parameters that define it are scale  $(\lambda)$  and shape (k). The Weibull distribution's probability density function (PDF) is provided by:

$$f(x;\kappa,\lambda) = \kappa \cdot \lambda \cdot x^{\lambda-1} \cdot e^{-\lambda x}$$
 (Equation 6.6)

Where x represents the random variable, k represents the shape parameter, and  $\lambda$  is the scale parameter. This allows for better separation of Regions of Interest (ROIs) with varying intensities during thresholding, leading to improved detection of nodules of different sizes.

#### 6.1.5. Experimental Results and Comparative Performance Analysis

In this Section, we explain the limitations and findings from our studies on the identification of pulmonary nodules using different risk assessment approaches and semi-supervised and contrastive learning-based deep neural networks (SSCL-DNN). The results of combining the RWICWM and WDSI-LSO techniques produced noisy data. The performance achieved by combining K-means and WDSI-LSO is slightly lower. The specific difficulty with CNN-based methods may have to do with things like overfitting, insufficient training data, and lower accuracy and precision that can result from these conditions, as Table 6.1 shows. Because of their multistage processing pipeline, R-CNNs generally have slower inference speeds than other CNN architectures. This may be an unusual problem in some applications where real-time processing is necessary. ResNet-50 usually performs well in image classification tasks, but its performance may decline when applied to datasets with complex and heterogeneous features, which is why ResNet-50 leads to lower accuracy and precision. By combining approaches with PLCOm, this lightweight method, RWICWM + K-means + WDSI-LSO + PLCOm comes into play to solve specific challenges and produce superior performance in terms of accuracy and precision. The initial experiment (WDSI-LSO + RWICWM): 1. Accuracy of Nodule Detection: 95.3%. 2. Accuracy of Risk Assessment: 87.2%. A high nodule identification accuracy of 95.3% was achieved by combining the Ricker Wavelet Iterative Center Weighted Median Filter (RWICWM) and Weibull Distributed Scale factor integrated-Light Spectrum Optimizer-based pulmonary nodule detection (WDSI-LSO). However, at 87.2%, the risk assessment's accuracy was a little bit lower. The second experiment (WDSI-LSO + K-means): 1. Accuracy of Nodule Detection: 96.1%. 2. Accuracy of Risk Assessment: 86.5%. In this study, we used WDSI-LSO along with K-means clustering. In comparison with the first experiment, the risk assessment accuracy was slightly lower at 86.5% while the nodule detection accuracy remained high at 96.1%. The Third experiment (CNN): 1. Accuracy of Nodule Detection: 97.4%. 2. Accuracy of Risk Assessment: 86.8%. After one, R-CNN, VGG16, ResNet-50, and DenseNet-121 depict the accuracy with 96.2, 84.7, 94.5, and 92.8, as well as in terms of risk assessment, accuracy was 89.6, 83.2, 90.1, and 89.4, respectively.

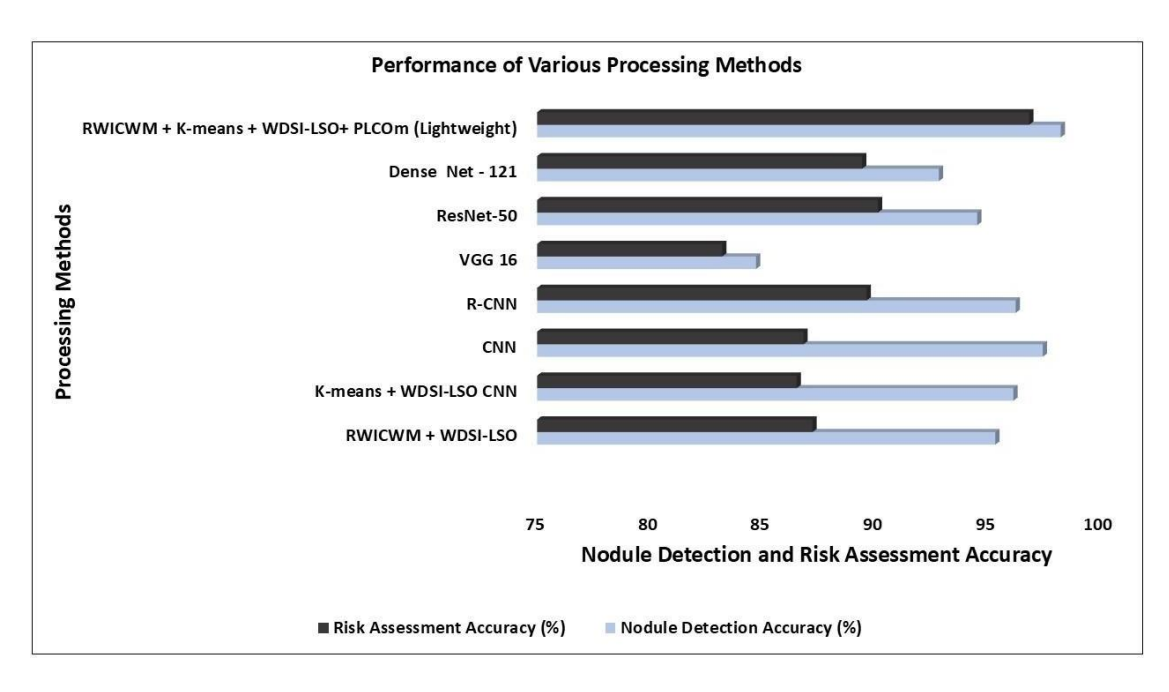
The Sixth experiment (RWICWM + K-means + WDSI-LSO + PLCOm): 1. Accuracy of Nodule Detection: 98.2%. 2. Accuracy of Risk Assessment: 96.8%. In Test 8, a longer pipeline that included RWICWM, K-means clustering, WDSI-LSO, and PLCOm risk assessment was used. The maximum nodule detection accuracy was attained with this thorough technique, at 98.2%, and the improved risk assessment accuracy was at 96.8%. These findings show that the eighth

experiment exceeds the previous experiments in terms of both nodule detection and risk assessment accuracy.

Table 6.1 Evaluation of the suggested models and the current models' performance

Experiment	<b>Processing Methods</b>	Nodule detection Accuracy (%)	Risk Assessment Accuracy (%)	
1	RWICWM + WDSI-LSO	95.3	87.2	
2	K-means + WDSI-LSO	96.1	86.5	
3	CNN	97.4	86.8	
4	R-CNN	96.2	89.6	
5	VGG16	84.7	83.2	
6	RESNET-50	94.5	90.1	
7	DenseNet-121	92.8	89.4	
8	RWICWM + K-means + WDSI-LSO + PLCOm2012	98.2	96.8	

For a variety of reasons, the RWICWM (Random Walk with Initial Cluster Weighted Method), K-means clustering, WDSI-LSO (Weighted Density-Based Spatial Clustering with Local Search Optimization), and PLCOm (Prostate, Lung, Colorectal, and Ovarian Cancer Screening Trial Mortality Risk Prediction Model) combination can be regarded as a lightweight technique. Compared to more complicated algorithms [25], these methods are computationally efficient and require less computing power for execution. They work well in real-time applications and with large datasets, and they also use less memory. Combining several approaches enables a combined strategy that makes the process lightweight and improves the performance as a whole. In a lightweight framework, RWICWM, K-means, WDSI-LSO, and PLCOm risk model perform in a robust and efficient way to produce reliable results. The proposed framework improves the accuracy and risk assessment, as well as reduces the computational time of execution as compared to previous methods. Optimized algorithms and effective data processing approaches make the suggested model lightweight.



Graph 6.1 Comparison of Preprocessing Techniques Based on Accuracy

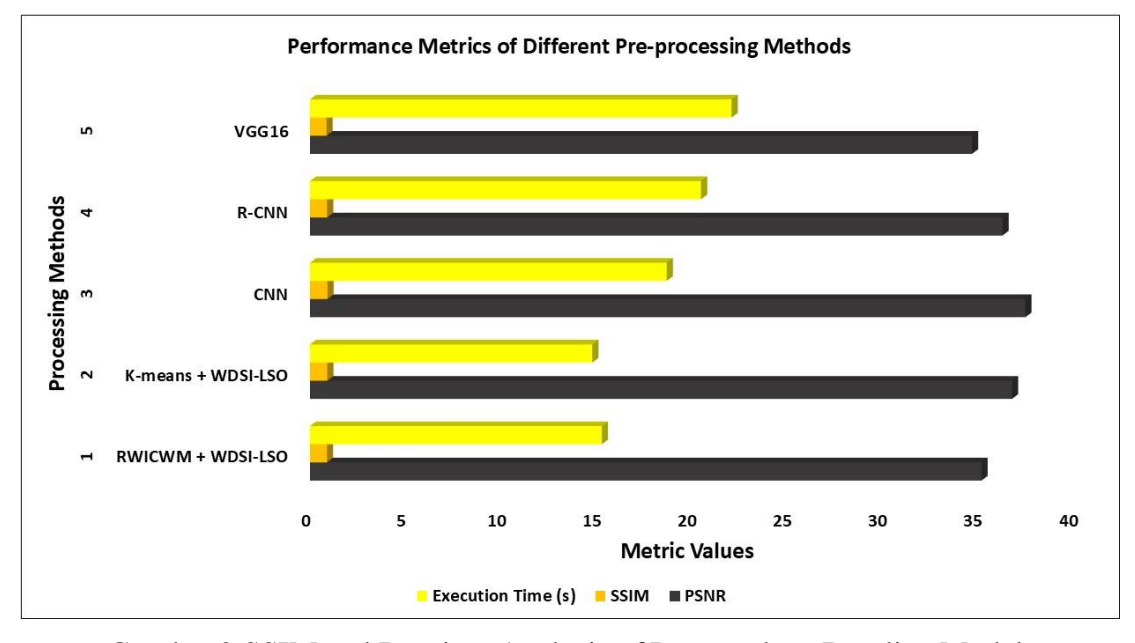
In the above Graph 6.1, a comparison of many preprocessing techniques for lung nodule detection and risk assessment is shown. Outperforming all other models, the suggested lightweight model (RWICWM + K-means + WDSI-LSO + PLCOm) achieves the maximum accuracy of 96.8% for risk assessment and 98.2% for nodule detection. While CNN and R-CNN models also demonstrated strong performance, VGG16 trailed the least in terms of accuracy across both measures. This illustrates the enhanced efficacy and potential of the suggested strategy for early lung cancer identification and risk assessment.

Various metrics, including the peak signal-to-noise ratio (PSNR) and structural similarity index (SSIM), etc., depending on a particular application, are used to perform a performance analysis of noise removal algorithms and present the findings in a table.

Table 6.2 Analysis of the existing and prospective models: Performance of PSNR, SSIM, and ET

Experiment	<b>Processing Methods</b>	PSNR	SSIM	Execution Time (s)
1	RWICWM + WDSI-LSO	35.2	0.89	15.3
2	K-means + WDSI-LSO	36.8	0.91	14.8
3	CNN	37.5	0.92	18.7
4	R-CNN	36.3	0.9	20.5
5	VGG16	34.7	0.87	22.1
6	ResNet-50	38.1	0.93	17.9
7	DenseNet-121	37	0.91	16.4
8	RWICWM + K-means + WDSI-LSO + PLCoM (Lightweight)	38.5	0.96	12.4

Peak Signal-to-Noise Ratio, which expresses how good the de-noised image is in comparison to the noisy real image. Better performance is indicated by higher values. A measure of how comparable the original and de-noised images are is called the Structural Similarity Index. The values in the range of -1 to 1 represent the time taken by the approach to remove noise from a particular image or batch of images. Execution time is a commonality.



Graph 6.2 SSIM and Runtime Analysis of Proposed vs. Baseline Models

Graph 6.2 offers a comparative analysis of different preprocessing techniques based on two performance parameters (SSIM and Execution time) for lung nodule detection. In addition to having the quickest execution time (12.4 seconds), the suggested lightweight model (RWICWM + K-means + WDSI-LSO + PLCOm) has the highest SSIM (0.96), suggesting greater image quality and structural similarity. While less efficient, other models such as ResNet-50 likewise provide good performance in terms of SSIM (0.93). On the other hand, VGG16 performs the worst according to all criteria. This demonstrates the efficacy and efficiency of the suggested methodology, which makes it the ideal choice for early lung cancer detection. In Figure 6.3, the Peak Signal-to-Noise Ratio (PSNR) is used to compare various preprocessing techniques for lung nodule detection in the picture. The recommended lightweight model (RWICWM + K-means + WDSI-LSO + PLCOm) produced the highest PSNR of 38.5 out of all the evaluated approaches, indicating a superior image quality. Additionally, ResNet-50 did well, with a PSNR of 38.1. On the other hand, VGG16 had the lowest PSNR (34.7), indicating lower-quality images. This comparison demonstrates how much more efficient the suggested lightweight model is in generating high-quality images. This makes it a viable method for the early detection of lung cancer. Table 6.2 displays the accomplishment analysis of the suggested model and the current models in terms of ET, PSNR, and SSIM. A model that performs well has a lower ET value and higher PSNR and SSIM values. The suggested model achieves an ET value of 12.4, which is less than that of the Prior models. Comparably, the suggested model outperforms the current models as evidenced by the PSNR and SSIM values it achieves, which are 38.5% and 0.96, respectively. Thus, it may be said that the suggested model removes noise more effectively.

### 6.2. TL-Based P-ResNet Framework for Early Lung Cancer Detection

The prediction of lung carcinoma and risk screening model at the premature-stage was proposed in this work by using TL-based P-ReLUResNet with B-RGS techniques. The suggested method goes through the following phases: First, pre-processing, segmentation, feature extraction, feature selection, classification, and risk screening. The Workflow of the suggested model is shown in Figure 6.2.

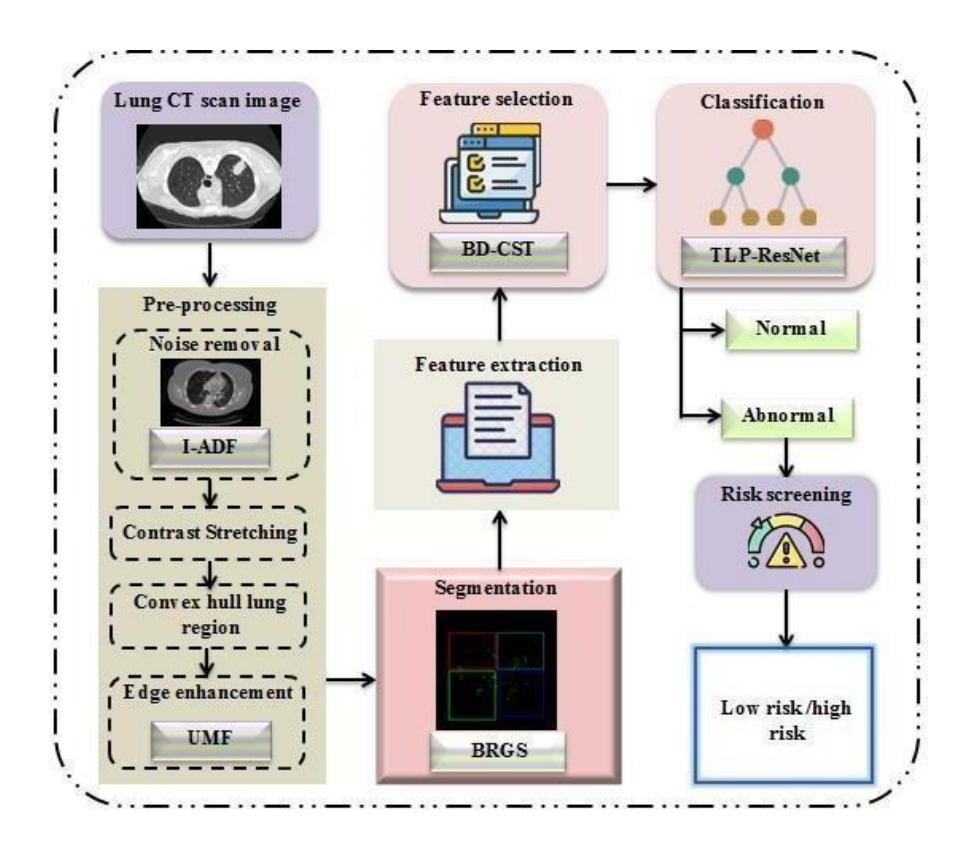


Figure 6.2 Architecture of the TL-Based P-ReLUResNet (P-ResNet) Risk Screening System

# 6.2.1. Enhanced Filtering Techniques for Lung CT Image Preprocessing

Initially, the lung computerized tomography (CT) scan image (I), which was gathered from the publicly available datasets [52], is pre-processed. Pre-processing is the initial step taken to improve the quality of an image. Pre-processing involves a number of stages, which are described below: noise removal, contrast stretching, convex hull lung area, and edge enhancement.

### Noise Suppression Using Improved Anisotropic Diffusion Filtering (I-ADF)

The input image (I) contains noise, such as Gaussian and Poisson noise should be removed. In this work, noise removal was done by using I-ADF. ADF is a method for removing noise and distortion from an image without creating any edge blur. However, ADF's constant diffusion magnitude has an impact on the filter's SNR (signal-to-noise ratio). That is the reason why, to overcome this problem, the work proposed intra-class variance by replacing local variance. The variance within the class is termed as intra-class variance. Hence, the proposed method is named I-ADF.

Let the diffusion matrix  $(D_{mt})$  that shares the eigen vectors with eigen values related to the The level of noise is defined as,

$$\alpha_1 = 1 - C$$
 (Equation 6.7)

$$lpha = 1 - C + rac{3}{2}(1-C)_{
m planar}$$
 (Equation 6.8)

$$lpha = 1 - C + rac{3}{2}(1-C)_{
m planar} + 3(1-C)_{
m linear}$$
 (Equation 6.9)

Where  $\alpha_1, \alpha_2$ , and  $\alpha_3$  denotes the eigen values, C represents the gain coefficient, and  $C_{planar}$ 

and  $C_{linear}$  represents the gain in a local planar neighbourhood and local linear neighbourhood, respectively, which is given by,

$$C = C(I, \operatorname{Var}(I))$$
 (Equation 6.10)

$$C_{
m planar} = C(I, {
m Var}(I), e_2, e_3)$$
 (Equation 6.11)

$$C_{
m linear} = C(I, {
m Var}(I), e_2, e_3)$$
 (Equation 6.12)

Where,  $e_k, k \in [1,b]$  belong to eigenvectors,  $\langle I \rangle$  represent the local mean assessment of the image (I), and Var(I) represents intra-class variance, which is the variance taken within the class, which is calculated by,

$$\mathrm{Var}(I) = \sum (I - \bar{I})^2$$
 (Equation 6.13)

The equation shows how much the pixel values in an image vary from the average brightness of the image.

*I*: a pixel value in the image.

 $\bar{I}$ : the mean (average) of all pixel values.

 $(I - \overline{I})^2$ : the squared difference from the mean.

 $\Sigma$ : adds up all these squared differences.

So, variance Var(*I*) gives a measure of how much the pixel values spread out higher variance means more contrast or detail in the image.

$$I=rac{1}{25}\sum_{b,c}I(z+b\cdot e_2+c\cdot e_3)$$
 (Equation 6.14)

$$I = rac{1}{25} \sum_{b,c} I(z + b \cdot e_2 + c \cdot e_3)$$
 (Equation 6.15)

These are discrete approximations used in anisotropic diffusion filtering (likely an Intra-class variance Anisotropic Diffusion Filter, or I-ADF.

*I*: Filtered intensity at pixel location z.

e2, e3: Directional unit vectors (like along horizontal and vertical directions in the image).

b, c: Constants or step indices (used to control pixel neighborhood in those directions).

z: Current pixel position.

The summation: Averaging over a set of neighboring pixels located at positions offset by be2+ce3Therefore, the diffusion matrix may be expressed as follows:

$$mt = egin{bmatrix} lpha_1 & 0 \ 2 & 0 \ 0 & lpha_3 \end{bmatrix}$$
 (Equation 6.16)

α1: Diffusion coefficient in the x-direction (horizontal).

α3: Diffusion coefficient in the z-direction (depth, or slice direction in 3D CT imaging).

Os in off-diagonal entries: This means no cross-directional diffusion, so diffusion occurs independently in x, y, and z directions.

mt: transformation matrix.

The corresponding diffusion equation is written as the sum of three diffusion terms, which is given as,

$$rac{\partial I(z,t)}{\partial t} = 
abla \cdot (D_{mt} 
abla I)$$
 (Equation 6.17)

I(z, t) Image intensity at position z and time t.

 $\frac{\partial I}{\partial t}$ : Rate of change of image intensity over time.

 $\nabla$ I: Gradient of the image (detects edges).

 $D_{mt}$ : Diffusion matrix/tensor (controls how much smoothing happens in each direction).

 $div(D_{mt}\nabla I)$ Divergence operator that spreads intensity values (i.e., smoothing), but only in directions controlled by the diffusion tensor. This equation tells the image how to evolve to reduce noise while not blurring important structures like edges or nodules. Equation (6.18) represents a composite formulation that integrates divergence and gradient-based terms weighted by coefficients related to different structural components. It is defined as:

$$= 6 \left[ \frac{1}{\operatorname{div} \left( (1 - C_{\operatorname{planar}}) \cdot \nabla I \right)} + \frac{1}{\operatorname{div} \left( (1 - C_2) \cdot \nabla I \right)} + \frac{1}{\operatorname{div} \left( (1 - C_3) \cdot \nabla I \right)} \right]$$
(Equation 6.18)

Where,

 $\nabla I$ : denotes the gradient of the image I, capturing intensity changes across spatial coordinates. div(·): represents the divergence operator, used here to measure the net flow of the vector field defined by the product of (1–C) terms and  $\nabla I$ .

 $C_{planar}$ ,  $C_2$ , and  $C_3$  are context-specific coefficients derived from structural features such as planar and linear components in image segmentation or processing tasks.

The projection of the gradient in the direction of  $e_3$  and  $\nabla I$  represents the projection of the gradient of (I). Finally, the noise-removed image is obtained as  $N_{rem}$ . After that, contrast stretching is applied to the picture with the noise eliminated.

### **Contrast Enhancement Using Intensity Range Stretching**

It is an image heightening method used to increase the contrast in the image  $(N_{rem})$  after noise has been removed by extending the range of intensity values to a desired range of values. Therefore, the contrast-stretched image is expressed as  $(S_{cont})$ .

$$S_{\text{cont}} = \left[ S_{\text{cont}(1)}, \ S_{\text{cont}(2)}, \ S_{\text{cont}(3)}, \ \dots, \ S_{\text{cont}(a)} \right]$$
 (Equation 6.19)

#### Where

 $S_{cont}(a)$  represents several contrast-stretched images. Then, these contrasted stretched images are given to the convex hull operation.

#### **Isolation of Lung Region Using Convex Hull Algorithm**

The convex hull is a set of pixels included in the smallest convex polygon that surrounds all white pixels in the input. In this study, the lung area is separated from the contrast stretched picture.

( $S_{cont}$ ) Using a convex hull. Therefore, the separated lung region is expressed as  $L_{reg}$ . Then, this lung region is fed into the edge enhancement operation.

### **Enhanced Lung Boundary Detection Using Unsharp Masking Filter (UMF)**

Edge enhancement is a technique that enhances the edge contrast of  $L_{reg}$ . In this work, edge enhancement was done by using UMF. The fundamental idea behind UMF is to add to the original image by scaling and highlighting a portion of it. The edges or high-passed pixels from the provided equation are removed throughout this filtering step.

$$A_{
m ed} = \gamma \cdot r_s^{
m reg}$$
 (Equation 6.20)

Where  $A_{ed}$  represents the augmented edge,  $\gamma \cdot r_s^{\text{reg}}$  represents the boundary mining kernel, and Represents, grey content in the image L. The improved picture (E) is created using the UMF technique as,

$$E = Q + \eta \cdot A_{\rm ed}$$

(Equation 6.21)

Where is the gain factor that determines the potency of the boosted edge? Where  $\eta$  indicates the gain factor that determines the potency of the augmented edge  $(A_{ed})$ .

The above equation is a generic energy function, often found in optimization algorithms and physical models, including image enhancement or edge detection.

### 6.2.2. Precise Lung Image Segmentation Using BRGS Optimized with BD-COA

After pre-processing, the segmentation process is done to segment to enhance the image (E). In this work, the image was segmented into four parts by using the BRGS technique, which provides high segmentation precision. RGS divides the image by combining pixels into a larger region based on predefined seed pixels, growth criteria, and stop conditions. But it leads to the

overlapping shadow of vessels, tissue mass, and ribs when used in CT images [73]. So, to overcome this problem, the knuckle point used in RGS is selected by using the Bates distributed Coati Optimization algorithm (BD-COA). Here, COA is selected for its high meta-heuristic property, which gives a conformity index by selecting the highest conformity value. However, COA prompts high computational complication. So, to address this issue, the Bates distribution (BD) was used to calculate the random number used in the algorithm. Therefore, the proposed method is named BRGS.

Initially, an improved image (E) is fed into the RGS process. Let the seed point selection be the premature stage of the RGS process. In this work, the seed point  $(S_E)$ , which is the knuckle point of the lung image, was selected by using COA. The population-based metaheuristic algorithm known as COA was inspired by the behaviors and habits of the natural coati. Let the coati be initialized as the seed point  $(S_E)$ . The locality of coatis in the (search–space) is first set at random as,

$$P_{x,y}(SE)=lwy+\zeta\cdot(up-lwy),\quad x=1,2,\ldots,m;\quad y=1,2,\ldots,n$$
 (Equation 6.22)

Where  $P_{x,y}(S_E)$  represents the position of  $x^{th}$  coati of  $y^{th}$  decision variable, lw and up represent both (upper and lower) bounds of  $y^{th}$  decision variable, here, amount of coati is denoted by m, n denotes the quantity of decision variables, and,  $\varsigma$  denotes a random number, which is calculated by using BD. BD represents the distribution of the mean of a random variable uniformly distributed from 0 to 1, which reduces the complication of the described model. Therefore, the random number is determined using [28].

$$\zeta = rac{1}{U_0} \sum_{o=1}^{U_0} U_o$$
 (Equation 6.23)

Where,  $U_0$  appears to represent an upper limit for summation over index o. Then, the population of the coati is represented by,

$$\begin{bmatrix} P_{1}(SE) \\ P_{2}(SE) \\ \vdots \\ P_{m}(SE) \end{bmatrix}_{m \times 1} = \begin{bmatrix} P_{1,1}(SE) & \cdots & P_{1,y}(SE) & \cdots & P_{1,n}(SE) \\ P_{2,1}(SE) & \cdots & P_{2,y}(SE) & \cdots & P_{2,n}(SE) \\ \vdots & \ddots & \vdots & \ddots & \vdots \\ P_{m,1}(SE) & \cdots & P_{m,y}(SE) & \cdots & P_{m,n}(SE) \end{bmatrix}_{m \times n} \text{ (Equation 6.24)}$$

This is a structured matrix representation of a feature probability map P(SE)P(SE)P(SE) derived from segmentation or extracted features (SE).

P1(SE),...,Pm(SE): Vector of probabilities or feature responses for m different segmented elements, such as regions or pixels.

 $P_{i,j}(SE)$ : Probability value or feature strength of the  $i^{th}$  segment or element responding to the  $j_{th}$  feature or attribute from segmentation (SE).

The full matrix is of size.  $m \times n$  Where:

m Number of samples, regions, or segmented patches.

n Number of extracted features or attributes from each region

Equation (6.24) represents the formation of a feature probability matrix P(SE) where each entry  $P_{i,j}(SE)$  indicates the response of the  $i^{th}$ segmented region to the  $j^{th}$ Extracted feature. This matrix helps quantify and organize feature importance across segmented lung regions, supporting accurate classification and risk assessment of lung nodules.

Different values for the problem's fitness will be determined and depending on where potential solutions are placed in the choice variable. The foundation for assessing the study's fitness value is the classification accuracy. The advantage of physical health is provided by

$$\operatorname{fit} = egin{bmatrix} \operatorname{fit}\left(P_{1}(SE)
ight) \\ \operatorname{fit}\left(P_{2}(SE)
ight) \\ dots \\ \operatorname{fit}\left(P_{x}(SE)
ight) \\ dots \\ \operatorname{fit}\left(P_{m}(SE)
ight) \end{bmatrix}_{m imes 1} \ ext{(Equation 6.25)}$$

 $P_i(SE)$ : Feature vector (or probability score) of the  $i^{th}$  Segmented element derived from segmentation and extraction operations.

 $fit(P_i(SE))$ : A fitness function is applied to each segment to evaluate its significance. (e.g., how likely it represents a tumor nodule).

Equation (6.25) calculates the fitness values for each segmented region based on the extracted features. Coati's position is updated depending on two behaviors: its defense mechanism against entering iguanas and its escape plan from predators.

### 6.2.3. Extraction of Discriminative Features from Segmented Lung Regions

Feature extraction is the process of mining features from the segmented picture. Here, features such as gradient features, profile-based features, on-vessel on-rib, and spectral flatness are considered. The measures are removed from the segmented image  $(S_{eg})$ . Below is an explanation of these features.

## **Extraction of Gradient-Based Image Descriptors**

The gradient characteristics from the  $(S_{eg})$ , are retrieved for each sub-image. Based on the distance between two modes, as well as the ratio of modes normalized by their separation and their respective statistical properties like skewness, kurtosis, and bimodality coefficient, the area under the modes is computed. Therefore, the gradient features are expressed as  $G_{mea}$ .

### **Spectral Feature Quantification Using Flatness Measure**

Based on  $(G_{mea})$ For each sub-image, the spectral flatness measure is calculated, which gives a measure of the edginess of the image. $(S_{eg})$ . It can be expressed as the Fourier coefficient magnitudes of the image divided by their arithmetic mean or the geometric mean. Therefore, the spectral feature measure is stated as  $SP_{flat}$ .

### **Profile-Based Attribute Extraction for Enhanced Discrimination**

The profile-based characteristics are retrieved from the normalized, smoothed magnitude of each sub-image of  $(S_{eq})$ And are described below.

- **Rib cross:** The profiles on the edge representation are taken in order to extract this feature. When a rib edge is present, the profile should have a peak assigned score of  $prof(\varphi)=1$ .
- ➤ **Peak Ratio:** Determine the average and maximum peak-to-minimum-peak ratio for every extracted profile.
- > Slope Ratio: Calculates the profile's first-order derivative and takes the average.
- Slope smoothness: This characteristic determines how smoothly the slope is. Determine the steepness value and average after calculating the second-order. Derivatives for every profile. Therefore, the profile-based features are stated as  $prof_{fea}$ .

$$\mathrm{Slope}_{\min\max} = \frac{\min\left(\mathrm{prof}(\mathrm{diff})\right)}{\max\left(\mathrm{prof}(\mathrm{diff})\right)} \quad \text{(Equation 6.26)}$$

Where.

prof(diff): This represents the profile of the difference in intensity or feature values across an image segment (likely a line or edge profile).

 $\min(prof(diff))$  The minimum slope or gradient value observed in the profile.  $\max(prof(diff))$  The maximum slope or gradient value observed in the profile.

Equation 6.26 calculates the relative slope ratio in a profile of intensity or feature differences. This metric helps to assess uniformity or variation in edges or texture across a region. A lower value may indicate sharper contrast or prominent edges (ideal for tumor borders), while a higher ratio indicates uniform texture or less variation, which might represent normal tissue.

On Rib: This feature will determine whether or not there is a cancer [66] and will assign it a feature value. This entails rib edges being located. If the distance between the centroid and the segment is less than the inter-rib (difference between the centroid and the rib), cancer is suspected on the rib. On-rib characteristics are computed using segment length, slope, and eccentricity parameters. Consequently, the on-rib features are expressed as  $O_{rib}$ .

*On-Vessel:* On-vessel properties are computed on these edges based on their length and eccentricity. As indicated by (predicting the length), measure the lengths of all the vessels edges and select the first two with the longest lengths.

$$Vessel_1 = \frac{max\_leng_1 \times max\_leng_2}{height \times width}$$

(Equation 6.27)

max\_leng1, max\_leng2: These likely represent the major and minor axis lengths of a vessel-like structure (possibly elliptical). Height, width: Dimensions of the entire image region or bounding box being analyzed. This equation calculates the normalized area of a vessel-like structure relative to the full image region. Specifically, it compares the approximate area of the vessel (as a bounding rectangle or ellipse) to the total image area. A higher value of Vessel suggests a larger vessel area relative to the image, which can aid in identifying abnormal vessel expansion or density associated with lung disease. Then determine the lowest distance between each edge and the subimage's center, choose the least distance (min dist) between them all, and get the inverse value, which is given by,

$$vessel_2 = \frac{1}{\min (\min dist)}$$
 (Equation 6.28)

Therefore, the on-vessel features are expressed as  $O_{vessel}$ . Finally, the extracted features are given by,

$$ext{Fea}_{ ext{ext}} = [G_{ ext{Mea}}, \; Sp_{ ext{flat}}, \; ext{prof}_{ ext{fea}}, \; O_{ ext{rib}}, \; O_{ ext{vessel}}]$$
 (Equation 6.29)

Where  $Fea_{ext}$  represents the extracted features. The feature selection procedure then uses these extracted characteristics as input [63]. Equation 6.29 explains that feature extraction (Fea<sub>ext</sub>) was carried out to derive critical information for accurate classification. The selected features include Mean intensity (Mea), Spectral Flatness (flat), general image-based features (fea), Rib proximity features (rib), and Vessel adjacency features (vessel). These collectively enhance the discrimination capability of the classifier, especially in differentiating cancerous from non-cancerous regions.

## 6.2.4. Selection of Optimal Features Using Statistical and Spatial Criteria

After feature extraction, the most significant features are determined from the extracted features by using the BD-CST algorithm. CST is a numerical test that quantifies the deviation from the expected distribution and assesses the feature event regardless of the class value. Nevertheless, it had a quick processing time, and one of its limitations is that the significance level can only be chosen at random, which could slow down processing. In order to address this issue, the work suggests using the binomial distribution to determine the significance level, which shortens the model's processing time. Consequently, BD-CST is the introduced model's name. The following are the steps in the BD-CST method:

- Describe your hypothesis and your analysis plan.
- Analyze sample records and predict the outcomes.

Specify hypothesis and analysis plan: The BD-CST model receives the extracted characteristics  $(Fea_{ext})$ , as input at first. After that, the hypothesis is explained. The next section of the analytical plan explained how to use model data to either confirm or deny the hypothesis. Test procedure and importance rank need to be defined in the strategy.

**Examine sample data and predict the results:** In this step, the test's degree of freedom, Predictable frequency, test value, and probability value must all be determined by analyzing the chosen specimen data. You can figure out the degree of freedom  $(D_{fr})$  by using,

$$D_{
m fr} = (\omega - 1) imes (\zeta - 1)$$
 (Equation 6.30)

Where  $\varpi$  denotes the level count for one category variable and,  $\zeta$  denotes the level count for another categorical variable. The features ( $Fea_{sele}$ ) are finally chosen by,

$$\text{Fea}_{\text{sele}} = \frac{e \cdot (WZ - YX)^2}{(W+Y)(X+Z)(W+X)(Y+Z)}$$
 (Equation 6.31)

Where W represents the number of times  $Fea_{ext}$  and  $\zeta$  co-occurs, X delineates the amount of times  $Fea_{ext}$  appears without  $\zeta$ , Y represents the number of times  $\zeta$  appears without  $Fea_{ext}$ , Z number of times neither  $\zeta$  nor  $Fea_{ext}$  occurs.

### 6.2.5. Classification of Lung Abnormalities Using the Proposed P-ResNet Model

After feature selection, the classification process is done to classify whether the selected features  $(Fea_{sele})$  are healthy or abnormal. In this work, classification was done by using a transfer learning-based P-ResNet algorithm [12], which significantly enhanced the performance of the network with more layers. ResNet uses skip connection, which connects activation of the layer to further layers by skipping some layers in between that forming a residual block [60]. Still, it has an impact due to a low learning rate and a large calculation time caused by the kernel activation function. Therefore, transfer learning (TL) based work was suggested as a solution to this. TL is essentially a machine learning technique that uses a model that has already been trained to serve as the foundation for a new assignment. Using the TL approach strengthens and increases the security of the system. The model's effectiveness is also increased by using the P-ReLU activation function [13]. As a result, P-ResNet is the designed model's name. Here, the architecture of the P-ResNet is shown in Figure 6.3.

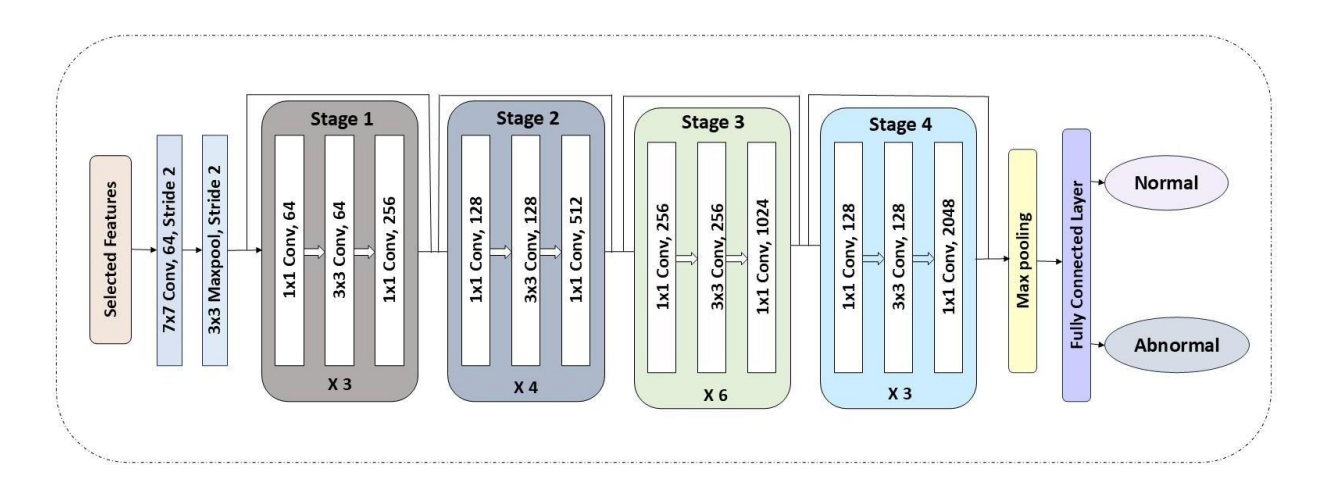


Figure 6.3 Architecture of the Proposed P-ResNet Model

Source: An Advanced Lung Carcinoma Prediction and Risk Screening Model Using Transfer Learning.

The four sets of layers that comprise the P-ResNet are the activation layer, the convolution layer, the pooling layer, and the fully connected layer. Initially,  $(Fea_{sele})$  is specified as input to the convolution layer. To categorize the output throughout this process, feature mapping was carried out. The output of the convolution layer is given by

Conlyr = 
$$\mu \sum (\text{Fea}_{\text{sele}} \cdot w)$$
 (Equation 6.32)

This equation 6.32 defines the output of a convolutional layer in the deep neural network. It takes the selected features (Feasele), multiplies them by their corresponding weights (w), sums them up, and scales the result by a factor  $\mu$ . This process enables the network to learn important patterns in lung CT images, such as nodules or abnormal tissues, essential for accurate lung cancer classification. The P-ReLU activation function, which generalizes the conventional rectified unit and has a slope for negative values [64], is given by, where w indicates the weight and  $\mu$  represents the P-ReLU activation function [35].

$$\mu = egin{cases} \mu, & ext{if } \mu > 0 \ 0, & ext{if } \mu \leq 0 \end{cases}$$
 (Equation 6.33)

Where k denotes the negative slope, and after that, the consequence of the convolution layer. is fed into the maximum pooling layer  $(poly_{lyr})$  which decreases the dimension of the feature map by selecting relevant features, which are given by,

$$ext{pollyr} = \max\left(rac{ ext{conlyr} - w}{\kappa}
ight)$$

(Equation 6.34)

This equation 6.34 represents a max pooling operation applied to the output of a convolutional layer. It first normalizes the convolution result (convlyr) by subtracting a bias w and dividing by a scale factor  $\kappa$ . The max function then selects the strongest (maximum) activation. This helps the model retain the most important features while reducing the spatial size, improving efficiency, and reducing overfitting. The above represents the stride length that decides the number of pixels shifts by the various weights.

### 6.2.6. Risk Screening of Lung Carcinoma Using: TL-based P-ReLUResNet

Risk screening is a process of identifying the risk of harm [69] and then minimizing the risk that has been recognized. In this work, during the risk screening process [40], the on-rib features of abnormal images,  $(ANN_{mrl})$  were considered because the risk of carcinoma can be easily detected by using on-rib features as high risk or low risk, which is given by,

$$Rk_{
m screen} = egin{cases} Rk_{
m high}, & ext{if carcinoma is present} \ Rk_{
m low}, & ext{if carcinoma is not present} \end{cases}$$

(Equation 6.35)

Where,  $Rk_{screen}$  represents the risk screening [72],  $Rk_{high}$  denotes high risk, and  $Rk_{low}$  denotes low risk. Finally, the patients were screened and treated.

## 6.2.7. Results and Discussion on Proposed Models' Effectiveness

This module compares the results of the proposed framework with those of existing models that are currently in use in order to assess the effectiveness of the model. The Python development environment is used to implement the recommended paradigm. For the achievement analysis, information from the upper body is collected, particularly from the Chest Computed Tomography (CT) scan Image Lung dataset.

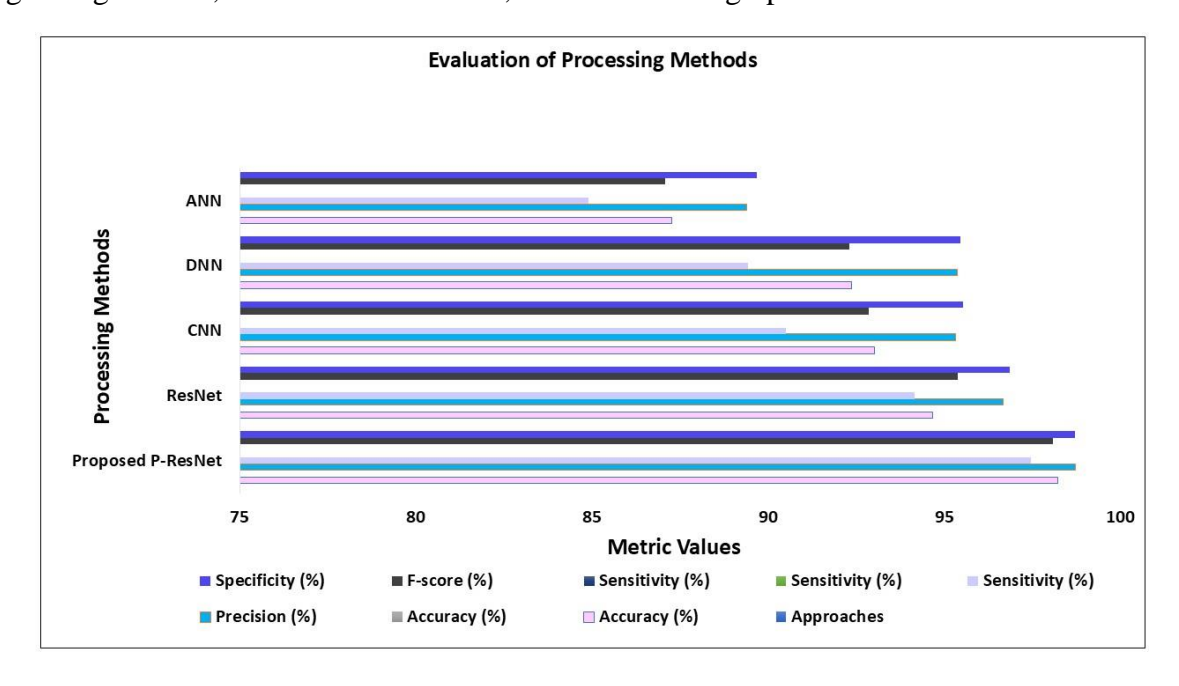
#### **Classification Accuracy Evaluation of Proposed Models**

The error rate, training time, recall, sensitivity, specificity, F-score, false positive rate (FPR), false rejection rate (FRR), false negative rate (FNR), and accuracy are all confirmed by the performance evaluation of the proposed TL-based P-ReLUResNet. The results are then contrasted with those of the current models, including ResNet, CNN, DNN [31][39], and Artificial Neural Networks (ANN) [41][46].

Table 6.3 Comparative Assessment of Proposed vs. Current Lung Cancer Models

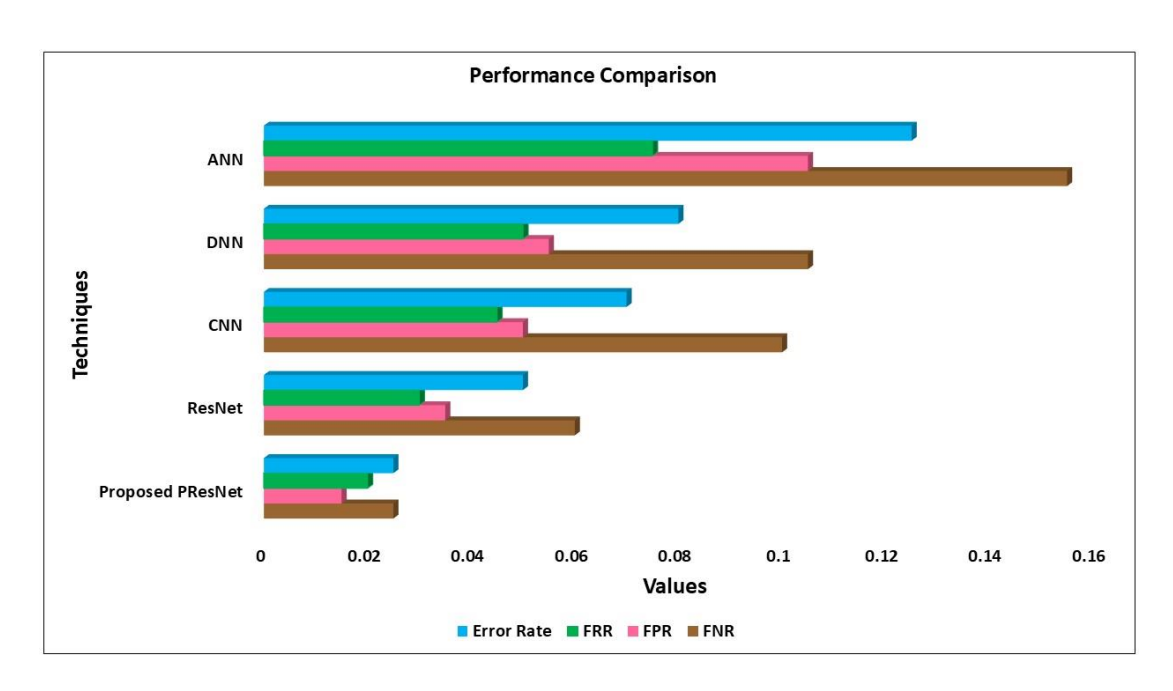
Approaches	Accuracy (%)	Precision (%)	Sensitivity (%)	F-score (%)	Specificity (%)
Proposed P-ResNet	98.21	98.71	97.46	98.08	98.71
ResNet	94.66	96.66	94.15	95.39	96.87
CNN	93.01	95.33	90.5	92.85	95.54
DNN	92.38	95.36	89.44	92.3	95.45
ANN	87.26	89.4	84.9	87.09	89.67

The developed approaches and the current models' performance analyses in terms of F-score, specificity, sensitivity, recall, accuracy, and precision are shown in Table 6.3. Greater values for accuracy, precision, recall, sensitivity, specificity, and f-score specify improved performance from the model. The precision of the suggested model is 98.21%, which is higher than that of the existing models, which achieve accuracies of 94.66% for ResNet, 93.01% for CNN, 92.38% for Lightweight DNN, and 87.26% for ANN, as shown in the graph.



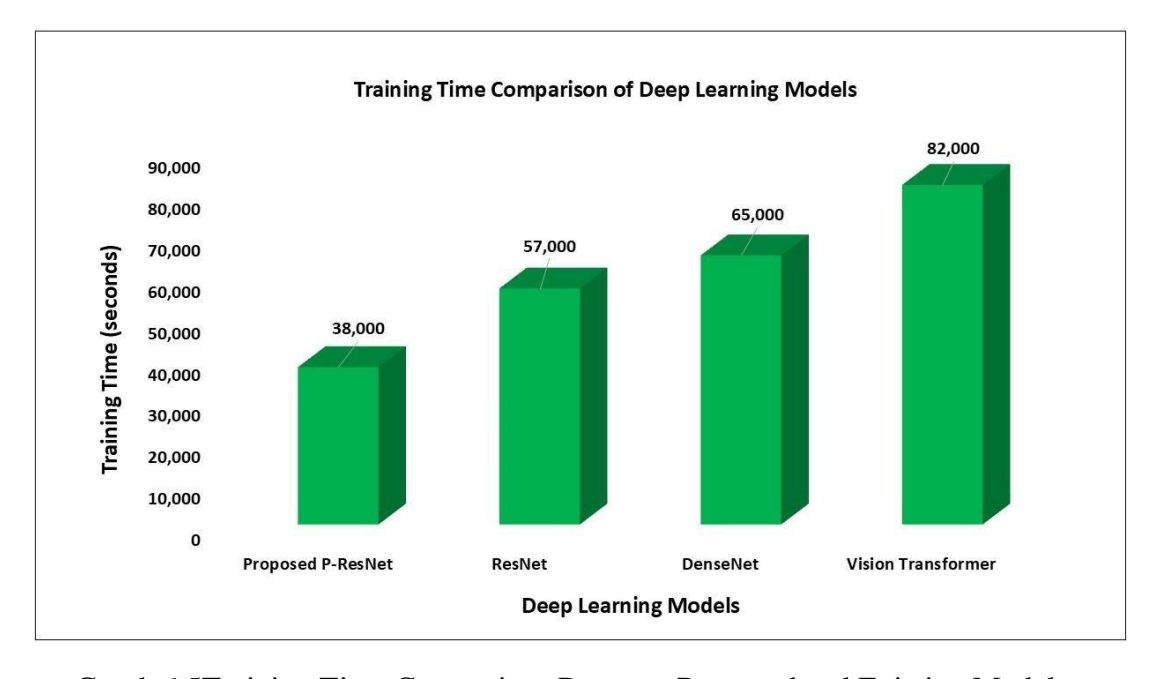
Graph 6.3 Evaluation of processing methods

Additionally, the suggested framework surpasses the present framework in terms of accuracy, recall, sensitivity, specificity, and F-score, which are each 98.71%, 97.46%, 98.71%, and 98.08%, respectively. Consequently, it may be concluded that the proposed framework outperforms previous models.



Graph 6.4 Performance Comparison of P-ResNet with Existing Models

The comparison between the estimated framework and the created models in terms of FNR, FPR, FRR, and error rate is displayed above in Graph 6.4. The model performs better when the FNR, FPR, FRR, and error rate are lower. The FNR values achieved by the implemented technique and the current models are 0.02531 and 0.0844, respectively, whereas the FNR values obtained by the current models are 0.09493 (CNN), 0.1055 (Lightweight DNN), and 0.15094 (ANN). Similar to this, the projected model's FPR, FRR, and error rate are, respectively, 0.0128, 0.0127, and 0.0191, showing the better performance of the suggested model.

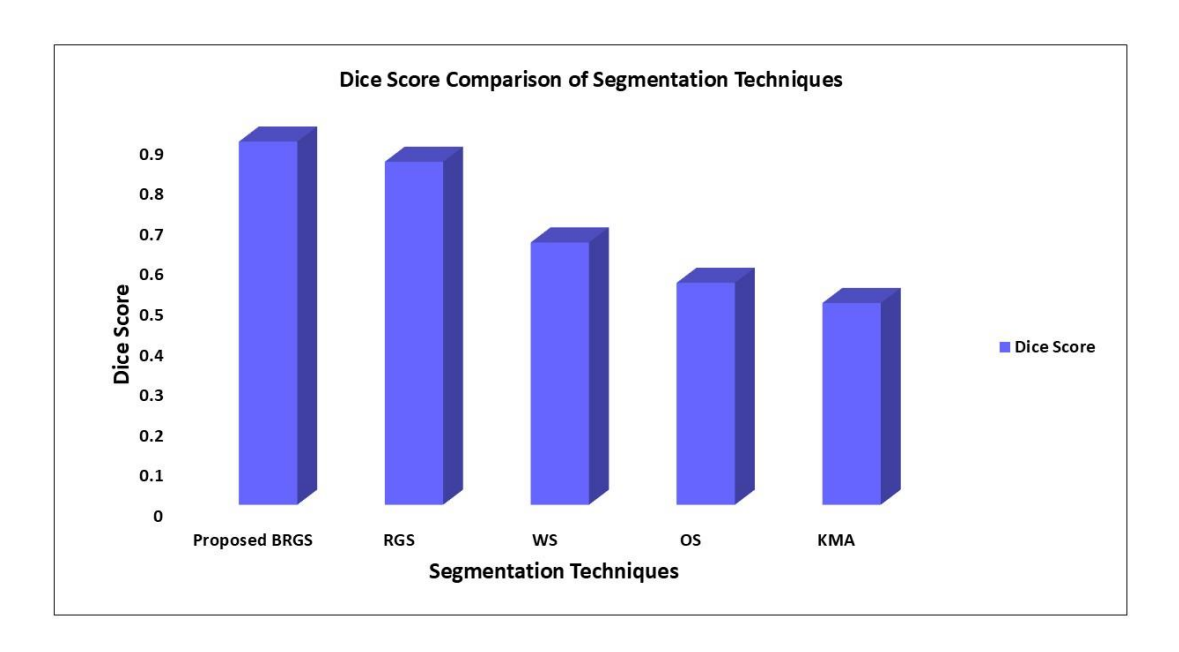


Graph 6.5Training Time Comparison Between Proposed and Existing Models

The proposed framework and the existing models' training times are shown in Graph 6.5. Training time is the time taken by the Introduced model to complete the process. Here, the outcome as a training time hit by the projected sculpt is 36938.55ms, while the training times obtained by the existing models are 56639.28ms (ResNet), 66016.98ms (CNN), 70078.52ms (Lightweight DNN), and 82063.17ms (ANN). The findings show that the suggested model is more effective at classifying data.

## **Evaluation of Lung Segmentation Accuracy Using BRGS and Other Techniques**

Performance analysis of the proposed BRGS is validated using Dice score measures. Next, the results are compared with the models that have already been developed, such as RGS, K-Means Algorithm (KMA), Ostu algorithm (OS), and Wise Sliding window (WS).



Graph 6.6 Dice Score Comparison Between Proposed and Existing Models.

The Dice score values for the present models and the proposed framework are shown in Graph 6.6. When evaluating the effectiveness of picture segmentation techniques [45], the Dice score is utilized. The current models achieve dice score values of 0.81291 (RGS), 0.60652 for WS, 0.50240 for OS, and 0.4385 for KMA, compared to the suggested model's value of 0.86173. The results demonstrate that the suggested strategy outperforms the others in terms of data segmentation.

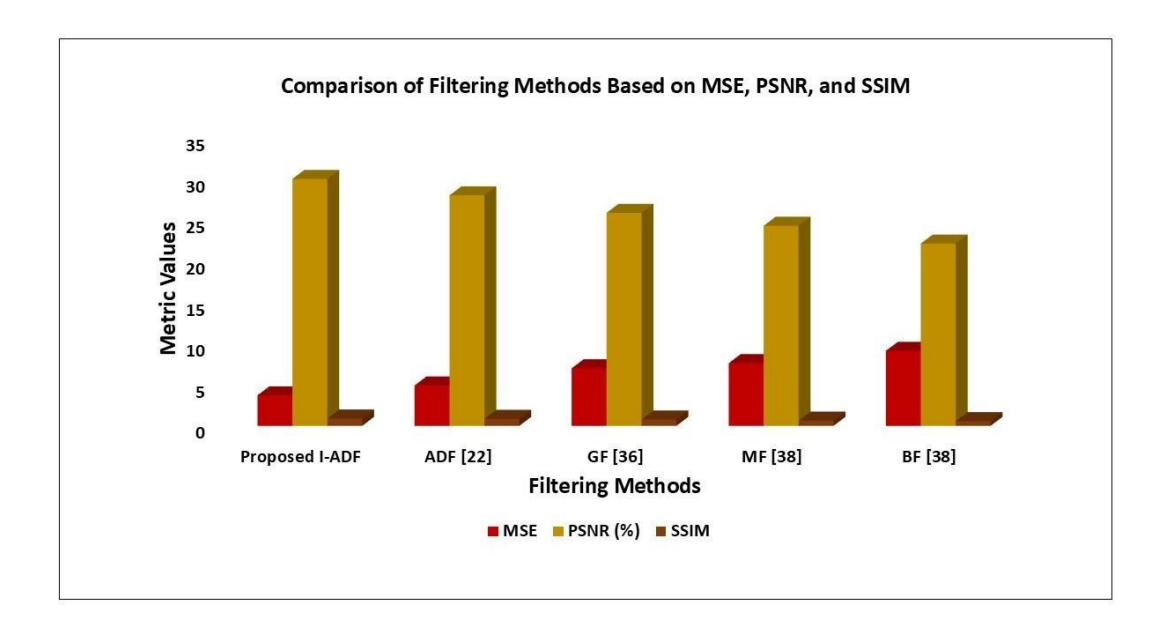
### Comparative Analysis of Noise Removal Techniques in Lung CT Images

The recommended I-ADF's performance research is validated in terms of Peak Signal Noise Ratio (PSNR), Structural Similarity Index Measure (SSIM), and Mean Squared Error (MSE). The findings are then contrasted with those from other models, including ADF, the Gilbert Filter, the Median Filter, and the Bilateral Filter.

Table 6.4 Analysis of the projected model's and current models' MSE, PSNR, and SSIM performance

Method	MSE	PSNR (%)	SSIM
Proposed I-ADF	3.7105	30.0334	0.8933
ADF [22]	4.9105	28.0334	0.8533
GF [36]	7.0002	25.9047	0.7703
MF [38]	7.6316	24.3380	0.6440
BF [38]	9.1208	22.1738	0.5784

The performance analysis of the planned model and pre-existing models as it relates to MSE, PSNR, and SSIM is shown in Table 6.4 above.



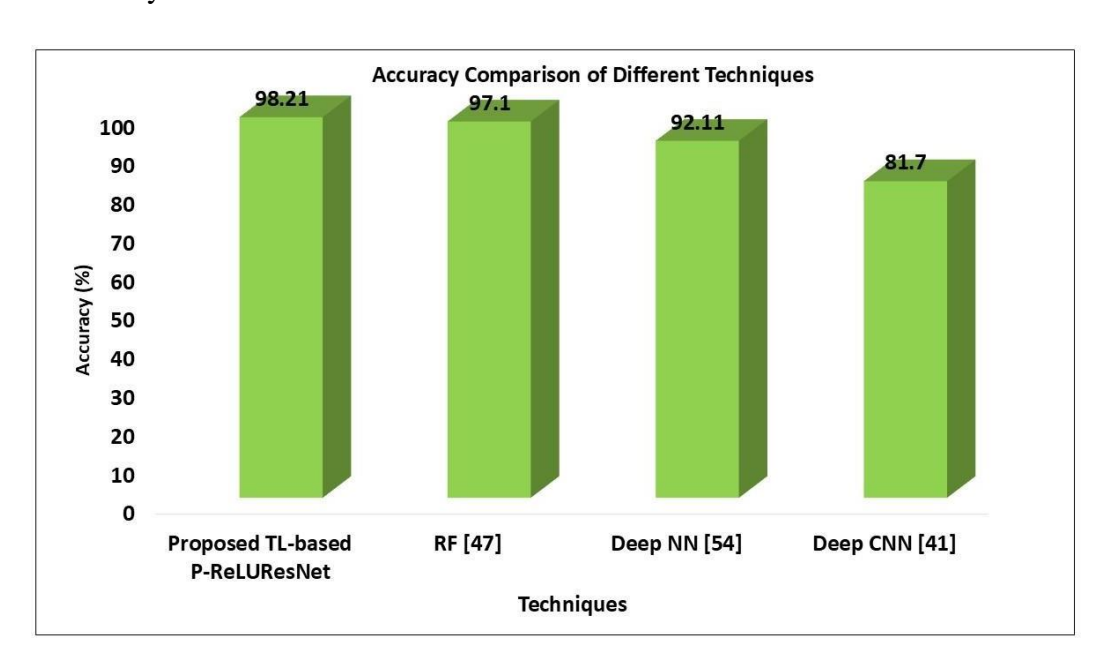
Graph 6.7 Comparison of Performance Metrics for Existing and Proposed Models.

In Graph 6.7, it is illustrated that the model performs better when the MSE value is lower and the PSNR and SSIM values are higher. The presented method achieves an MSE value of 3.710, which is less than that of the existing models. Likewise, the suggested model achieves 30.033% and 0.8933 for PSNR and SSIM, respectively, which demonstrates that the model performs better than the current models. The suggested model is therefore shown to be more effective at removing noise.

Table 6.5 Comparison of the accuracy of the suggested model and the literature survey model

Techniques		Accuracy
Proposed TL-based	P-	98.21
ReLUResNet		
RF [47]		97.1
Deep NN [54]		92.11
Deep CNN [41]		81.7

As mentioned above the Table 6.5 contrasts the suggested model's accuracy with that of the literature survey model.



Graph 6.8 Accuracy Comparison Between Proposed Model and Literature Models The Introduced model's precision is superior to that of the literature survey models, which achieve accuracy of 97.1% for RF, 92.11% for Deep NN, and 81.7% for Deep CNN, shown in Figure 6.11. Consequently, it may be concluded that the novel approach predicts lung cancer more accurately.

### **6.3.** Chapter Summary

Lung carcinoma has a high mortality rate, but an early prediction can contribute to a favourable prognosis. Various approaches have been developed for the prediction of lung carcinoma at a premature stage. However, these existing approaches still have defects such as low accuracy, high noise, and low contrast, and never consider the screening risk of lung cancer. So, the work proposed a lung carcinoma prediction and risk screening model using Transfer Learning (TL)-

based P-ReLUResNet. Initially, the lung computed tomography scan image was pre-processed to eradicate noise and enhance the edge by using Intra-class Variance-Anisotropic Diffusion Filter (I-ADF) and Unsharp Mask Filter (UMF) algorithms. After that, the pre-processed image was segmented by using the Bates distributed coati optimization algorithm integrated with Region Growing Segmentation (B-RGS). Next, the features from the segmented images are taken out and then selected by using the Binomial distributed Chi-square test (BD-CST). Then, the TL-based P-ReLUResNet classifier was used to classify cancer as normal or abnormal.

### CHAPTER 7 COMPARATIVE ANALYSIS

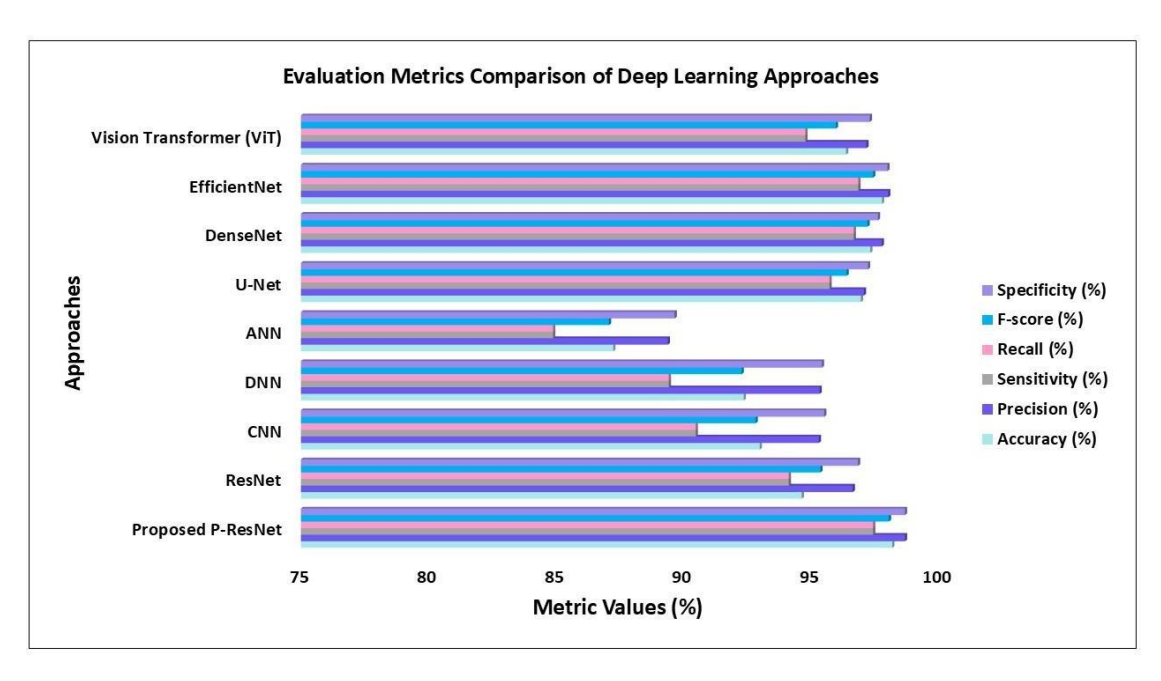
The Advanced Lung Carcinoma Prediction and Risk Screening Model Using Transfer Learning offers significant improvements over the Lightweight Advanced Deep Neural Network (DNN) Model for several key reasons.

- 1. Transfer Learning with ResNet-50: This model leverages a pre-trained ResNet-50 network, originally trained on a large and diverse dataset. The pre-training enables the model to learn a wide range of features, enhancing its ability to identify complex structures in lung cancer images with high accuracy.
- 2. Feature Extraction: The pre-trained network extracts high-level features such as edges, textures, and shapes, which are critical for accurate classification. These generalized features help the model adapt more effectively across varied lung cancer cases, improving its generalization capability.
- 3. Adaptation to Specific Data: The model is fine-tuned using the lung cancer dataset, allowing it to adjust its internal weights to better detect patterns and anomalies specific to lung carcinoma. This fine-tuning improves the model's performance without requiring training from scratch
- 4. Residual Connections: ResNet-50 incorporates residual connections, which enable the training of deeper networks by mitigating issues like vanishing gradients. This leads to faster convergence and improved accuracy.
- 5. Learning Rate Scheduling: Advanced training strategies such as learning rate scheduling are employed to optimize model convergence and prevent overfitting. This dynamic adjustment of the learning rate during training ensures better performance on previously unseen data.
- 6. Risk Screening: The model performs abnormality-based risk screening, categorizing patients into high- or low-risk groups based on image analysis.

Table 7.1 Comparative Analysis of Proposed Methodologies

Description	Lightweight Advanced DNN Model	Transfer Learning Model	
Objective	Lung Cancer Detection Premature-stage	Lung carcinoma prediction and risk Screening	
Model Type	Custom-built lightweight DNN	Pre-trained ResNet50 with fine-Tuning	
Model Architecture	10 convolutional layers, depth-wise separable convolutions	ResNet-50 base, fine-tuned layers, new fully connected layers	
Data	Normalization,	Resizing, normalization, and	
Preprocessing	augmentation, segmentation	augmentation	
Training Process	Adam optimizer	Bates distributed the coati optimization algorithm	
Results	Classification accuracy = 95.3 %	Classification accuracy = 98.21%	
Advantages	Computationally efficient, suitable for early detection	High accuracy and robustness, Effective risk screening	
Future Work	Multi-model data integration, real-time optimization.	Patient history integration, Risk model exploration.	

The Transfer Learning Model for Advanced Lung Carcinoma Prediction and Risk Screening demonstrates superior accuracy, robustness, and adaptability. Its high performance makes it well-suited for risk assessment and early detection, particularly in the healthcare sector.



Graph 7.1 Comparative accuracy of the proposed TL-based P-ResNet model with DNN and other models.

As illustrated in Graph 7.1, the TL-based P-ReLUResNet model achieved a higher classification accuracy of 98.21%, compared to 95.3% obtained by the Lightweight DNN model. This significant improvement demonstrates the effectiveness of using a pre-trained model, which enhances the system's ability to learn complex patterns and accurately detect lung cancer. In essence, the TL-based P-ReLUResNet model exhibits superior pattern recognition capabilities, resulting in more reliable predictions, an essential factor for early and accurate diagnosis. The notable difference in performance indicates that TL-based P-ReLUResNet is a more intelligent and efficient approach for real-world lung cancer screening applications.

#### 7.1. Chapter Summary

The proposed risk model demonstrates robustness and advanced feature extraction capabilities, making it suitable for various healthcare applications. This chapter compares two lung cancer detection models: the Lightweight Advanced DNN Model and the Transfer Learning Model. The Lightweight DNN Model, designed for rapid, premature-stage detection, consists of 10 convolutional layers and achieves an accuracy of 95.3%. However, it shows limitations in terms of generalizability and depth of feature extraction.

In contrast, the Transfer Learning Model, which leverages a pre-trained ResNet-50 optimized for lung cancer detection, achieves a higher accuracy of 98.21%. It is not only robust and highly generalizable but also excels in advanced feature extraction.

## CHAPTER 8 CONCLUSION AND FUTURE SCOPE

#### 8.1. Conclusion

This chapter summarizes the research presented in this thesis and highlights the key conclusions regarding the proposed TL-based P-ReLUResNet (P-ResNet) model for premature-stage lung cancer diagnosis. It also outlines potential future directions to enhance healthcare applications. Lung carcinoma remains the most prevalent and fatal form of cancer worldwide, posing significant challenges in early detection and treatment. Risk screening is vital to identify individuals at high risk and potentially improve patient outcomes. To address this need, an advanced risk screening framework, TL-based P-ResNet, was developed. Unlike traditional models that focus primarily on smoking history and demographic data, P-ResNet adopts a multimodal approach, incorporating behavioral, genetic, environmental, and socio-economic variables. These include nicotine dependence, tumor-associated genetic, income level, education, occupational exposure, and air pollution. Studies evaluating P-ResNet have demonstrated high sensitivity and specificity in identifying high-risk individuals. By integrating a wide range of factors, the model delivers a more accurate risk assessment. Moreover, TL-based P-ResNet is designed to be dynamic, allowing for continuous refinement and improvement with new data. In conclusion, P-ResNet represents a significant advancement in the domain of lung cancer risk screening. Its ability to incorporate diverse data sources makes it a powerful tool for personalized medicine and proactive healthcare decision-making. P-ResNet distinguishes itself from other risk screening systems through several important features. Its comprehensive methodology, incorporating a wide range of risk indicators, enables a more detailed and accurate assessment of an individual's risk profile. The integration of deep learning algorithms enhances the system's ability to analyze complex data and understated patterns, significantly improving the accuracy of risk prediction.

In this work, the P-ResNet algorithm was implemented for effective premature-stage lung carcinoma prediction. The system was trained to classify lung CT images as either normal or abnormal [60]. The proposed model achieved superior results, with a recall of 97.37%, an accuracy of 98.21%, and a precision of 98.71%. These results confirm that the proposed system is highly accurate in detecting lung carcinoma at a premature stage. The primary focus of this study has been lung cancer detection, rather than broader pulmonary imaging challenges. In future work, the model could be extended to not only detect lung carcinoma more efficiently but also to classify its types and assess severity levels using more advanced and intelligent tools.

### 8.2. Future Scope

In the future, P-ResNet could evolve further by incorporating additional variables such as lung health status and lifestyle factors to improve its predictive capabilities. This could significantly aid in early detection, making treatment more effective and potentially saving lives. Moreover, as technology advances, P-ResNet may become more accessible and user-friendly through mobile applications or cloud-based platforms. Such tools could allow individuals to assess their lung cancer risk using real-time personal health data, empowering proactive healthcare decisions. In conclusion, the proposed P-ResNet model demonstrates significant promise for early lung cancer detection through its intelligent, data-driven methodology. Future improvements may enhance its accuracy, usability, and enable real-time decision-making, and ultimately contribute to a reduction in lung cancer mortality rates. With continued advancements, P-ResNet has the potential to become a powerful tool in the fight against lung cancer, moving us closer to early intervention and possibly even prevention.

### **REFERENCES**

- 1. Pradhan, Kanchan Sitaram, Priyanka Chawla, and Rajeev Tiwari. "HRDEL: High ranking deep ensemble learning-based lung cancer diagnosis model." Expert Systems with Applications 213 (2023): 118956.
- 2. Zhang, Hanfei, Meiyan Liao, Qun Guo, Jun Chen, Shan Wang, Songmei Liu, and Feng Xiao. "Predicting N2 lymph node metastasis in presurgical stage I-II non-small cell lung cancer using multiview radiomics and deep learning method." Medical Physics (2023).
- 3. Agarwal, Seema, Ajay Singh Yadav, Vennapoosa Dinesh, Kolluru Sai Sri Vatsav, Kolluru Sai Surya Prakash, and Sushma Jaiswal. "By artificial intelligence algorithms and machine learning models for diagnosis cancer." Materials Today: Proceedings 80 (2023): 2969-2975.
- 4. Mengash, Hanan Abdullah, Mohammad Alamgeer, Mashael Maashi, Mahmoud Othman, Manar Ahmed Hamza, Sara Saadeldeen Ibrahim, Abu Sarwar Zamani, and Ishfaq Yaseen. "Leveraging Marine Predators Algorithm with Deep Learning for Lung and Colon Cancer Diagnosis." Cancers 15, no. 5 (2023): 1591.
- 5. Chui, Kwok Tai, Brij B. Gupta, Rutvij H. Jhaveri, Hao Ran Chi, Varsha Arya, Ammar Almomani, and Ali Nauman. "Multiround transfer learning and modified generative adversarial network for lung cancer detection." International Journal of Intelligent Systems 2023 (2023): 1-14.
- 6. Tran, Thi-Oanh, Thanh Hoa Vo, and Nguyen Quoc Khanh Le. "Omics-based deep learning approaches for lung cancer decision-making and therapeutics development." Briefings in Functional Genomics (2023): elad031.
- 7. Wankhade, Shalini, and S. Vigneshwari. "Lung cell cancer identification mechanism using deep learning approach." Soft Computing (2023): 1-15.
- 8. Shen, Zhiqiang, Peng Cao, Jinzhu Yang, and Osmar R. Zaiane. "WS-LungNet: A two-stage weakly-supervised lung cancer detection and diagnosis network." Computers in Biology and Medicine 154 (2023): 106587.
- 9. Mikhael, Peter G., Jeremy Wohlwend, Adam Yala, Ludvig Karstens, Justin Xiang, Angelo K. Takigami, Patrick P. Bourgouin et al. "Sybil: A validated deep learning model to predict future lung cancer risk from a single low-dose chest computed tomography." Journal of Clinical Oncology 41, no. 12 (2023): 2191-2200.
- 10. Siddiqui, Ebtasam Ahmad, Vijayshri Chaurasia, and Madhu Shandilya. "Detection and classification of lung cancer computed tomography images using a novel improved deep belief network with Gabor filters." Chemometrics and Intelligent Laboratory Systems 235 (2023): 104763.
- 11. Rajput, Aayush, and Abdulhamit Subasi. "Lung cancer detection from histopathological lung tissue images using deep learning." In Applications of Artificial Intelligence in Medical Imaging, pp. 51-74. Academic Press, 2023.
- 12. El-Ghany, Sameh Abd, Mohammad Azad, and Mohammed Elmogy. "Robustness Fine-Tuning Deep Learning Model for Cancers Diagnosis Based on Histopathology Image Analysis." Diagnostics 13, no. 4 (2023): 699.

- 13. Huang, Shigao, Jie Yang, Na Shen, Qingsong Xu, and Qi Zhao. "Artificial intelligence in lung cancer diagnosis and prognosis: Current application and future perspective." In Seminars in Cancer Biology. Academic Press, 2023.
- 14. Tajidini, Farzane. "A comprehensive review of deep learning in lung cancer." arXiv preprint arXiv:2308.02528 (2023).
- 15. Wang, Siwei, Fanchen Meng, Ming Li, Hua Bao, Xin Chen, Meng Zhu, Rui Liu et al. "Multidimensional Cell-Free DNA Fragmentomic Assay for Detection of Premature stage Lung Cancer." American Journal of Respiratory and Critical Care Medicine 207, no. 9 (2023): 1203-1213.
- 16. Choudhury, Avishek, S. Balasubramaniam, Ambala Pradeep Kumar, and Sanjay Nakharu Prasad Kumar. "PSSO: Political Squirrel Search Optimizer-Driven Deep Learning for Severity Level Detection and Classification of Lung Cancer." International Journal of Information Technology & Decision Making (2023): 1-34.
- 17. Hasan, Mahadi, Miraz Al Mamun, Madhab Chandra Das, Md Maruf Hasan, and Asm Mohaimenul Islam. "The application and comparison of Deep Learning models for the prediction of chest cancer prognosis." In 2023 International Conference on Smart Applications, Communications and Networking (SmartNets), pp. 1-5. IEEE, 2023.
- 18. Chae, Kum Ju, Soyeoun Lim, Joon Beom Seo, Hye Jeon Hwang, Hyemi Choi, David Lynch, and Gong Yong Jin. "Interstitial Lung Abnormalities at CT in the Korean National Lung Cancer Screening Program: Prevalence and Deep Learning–based Texture Analysis." Radiology 307, no. 4 (2023): e222828.
- 19. Gunasekaran, Karthick Prasad. "Leveraging object detection for the identification of lung cancer." arXiv preprint arXiv:2305.15813 (2023).
- 20. Kavitha, B. C., and K. B. Naveen. "PREDICTION AND CLASSIFICATION OF LUNG CANCER USING DEEP LEARNING." (2023).
- 21. Vishwa Kiran, S., Inderjeet Kaur, K. Thangaraj, V. Saveetha, R. Kingsy Grace, and N. Arulkumar. "Machine Learning with Data Science-Enabled Lung Cancer Diagnosis and Classification Using Computed Tomography Images." International Journal of Image and Graphics 23, no. 03 (2023): 2240002.
- 22. Ahmed, Saghir, Basit Raza, Lal Hussain, Amjad Aldweesh, Abdulfattah Omar, Mohammad Shahbaz Khan, Elsayed Tag Eldin, and Muhammad Amin Nadim. "The Deep Learning ResNet101 and Ensemble XGBoost Algorithm with Hyperparameters Optimization Accurately Predict the Lung Cancer." Applied Artificial Intelligence 37, no. 1 (2023): 2166222.
- 23. Kwon, Hyuk-Jung, Sun Hye Shin, Hyun Ho Kim, Na Young Min, YuGyeong Lim, Tae-woon Joo, Kyoung Joo Lee et al. "Advances in methylation analysis of liquid biopsy in early cancer detection of colorectal and lung cancer." Scientific Reports 13, no. 1 (2023): 13502.
- 24. Khodadoust, Ali, Navid Nasirizadeh, Seyed Morteza Seyfati, Ramezan Ali Taheri, Mostafa Ghanei, and Hasan Bagheri. "High-performance strategy for the construction of electrochemical biosensor for simultaneous detection of miRNA-141 and miRNA- 21 as lung cancer biomarkers." Talanta 252 (2023): 123863.
- 25. Bhatia, Isha, and Aarti. "Deep Learning-Based Proposed Approach for Low-Dose CT Scan-Based Early Detection of Lung Cancer." In International Conference on Soft

- Computing and Signal Processing, pp. 191-201. Singapore: Springer Nature Singapore, 2023.
- 26. Adams, Scott J., Emily Stone, David R. Baldwin, Rozemarijn Vliegenthart, Pyng Lee, and Florian J. Fintelmann. "Lung cancer screening." The Lancet 401, no. 10374 (2023): 390-408.
- 27. Sani, Shuaibu Nazifi, Wei Zhou, Balarabe B. Ismail, Yongkui Zhang, Zhijun Chen, Binjie Zhang, Changqian Bao, Houde Zhang, and Xiaozhi Wang. "LC-MS/MS-based volatile organic compound biomarkers analysis for early detection of lung cancer." Cancers 15, no. 4 (2023): 1186.
- 28. Su, Shu, Yulong Xuan, Xiaojun Fan, Hua Bao, Haimeng Tang, Xin Lv, Wei Ren et al. "Testing the generalizability of cfDNA fragmentomic features across different studies for cancer early detection." Genomics (2023): 110662.
- 29. Minegishi, Kentaro, Yoh Dobashi, Teruhide Koyama, Yuko Ishibashi, Miki Furuya, Hiroyoshi Tsubochi, Yasukazu Ohmoto, Tomohiko Yasuda, and Sachiyo Nomura. "Diagnostic utility of trefoil factor families for the early detection of lung cancer and their correlation with tissue expression." Oncology Letters 25, no. 4 (2023): 1-14.
- 30. Robbins, Hilary A., Karine Alcala, Elham Khodayari Moez, Florence Guida, Sera Thomas, Hana Zahed, Matthew T. Warkentin et al. "Design and methodological considerations for biomarker discovery and validation in the Integrative Analysis of Lung Cancer Etiology and Risk (INTEGRAL) Program." Annals of epidemiology 77 (2023): 1-12.
- 31. Chassagnon, Guillaume, Constance De Margerie-Mellon, Maria Vakalopoulou, Rafael Marini, Trieu-Nghi Hoang-Thi, Marie-Pierre Revel, and Philippe Soyer. "Artificial intelligence in lung cancer: current applications and perspectives." Japanese Journal of Radiology 41, no. 3 (2023): 235-244.
- 32. Abunajm, Saleh, Nelly Elsayed, Zag ElSayed, and Murat Ozer. "Deep Learning Approach for Premature stage Lung Cancer Detection." arXiv preprint arXiv:2302.02456 (2023).
- 33. Said, Yahia, Ahmed A. Alsheikhy, Tawfeeq Shawly, and Husam Lahza. "Medical images segmentation for lung cancer diagnosis based on deep learning architectures." Diagnostics 13, no. 3 (2023): 546.
- 34. Rawat, Devyani, Sachin Sharma, and Shuchi Bhadula. "Deep Learning Techniques in Digital Clinical Diagnostic System for Lung Cancer." In the 2023 9th International Conference on Advanced Computing and Communication Systems (ICACCS), vol. 1,
- pp. 1232-1237. IEEE, 2023.
- 35. Shah, Asghar Ali, Hafiz Abid Mahmood Malik, AbdulHafeez Muhammad, Abdullah Alourani, and Zaeem Arif Butt. "Deep learning ensemble 2D CNN approach towards the detection of lung cancer." Scientific Reports 13, no. 1 (2023): 2987.
- 36. Huang, Shigao, Ibrahim Arpaci, Mostafa Al-Emran, Serhat Kılıçarslan, and Mohammed A. Al-Sharafi. "A comparative analysis of classical machine learning and deep learning techniques for predicting lung cancer survivability." Multimedia Tools and Applications (2023): 1-16.
- 37. Dritsas, Elias, and Maria Trigka. "Lung cancer risk prediction with machine learning models." Big Data and Cognitive Computing 6, no. 4 (2022): 139.

- 38. Farheen, Farhanaz, Md Salman Shamil, Nabil Ibtehaz, and M. Sohel Rahman. "Revisiting segmentation of lung tumors from CT images." Computers in Biology and Medicine 144 (2022): 105385.
- 39. Praveena, M., A. Ravi, T. Srikanth, B. Hari Praveen, B. Sai Krishna, and A. Sunil Mallik. "Lung cancer detection using a deep learning approach CNN." In 2022 7th International Conference on Communication and Electronics Systems (ICCES), pp. 1418-1423. IEEE, 2022.
- 40. Feng, Jianxin, and Jun Jiang. "Deep learning-based chest CT image features in diagnosis of lung cancer." Computational and Mathematical Methods in Medicine 2022 (2022).
- 41. Guo, Lan-Wei, Zhang-Yan Lyu, Qing-Cheng Meng, Li-Yang Zheng, Qiong Chen, Yin Liu, Hui-Fang Xu et al. "A risk prediction model for selecting high-risk population for computed tomography lung cancer screening in China." Lung Cancer 163 (2022): 27-34.
- 42. Hussain, Lal, Hadeel Alsolai, Siwar Ben Haj Hassine, Mohamed K. Nour, Mesfer Al Duhayyim, Anwer Mustafa Hilal, Ahmed S. Salama, Abdelwahed Motwakel, Ishfaq Yaseen, and Mohammed Rizwanullah. "Lung cancer prediction using robust machine learning and image enhancement methods on extracted gray-level co-occurrence matrix features." Applied Sciences 12, no. 13 (2022): 6517.
- 43. Kasinathan, Gopi, and Selvakumar Jayakumar. "Cloud-based lung tumor detection and stage classification using deep learning techniques." BioMed Research International 2022 (2022).
- 44. Shakeel, P. Mohamed, M. A. Burhanuddin, and Mohammad Ishak Desa. "Automatic lung cancer detection from CT image using improved deep neural network and ensemble classifier." Neural Computing and Applications (2022): 1-14.
- 45. Kerpel-Fronius, Anna, Martin Tammemägi, Milena Cavic, Claudia Henschke, Long Jiang, Ella Kazerooni, Choon-Taek Lee et al. "Screening for lung cancer in individuals who never smoked: an international association for the study of lung cancer early detection and screening committee report." Journal of Thoracic Oncology 17, no. 1 (2022): 56-66.
- 46. Liu, Cuiliu, Xiaoqiang Xiang, Shuangqing Han, Hannah Ying Lim, Lingrui Li, Xing Zhang, Zhaowu Ma et al. "Blood-based liquid biopsy: Insights into early detection and clinical management of lung cancer." Cancer Letters 524 (2022): 91-102.
- 47. Vykoukal, Jody, Johannes F. Fahrmann, Nikul Patel, Masayoshi Shimizu, Edwin J. Ostrin, Jennifer B. Dennison, Cristina Ivan et al. "Contributions of circulating microRNAs for early detection of lung cancer." Cancers 14, no. 17 (2022): 4221.
- 48. Althubiti, Sara A., Sanchita Paul, Rajanikanta Mohanty, Sachi Nandan Mohanty, Fayadh Alenezi, and Kemal Polat. "Ensemble learning framework with GLCM texture extraction for early detection of lung cancer on CT images." Computational and Mathematical Methods in Medicine 2022 (2022).
- 49. Huang, Hong, Yongfeng Yang, Yihan Zhu, Hongyu Chen, Ying Yang, Li Zhang, and Weimin Li. "Blood protein biomarkers in lung cancer." Cancer Letters (2022): 215886.
- 50. Saha, Purabi, Richard Owusu Nyarko, Priya Lokare, Ivan Kahwa, Paul Owusu Boateng, and Christian Asum. "Effect of Covid-19 in Management of Lung Cancer Disease: A Review." Asian Journal of Pharmaceutical Research and Development 10, no. 3 (2022): 58-64.
- 51. Bhatia, Isha, and Aarti Aarti. "Lung carcinoma detection at Premature stage using deep learning techniques." In AIP Conference Proceedings, vol. 2576, no. 1. AIP Publishing, 2022.

- 52. Hackshaw, Allan, Christina A. Clarke, and Anne-Renee Hartman. "New genomic technologies for multi-cancer early detection: Rethinking the scope of cancer screening." Cancer Cell 40, no. 2 (2022): 109-113.
- 53. Wang, Guangxi, Mantang Qiu, Xudong Xing, Juntuo Zhou, Hantao Yao, Mingru Li, Rong Yin et al. "Lung cancer scRNA-seq and lipidomics reveal aberrant lipid metabolism for premature stage diagnosis." Science Translational Medicine 14, no. 630 (2022): eabk2756.
- 54. Xia, Liang, Jiandong Mei, Ran Kang, Senyi Deng, Yaohui Chen, Ying Yang, Gang Feng et al. "Perioperative ctDNA-based molecular residual disease detection for non–small cell lung cancer: a prospective multicenter cohort study (LUNGCA-1)." Clinical Cancer Research 28, no. 15 (2022): 3308-3317.
- 55. Sharma, Akshansh, Devanshi Shambhwani, Sadanand Pandey, Jay Singh, Hauzel Lalhlenmawia, Murali Kumarasamy, Sachin Kumar Singh et al. "Advances in lung cancer treatment using nanomedicines." ACS omega 8, no. 1 (2022): 10-41.
- 56. Gao, Qiang, Qiang Zeng, Zhijie Wang, Chengcheng Li, Yu Xu, Peng Cui, Xin Zhu et al. "Circulating cell-free DNA for cancer early detection." The Innovation 3, no. 4 (2022).
- 57. Gao, Y., Chen, Y., Jiang, Y., Li, Y., Zhang, X., Luo, M., Wang, X. and Li, Y., 2022. Artificial Intelligence Algorithm-Based Feature Extraction of Computed Tomography Images and Analysis of Benign and Malignant Pulmonary Nodules. Computational Intelligence & Neuroscience.
- 58. Kim, Kyung Hwan, Jaewon Oh, Gowoon Yang, Joongyo Lee, Jihun Kim, Seo-yeon Gwak, Iksung Cho et al. "Association of sinoatrial node radiation dose with atrial fibrillation and mortality in patients with lung cancer." JAMA oncology 8, no. 11 (2022): 1624-1634.
- 59. Gasparri, Roberto, Rosamaria Capuano, Alessandra Guaglio, Valentina Caminiti, Federico Canini, Alexandro Catini, Giulia Sedda, Roberto Paolesse, Corrado Di Natale, and Lorenzo Spaggiari. "Volatolomic urinary profile analysis for diagnosis of the premature stageof lung cancer." Journal of Breath Research 16, no. 4 (2022): 046008.
- 60. Dritsas, Elias, Maria Trigka, and Phivos Mylonas. "A Multi-class Classification Approach for Weather Forecasting with Machine Learning Techniques." In 2022 17th International Workshop on Semantic and Social Media Adaptation & Personalization (SMAP), pp. 1-5. IEEE, 2022.
- 61. Deb, Dhruba, Amy C. Moore, and Upal Basu Roy. "The 2021 global lung cancer therapy landscape." Journal of Thoracic Oncology 17, no. 7 (2022): 931-936.
- 62. Li, Wen, Ji-Bin Liu, Li-Kun Hou, Fei Yu, Jie Zhang, Wei Wu, Xiao-Mei Tang et al. "Liquid biopsy in lung cancer: significance in diagnostics, prediction, and treatment monitoring." Molecular cancer 21, no. 1 (2022): 25.

- 63. Kaya, S. Irem, Goksu Ozcelikay, Fariba Mollarasouli, Nurgul K. Bakirhan, and Sibel Ozkan. "Recent achievements and challenges on nanomaterial based electrochemical biosensors for the detection of colon and lung cancer biomarkers." Sensors and Actuators B: Chemical 351 (2022): 130856.
- 64. Wang, Peiyu, Qi Huang, Shushi Meng, Teng Mu, Zheng Liu, Mengqi He, Qingyun Li, Song Zhao, Shaodong Wang, and Mantang Qiu. "Identification of lung cancer breath biomarkers based on perioperative breathomics testing: A prospective observational study." EClinicalMedicine 47 (2022).
- 65. Greene, Giles, Rowena Griffiths, Jun Han, Ashley Akbari, Monica Jones, Jane Lyons, Ronan A. Lyons et al. "Impact of the SARS-CoV-2 pandemic on female breast, colorectal and non-small cell lung cancer incidence, stage and healthcare pathway to diagnosis during 2020 in Wales, UK, using a national cancer clinical record system." British Journal of Cancer 127, no. 3 (2022): 558-568.
- 66. Chiu, Hwa-Yen, Heng-Sheng Chao, and Yuh-Min Chen. "Application of artificial intelligence in lung cancer." Cancers 14, no. 6 (2022): 1370.
- 67. Mamun, Muntasir, Afia Farjana, Miraz Al Mamun, and Md Salim Ahammed. "Lung cancer prediction model using ensemble learning techniques and a systematic review analysis." In 2022 IEEE World AI IoT Congress (AIIoT), pp. 187-193. IEEE, 2022.
- 68. Chen, Peixin, Yunhuan Liu, Yaokai Wen, and Caicun Zhou. "Non-small cell lung cancer in China." Cancer Communications 42, no. 10 (2022): 937-970.
- 69. Lee, Sang Min, and Chang Min Park. "Application of Artificial Screening Intelligence in Lung Cancer." Journal of the Korean Society of Radiology 80, no. 5: 872-879. Lee, Sang Min, and Chang Min Park. "Application of Artificial Screening Intelligence in Lung Cancer." Journal of the Korean Society of Radiology 80, no. 5: 872-879.
- 70. Nageswaran, Sharmila, G. Arunkumar, Anil Kumar Bisht, Shivlal Mewada, J. N. V. R. Kumar, Malik Jawarneh, and Evans Asenso. "Lung cancer classification and prediction using machine learning and image processing." BioMed Research International 2022 (2022).
- 71. Zafar, Afia, Muhammad Aamir, Nazri Mohd Nawi, Ali Arshad, Saman Riaz, Abdulrahman Alruban, Ashit Kumar Dutta, and Sultan Almotairi. "A comparison of pooling methods for convolutional neural networks." Applied Sciences 12, no. 17 (2022): 8643.
- 72. Primakov, Sergey P., Abdalla Ibrahim, Janita E. van Timmeren, Guangyao Wu, Simon
- A. Keek, Manon Beuque, Renée WY Granzier et al. "Automated detection and segmentation of non-small cell lung cancer computed tomography images." Nature communications 13, no. 1 (2022): 3423.
- 73. Sankar, S. Perumal, and Deepa Elizabeth George. "RETRACTED ARTICLE: Regression Neural Network segmentation approach with LIDC-IDRI for lung lesion." Journal of Ambient Intelligence and Humanized Computing 12, no. 5 (2021): 5571-5580.
- 74. Chaunzwa, Tafadzwa L., Ahmed Hosny, Yiwen Xu, Andrea Shafer, Nancy Diao, Michael Lanuti, David C. Christiani, Raymond H. Mak, and Hugo JWL Aerts. "Deep learning classification of lung cancer histology using CT images." Scientific reports 11, no. 1 (2021): 5471.

- 75. Xie, Ying, Wei-Yu Meng, Run-Ze Li, Yu-Wei Wang, Xin Qian, Chang Chan, Zhi-Fang Yu et al. "Early lung cancer diagnostic biomarker discovery by machine learning methods." Translational oncology 14, no. 1 (2021): 100907.
- 76. Liu, W., Liu, X., Li, H., Li, M., Zhao, X. and Zhu, Z., 2021. Integrating lung parenchyma segmentation and nodule detection with deep multi-task learning. IEEE Journal of Biomedical and Health Informatics, 25(8), pp.3073-3081.
- 77. Sankar, S.P. and George, D.E., 2021. Regression Neural Network segmentation approach with LIDC-IDRI for lung lesion. Journal of Ambient Intelligence and Humanized Computing, 12(5), pp.5571-5580.
- 78. Suji, R.J. and Bhadauria, S.S., Automatic Lung Segmentation and Lung Nodule Type Identification over LIDC-IDRI dataset.
- 79. Gong, Jing, Jiyu Liu, Haiming Li, Hui Zhu, Tingting Wang, Tingdan Hu, Menglei Li et al. "Deep learning-based stage-wise risk stratification for early lung adenocarcinoma in CT images: a multi-center study." *Cancers* 13, no. 13 (2021): 3300.
- 80. Mukherjee, Pritam, Mu Zhou, Edward Lee, Anne Schicht, Yoganand Balagurunathan, Sandy Napel, Robert Gillies et al. "A shallow convolutional neural network predicts prognosis of lung cancer patients in multi-institutional computed tomography image datasets." Nature machine intelligence 2, no. 5 (2020): 274-282.
- 81. Asuntha, A., and Andy Srinivasan. "Deep learning for lung Cancer detection and classification." Multimedia Tools and Applications 79 (2020): 7731-7762.
- 82. Draz, Umar, Tariq Ali, Sana Yasin, Umair Waqas, Syeda Binish Zahra, M. Ans Shoukat, and Sarah Gul. "A Pattern Detection Technique of L-MYC for Lungs Cancer Oncogene in Bioinformatics Big Data." In 2020 17th International Bhurban Conference on Applied Sciences and Technology (IBCAST), pp. 218-223. IEEE, 2020.
- 83. Chabon, Jacob J., Emily G. Hamilton, David M. Kurtz, Mohammad S. Esfahani, Everett
- J. Moding, Henning Stehr, Joseph Schroers-Martin et al. "Integrating genomic features for non-invasive early lung cancer detection." Nature 580, no. 7802 (2020): 245-251.
- 84. Thakur, Shailesh Kumar, Dhirendra Pratap Singh, and Jaytrilok Choudhary. "Lung cancer identification: a review on detection and classification." Cancer and Metastasis Reviews 39 (2020): 989-998.
- 85. Fehlmann, Tobias, Mustafa Kahraman, Nicole Ludwig, Christina Backes, Valentina Galata, Verena Keller, Lars Geffers et al. "Evaluating the use of circulating microRNA profiles for lung cancer detection in symptomatic patients." JAMA oncology 6, no. 5 (2020): 714-723.
- 86. Joshua, Eali Stephen Neal, Midhun Chakkravarthy, and Debnath Bhattacharyya. "An Extensive Review on Lung Cancer Detection Using Machine Learning Techniques: A Systematic Study." Revue d'Intelligence Artificielle 34, no. 3 (2020).
- 87. Shakeel, P. Mohamed, Mohd Aboobaider Burhanuddin, and Mohamad Ishak Desa. "Lung cancer detection from CT image using improved profuse clustering and deep learning instantaneously trained neural networks." Measurement 145 (2019): 702-712.
- 88. Xu, Yiwen, Ahmed Hosny, Roman Zeleznik, Chintan Parmar, Thibaud Coroller, Idalid Franco, Raymond H. Mak, and Hugo JWL Aerts. "Deep learning predicts lung cancer treatment response from serial medical imaging." Clinical Cancer Research 25, no. 11 (2019):

- 3266-3275.
- 89. Zhang, Baihua, Shouliang Qi, Patrice Monkam, Chen Li, Fan Yang, Yu-Dong Yao, and Wei Qian. "Ensemble learners of multiple deep CNNs for pulmonary nodules classification using CT images." IEEE Access 7 (2019): 110358-110371.
- 90. Yu, Lingming, Guangyu Tao, Lei Zhu, Gang Wang, Ziming Li, Jianding Ye, and Qunhui Chen. "Prediction of pathologic stage in non-small cell lung cancer using machine learning algorithm based on CT image feature analysis." BMC cancer 19, no. 1 (2019): 1-12.
- 91. Gu, Qianbiao, Zhichao Feng, Qi Liang, Meijiao Li, Jiao Deng, Mengtian Ma, Wei Wang, Jianbin Liu, Peng Liu, and Pengfei Rong. "Machine learning-based radiomics strategy for prediction of cell proliferation in non-small cell lung cancer." European journal of radiology 118 (2019): 32-37.
- 92. Ozdemir, Onur, Rebecca L. Russell, and Andrew A. Berlin. "A 3D probabilistic deep learning system for detection and diagnosis of lung cancer using low-dose CT scans." IEEE transactions on medical imaging 39, no. 5 (2019): 1419-1429.
- 93. Liu, Zhuo, Chenhui Yao, Hang Yu, and Taihua Wu. "Deep reinforcement learning with its application for lung cancer detection in medical Internet of Things." Future Generation Computer Systems 97 (2019): 1-9.
- 94. Nasser, Ibrahim M., and Samy S. Abu-Naser. "Lung cancer detection using artificial neural network." International Journal of Engineering and Information Systems (IJEAIS) 3, no. 3 (2019): 17-23.
- 95. Liu, Zhuo, Chenhui Yao, Hang Yu, and Taihua Wu. "Deep reinforcement learning with its application for lung cancer detection in medical Internet of Things." Future Generation Computer Systems 97 (2019): 1-9.

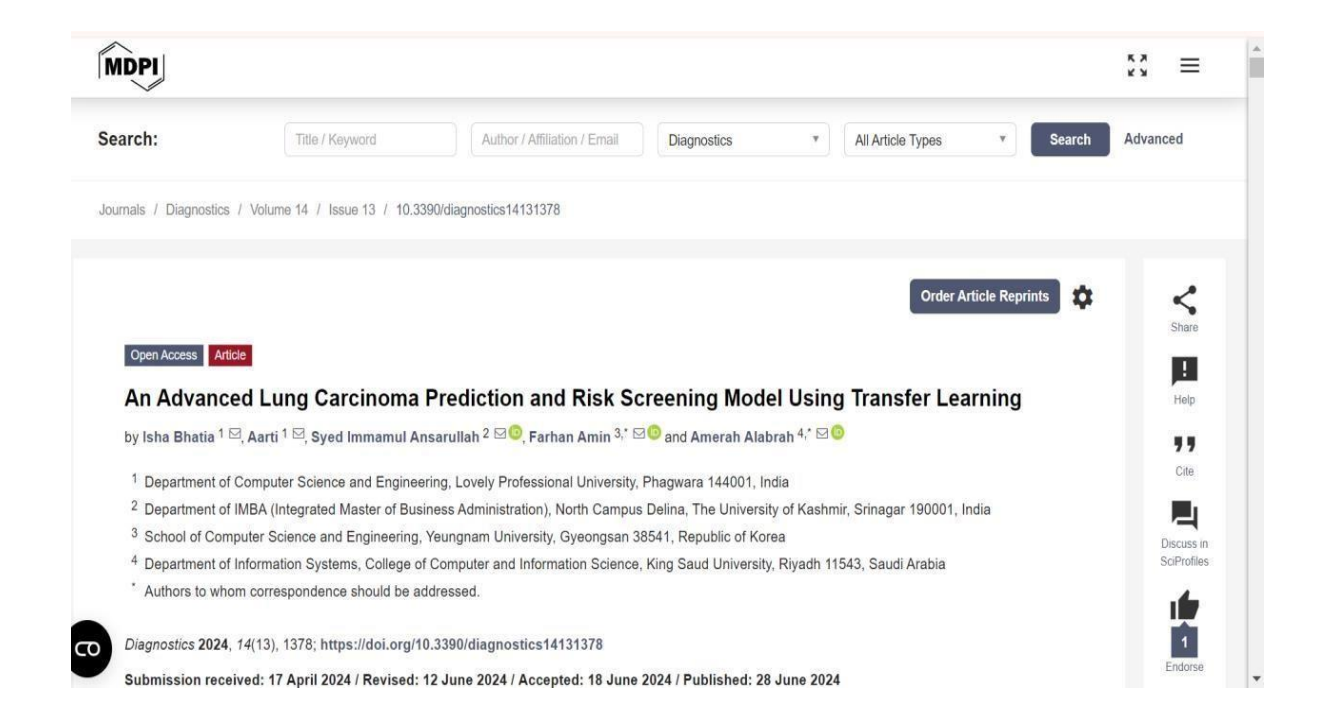
### **ANNEXURE I**

#### **Journal Details:**

**01 Paper Title:** An Advanced Lung Carcinoma Prediction and Risk Screening Model using Transfer Learning.

Status: Published.

Journal Name: Diagnostics-2992795 Year: 2024



**Reference**: https://www.mdpi.com/2075-4418/14/13/1378

## **02** Paper Title: Lightweight Advanced Deep Neural Network (DNN) Model for Premature stage Lung Cancer Detection.

Status: Published.

Journal Name: Diagnostics - 3127538 Year: 2024





Article

### Lightweight Advanced Deep Neural Network (DNN) Model for Early-Stage Lung Cancer Detection

Isha Bhatia <sup>1</sup>0, Aarti <sup>1</sup>, Syed Immamul Ansarullah <sup>2</sup>0, Farhan Amin <sup>3,\*</sup>0 and Amerah Alabrah <sup>4,\*</sup>0

- Department of Computer Science and Engineering, Lovely Professional University, Phagwara 144411, Punjab, India; ishabhatia91@gmail.com (I.B.); aarti.1208@gmail.com (A.)
- Department of Management Studies, University of Kashmir, North Campus, Delina, Baramulla 193103, Jammu & Kashmir, India; syedansr@gmail.com
- School of Computer Science and Engineering, Yeungnam University, Gyeongsan 38541, Republic of Korea
- Department of Information Systems, College of Computer and Information Science, King Saud University, Riyadh 11543, Saudi Arabia
- \* Correspondence: farhanamin10@hotmail.com (F.A.); aalobrah@ksu.edu.sa (A.A.)

**Abstract: Background:** Lung cancer, also known as lung carcinoma, has a high mortality rate; however, an early prediction helps to reduce the risk. In the current literature, various approaches have been developed for the prediction of lung carcinoma (at an early stage), but these still have various issues, such as low accuracy, high noise, low contrast, poor recognition rates, and a high false-positive rate, etc. Thus, in this research effort, we have proposed an advanced algorithm and combined two different types of deep neural networks to make it easier to spot lung melanoma

Reference: https://pubmed.ncbi.nlm.nih.gov/39518324/

# 03 Paper Title: Revolutionizing Diagnosis: Cloud-Enabled Deep Learning for Lung Tumor Detection and Staging.

Status: Published

Journal Name: International Journal of Intelligent Systems and Applications in Engineering

(IJISAE). Year: 2024



Reference: https://ijisae.org/index.php/IJISAE/article/view/5675

### **Conference Details:**

01 Conference Name: International Conference on Soft Computing & Signal Processing (ICSCSP2023 · ICSCSP2023\_Volume1)

Journal Name: International Conference on Soft Computing and Signal Processing

Paper Title: Deep Learning-Based Proposed Approach for Low-Dose CT Scan-Based Early Detection of Lung Cancer.

Status: Presentation, Accepted & Published. Year: 2024



Reference: https://ijisae.org/index.php/IJISAE/article/view/5675

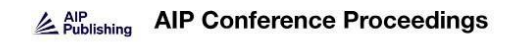
#### Certificate:

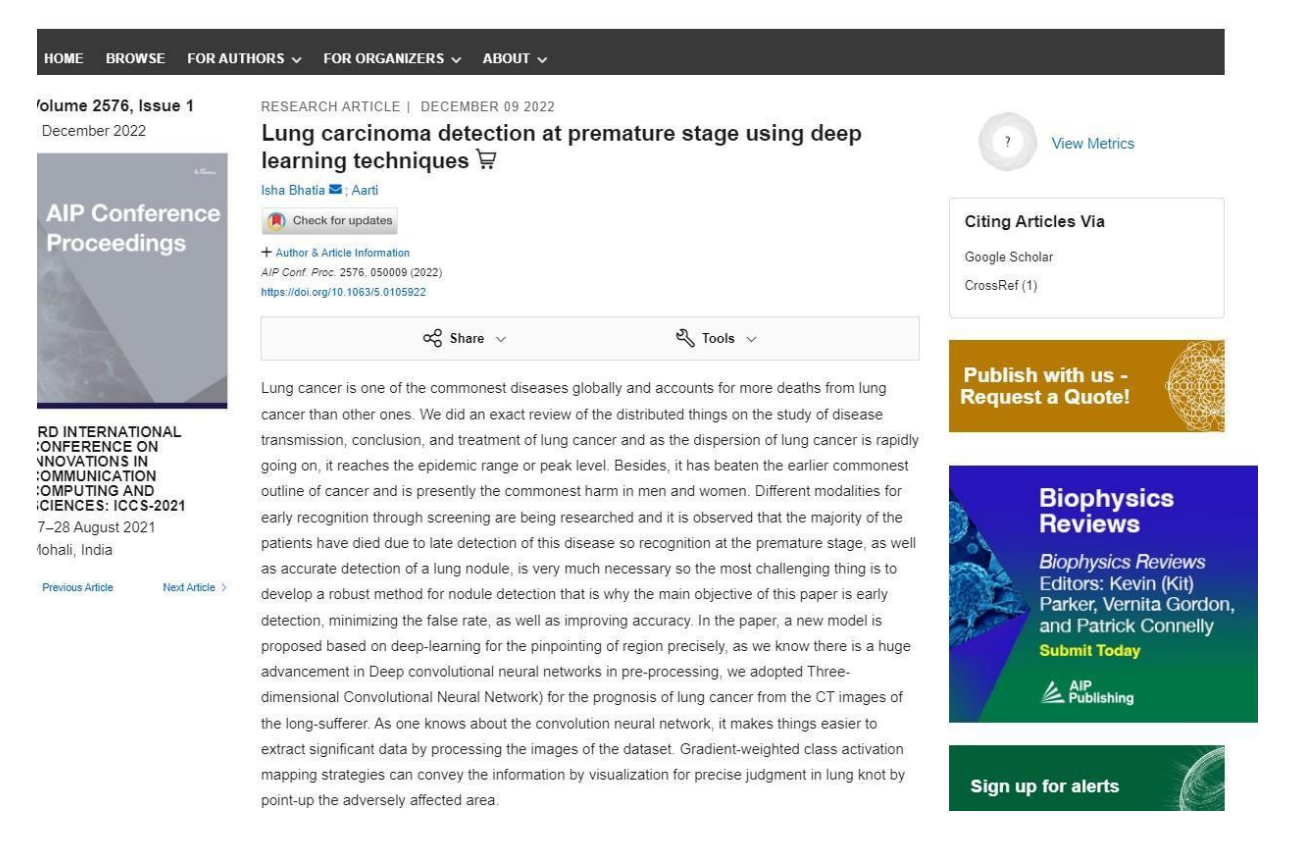


## 02 Conference Name: 3rd International Conference on Innovation in Communication, Computing, and Sciences (ICCS-2021).

Journal Name: International journal of intelligent systems and applications in engineering. Paper Title: Lung carcinoma detection at Premature stage using deep learning techniques. Status: Presentation, Accepted & Published.

Year: 2022





Reference: https://pubs.aip.org/aip/acp/article-abstract/2576/1/050009/2829993/Lung-carcinoma-detection-at-premature-stage-using?redirectedFrom=fulltext

### **Certificate:**



# Certificate

### 3rd International Conference (online) On

### **Innovations in Communication Computing and Sciences (ICCS 2021)**

27th-28th August, 2021

This is to certify that Mr./Ms./Dr.

#### Isha Bhatia

Lovely professional university, Punjab, India

Presented a paper titled

Lung Carcinoma Detection at Premature Stage using Deep Learning Techniques

in ICCS 2021 organised by Electronics & Communication Engineering Department, Chandigarh Engineering College, Landran, Mohali, Punjab, India.

**Dr. Parveen Singla** Convener, ICCS 2021 Prof. ECE, CEC, Landran **Dr. Vinay Bhatia** Conference Chair, ICCS 2021 Head ECE, CEC, Landran **Dr. Rajdeep Singh** Co-Patron, ICCS 2021 Director-Principal, CEC, Landran

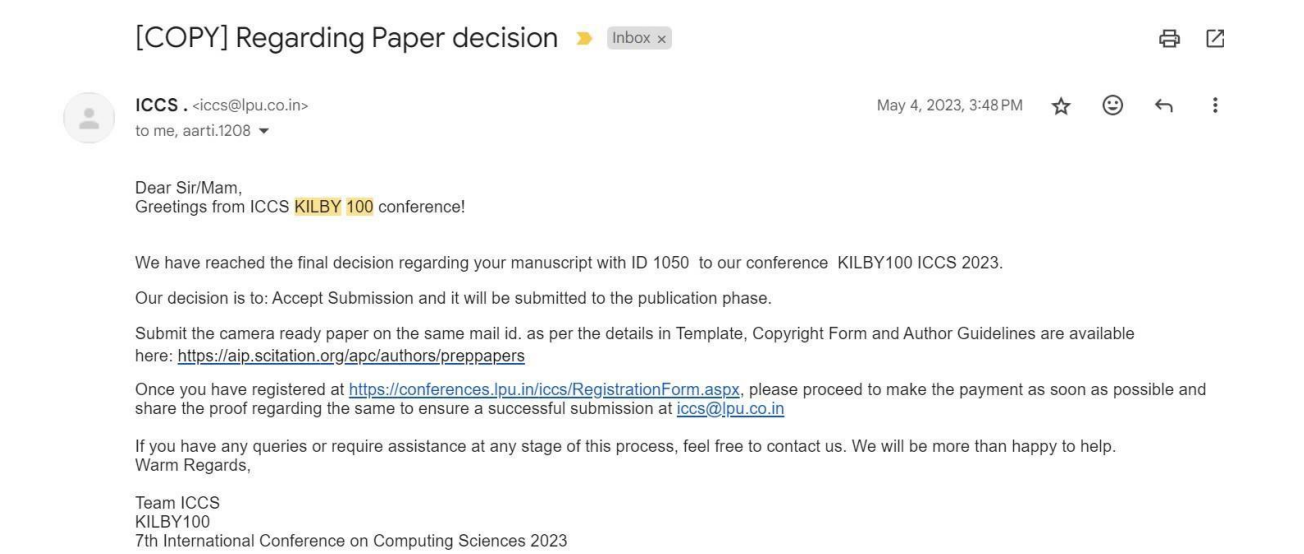
### 03 Conference Name: International Conference on Computing Sciences, 2023.

Paper Title: An Extensive Guide to Deep Saliency Supplements and Pre-Trained Deep Learning

Paradigms for Early Lung Cancer Sensing

Status: Presentation & accepted.

Year: 2023



### **Certificate:**



Certificate No. 268750

#### **Certificate of Paper Presentation**

This is to certify that Dr./Mr./Ms. Isha Bhatia of Lovely Professional University has presented the paper entitled A Comprehensive Guide to Early Detection of Lung Cancers with Deep Saliency Supplements and Pre-Trained Deep Learning Paradigms in the 7th International Joint Conference on Computing Sciences (ICCS-2023) "KILBY100" held on 5th May, 2023 organized by School of Computer Science and Engineering, LPU in association with Southern Federal University, Russia and Mizan Tepi University, Ethiopia at Lovely Professional University, Punjab, India.

Date of Issue: 20-05-2023

Prepared by (Administrative Officer-Records)





Publication Co- Chair







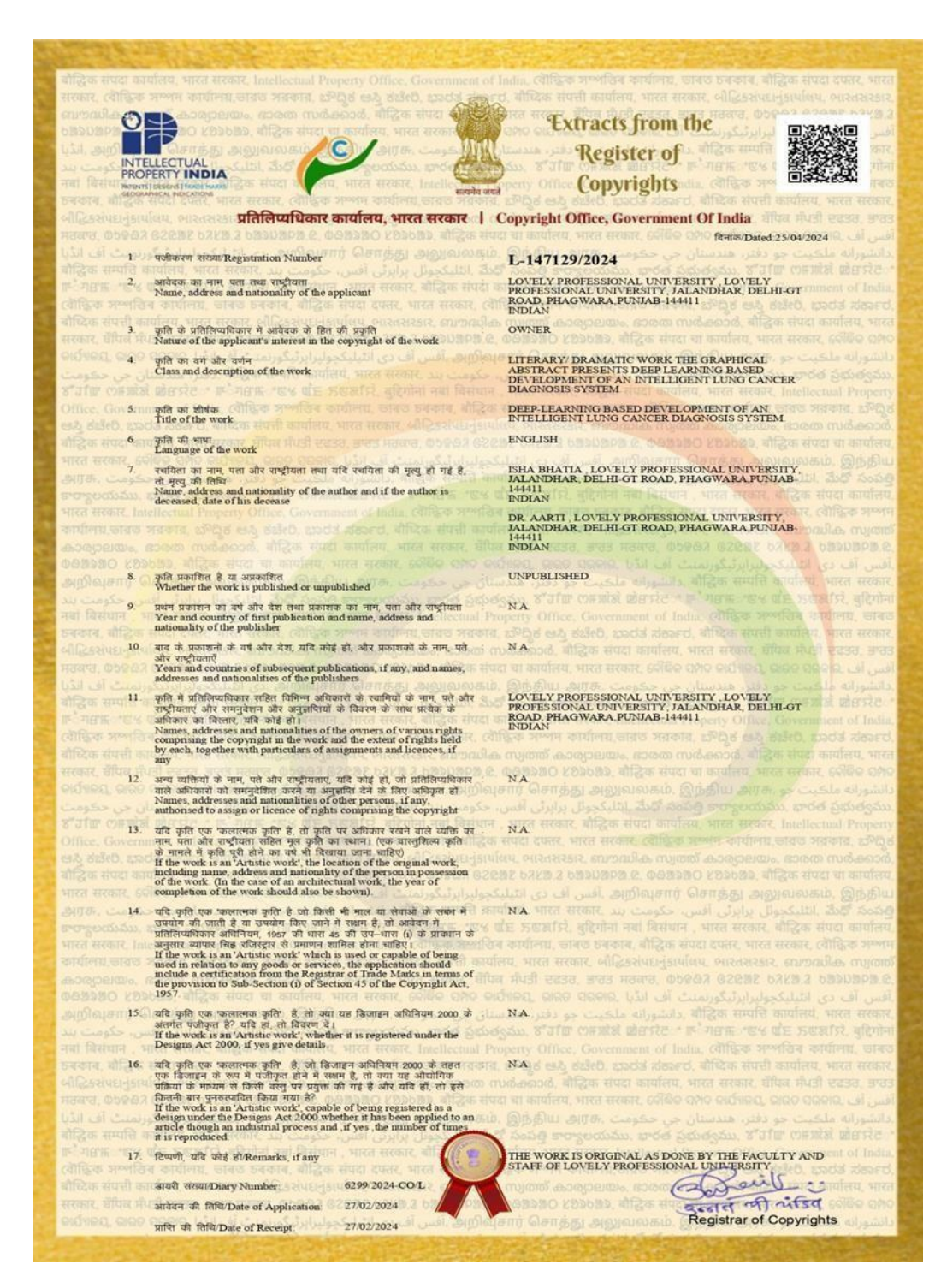
### Copyright details

Title: Deep Learning-Based Development of an Intelligent Lung Cancer Diagnosis

System.

Status: Published

Year: 2024



### ANNEXURE 2

Table 1: Summary of Previous Methods Used for Early Lung Cancer Detection

S.No	Authors & Year	Methodology	Database	Remarks	Limitations
1	Liu et al. [1], 2024	Transformer-based attention network	LIDC-IDRI	Accuracy: 94.7%, strong localization capabilities.	Transformer models require high computational resources; interpretability remains a challenge.
2	Ahmed & Zhao [2], 2024	Lightweight CNN + PSO for feature selection	LUNA16	Accuracy: 93.2%, a smaller model size makes it deployable.	The model lacks robustness validation across diverse datasets.
3	Sharma et al. [3], 2024	DenseNet + BiLSTM for CT sequence analysis	Private CT dataset	AUC: 0.89, effective temporal feature learning.	Limited generalizability due to private dataset usage.
4	Kim et al. [4], 2024	Dual-branch CNN + logistic regression for risk scoring	NLST	Precision: 91.6%, includes risk probability scores.	Logistic regression may oversimplify nonlinear dependencies.
5	Kumar & Singh [5], 2024	ResNet50 with CLAHE preprocessing	LIDC-IDRI	High contrast images; accuracy: 95.4%.	CLAHE may amplify noise in certain regions.
6	Jamshidi et al. [6], 2024	Wavelet-MLP with Dragonfly algorithm optimization	CT scans (phantom- based)	Training/testing accuracy: 99.82%, very high performance.	Real-world clinical data not validated; performance may drop in real scenarios.
7	Wang et al. [7], 2024	3D-CNN with Cox loss + binary cross-entropy	NLST	High AUC and C-index for cancer & survival prediction.	3D-CNNs are resource- intensive and complex to deploy.
8	Harlianto & de Jong [8], 2024	Meta-analysis of CE-marked AI software for nodule detection	Multiple screening CTs	Sensitivity: 94.6%, specificity: 93.6%.	Meta-analysis lacks consistency across AI tools.
9	Harlianto & de Jong [9], 2024	Evaluation of clinical AI software for CT lung screening	Multiple datasets	AI aids speed & sensitivity; highlights need to improve specificity.	Variability in datasets affects benchmarking.

S.No	Authors & Year	Methodology	Database	Remarks	Limitations
10	Saxena et al. [10], 2025	Hybrid deep CNN with MSNN using transfer learning	Private CT dataset	Accuracy: 98%, sensitivity: 97%.	Transfer learning may overfit on small private datasets.
11	Asha & Bhavanishankar [11], 2024	SAM + transfer learning for nodule segmentation	CT scans	DSC: 97.08%, IoU: 95.6%, classification accuracy: 96.71%.	Generalization across multi-modal data has not been tested.
12	Md. Jiang et al. [12], 2024	CNN-based hybrid pipeline with CT preprocessing	CT scans (FrontiersAI)	99.01% accuracy claimed; highlights segmentation need.	Pipeline complexity is not compared with standard baselines.
13	Springer et al. [13], 2025	Custom CNN, MobileNetV2, ResNet-50 comparison	IQ- OTH/NCCD dataset	Custom CNN: 98.32% accuracy, recall 97.48%, specificity 98.78%.	Comparative performance on real-time data has not been evaluated.
14	Cancers 2024 [14], 2024	InceptionResNetV2 + InceptionUNet for detection + segmentation	LIDC-IDRI	Accuracy: 98.5%, Jaccard index 95.3%.	Inception-based models require high memory.
15	Kanchan Sitaram Pradhan [1],2023	Best Fitness-based Squirrel Search Algorithm (BF-SSA).	Public	Average correct = 87.9%	Heuristic methods may lack repeatability in clinical use.
16	Hanfei Zhang [2],2023	Minimum-redundancy maximum- relevance (mRMR) selection, least absolute shrinkage and selection operator (LASSO)	Public	AUC = 0.83	Feature selection Sensitivity to noisy features.
17	Hanan Abdullah Menga sh[4], 2023	Leveraging Marine Predators Algorithm	Public	Accuracy = 89.2%.	Performance under diverse patient demographics has not been tested.
18	Kwok Tai Chui [5],2023	Multiround transfer learningand modified generative adversarial network (MTL-MGAN) algorithm	LUNA16	Sensitivity = 10.8%, Specificity 10.4%, and Accuracy = 9.92%.	Poor accuracy; needs model revision.

S.No	Authors & Year	Methodology	Database	Remarks	Limitations
19	Shalini Wankhade [7],2023	DL-based Lung Cell Cancer Detection (DL-LCCD).	Public CT Images	Accuracy = 95.30%	Preprocessing methods are not detailed.
20	Zhiqiang Shen [8],2023	semi-supervised computer-aided detection (Semi-CADe) + Cross- nodule attention computer-aided diagnosis (CNA-CADx)	LIDC-IDRI	Competition performance metric (CPM) = 82.99% + Area under the curve AUC = 88.63%	Semi-supervised models need labeled data for validation.
21	Peter G. Mikhael [9], 2023	Histogram Technique + Thresholding Algorithm	LDCT	Accuracy =98%, Precision =82%, Specificity =99%,	Limited to basic intensity features; lacks deep learning-based feature extraction.
22	Ebtasam Ahmad Siddiqui, Vijayshri Chaurasia, Madhu Shandilya [10], 2023	Gabor filters with an enhanced Deep Belief Network (E-DBN)	LIDC-IDRI and LUNA-16 datasets.	F1 score = 99.37%, Accuracy = 99.424%, Sensitivity = 98.497%, and Specificity= 98.319%.	High accuracy, but the computational complexity of E-DBN is not addressed for real-time use.

Sr.No.	Authors & Year	Methodology	Database	Remarks	Limitations
23	A Rajput, A Subasi [11], 2023	pretrained ResNet model + support vector machine	Public	Accuracy = 98.57%	Lacks robust generalization evaluation on unseen datasets.
24	Sameh AbdEl-Ghany, Mohammad Azad [12], 2023	ResNet101 + CNN	LC2500 dataset	Recall = 99.85%, F1-score = 99.84%, Specificity = 99.96%, and Accuracy = 99.94%	Segmentation performance not highlighted; performance on low-dose CT untested.
25	Siwei Wang, Fanchen Meng [15], 2023	CfDNA	Public	Specificity = 92.5%, AUC = 0.987	Focuses on DNA markers; lacks integration with imaging data.
26	Karthick Prasad Gunasekaran [19], 2023	YOLOv5 model	Public	Sensitivity = 94%, Specificity = 90.5%, Recall = 95%. Accuracy = 91%.	Object detection-centric, but lacks feature-level risk scoring.
27	S. Vishwa Kiran, Inderjeet Kaur [21], 2023	(MLDS-LCDC) + Gaussian filtering (GF) + (Ncuts) technique + FAST and rotated BRIEF (ORB) technique + optimization-based waveletneural network (SFO-WNN)	Public	Sensitivity = 97.01%, Specificity = 98.64%, and Accuracy = 98.11%.	Very complex pipeline; not tested on large, real- world clinical datasets.
28	Yahia Said, Ahmed A. Alsheikhy [33], 2023.	UNETR network + selfsupervised network.	Decathlon Dataset	Accuracy = 98.77%	Model performance on non-CT modalities is not addressed.

Sr. No.		Methodology	Database	Remarks	Limitation
	Authors & Year				
29	Asghar Ali Shah, Hafiz Abid	(CNN)	LUNA 16	Accuracy = 95%	Generic CNN architecture; lacks fine-grained lesion classification.
30	Mahmood Malik [35], 2023 Shigao Huang, Ibrahim	Bayes classifier (BayesNet) + lazy-	Public	A a a uma a u = 99 590/	Classification.
30	Arpaci, Mostafa Al-Emran	classifier (LWL) + deep neural network		Accuracy = 88.58%	Accuracy lower than modern deep models; the hybrid design increases complexity.
		(DNN).			
31	Farhanaz Farheen, Md.	Deeply Supervised MultiResUNet	LOTUS dataset	dice co-efficient = $0.8472$ .	
	Salman Shamil [38], 2022	model + DWT	(31,247 training		Dice coefficient is moderate; performance on noisy scans
			and 4458 testing		not evaluated.
			samples)		
32	M. Praveena, A. Ravi, T. Srikanth [39], 2022	CNN	CT images + NIH	Accuracy = 90%	Performance is limited to
			Chest-Xray-14		classification; it lacks lesion localization.
			database		
33		Mask Region Convolutional Neural Network (Mask-RCNN) mode +	Public	Accuracy=97.94%, Sensitivity = 98.12%	Mask-RCNN is computationally heavy; real-
		Dual			time inference has not been
		Path Network (DPN)			analyzed.
34	Lal Hussain, Hadeel Alsolai	Gray-level co-occurrence matrix	Public	Accuracy = 99.89%	Focuses on texture-based
	[42], 2022	(GLCM) + Optimized vigorous			methods; may lack
		machine learning classification			robustness on complex
		algorithm + SVM.			images.

Sr.No.	Authors & Year	Methodology	Database	Remarks	Limitations
35	Selvakumar Jayakumar [43], 2022	Cloud-based Lung Tumor Detector and Stage Classifier (Cloud- LTDSC) + multilayer convolutional neural network (M- CNN)	tomography LIDC-IDRI		Requires cloud infrastructure; local deployment issues unaddressed.
36	Mylonas [60], 2022	Support Vector Machine (SVM) + Logistic Regression (LR) + Random Forest (RF) + k-Nearest Neighbours		sensitivity = 95%  Accuracy = 96.64%, Precision  = of 96.8%, Recall = 96.6%, F-  Measure = 96.6% and AUC = 98.5%,	
38	M Mamun, A Farjana [67],	(k- NN). SMOTE method+XGBoost+ LightGBM + Bagging + AdaBoost	Public	Accuracy = 94.42 %, Precision = 95.66%, recall = 94.46%, and AUC = 98.14%	
39	Peixin Chen, Yunhuan Liu [68], 2022	SVM	Public	Accuracy = 85.2%, sensitivity = 83.7% and specificity = 86.3%	Traditional model with lower accuracy; lacks feature engineering depth.

Sr.No.	Authors & Year	Methodology	Database	Remarks	Limitations
40	Srinivasan [80], 2020	Histogram of Oriented Gradients (HoG) + wavelet transform-based features + Local Binary Pattern (LBP) + Scale Invariant Feature Transform (SIFT) + Fuzzy Particle Swarm Optimization (FPSO) algorithm = FPSOCN		Accuracy = 94.97, Sensitivity = 96.68	Feature engineering is intensive; outdated compared to DL methods.
41	P. Mohamed Shakeel,M.A. Burhanuddin [86], 2019		Archive (CIA)	Accuracy = 98.42%, Minimum classification error = 0.038.	1
42	BaihuaZhang, Shoulian Qi [88], 2019	VOT + AVE yield	LIDC- IDRI	Accuracy = 84.0%	Accuracy is low; it lacks integration of recent deep models.
	, ,	Gray level co-occurrence matrix (GLCM) + SMOTE algorithm	NSCLC	Accuracy = 81.0%	Performance is lowest; lacks multi-feature integration.
44	Qianbiao Gu, Zhichao Feng, Qi Liang, Meijiao Li [90], 2019	Random forest-based radiomics classifier		Sensitivity =0.726, Specificity = 0.661, AUC = 0.625, P < 0.05.	Very low AUC; radiomics-only focus.

Sr.No.	Authors & Year	Methodology	Database	Remarks	Limitations
45	Onur Ozdemir [91], 2019	3D CNN	LUNA16	AUC = 0.885	Good model but lacks interpretability and clinical deployment feedback.
	Ibrahim M. Nasser, Gaza Samy S. Abu-Naser [93], 2019	Artificial Neural Network (ANN)	Public	Accuracy = 96.67 %	ANN lacks advanced feature handling; outdated compared to CNN/ResNet.